Chapter 1. Present State of Approaches for Ensuring Safety against Tsunami

This chapter consolidates the history of tsunami assessments and approaches employed to ensure the safety of nuclear power plants against tsunami.

1.1. History of tsunami assessments and approach to ensuring safety against tsunami since 2011 Tohoku earthquake

1.1.1. Research on tsunami by the Japan Society of Civil Engineers

The Japan Society of Civil Engineers is a key presence promoting the public interest by ascertaining long-term social infrastructure and system needs as well as engaging in exchange and evaluation of research, scholarly study and technology on how social infrastructure and systems, capable of flexibly addressing such needs, should be structured and provided. Also, the Japan Society of Civil Engineers is an academic society that undertakes research on tsunami and the development of technology for Japan with its tsunami-prone regions, such as the Pacific coast and the coastline along the eastern margin of the Japan Sea.

Coastal engineering is a type of civil engineering that studies, among other things, natural phenomena, structures, plans for preserving and developing coastlines and the accompanying water areas. The Japan Society of Civil Engineers' Coastal Engineering Committee publishes annual collections of papers on coastal engineering and holds lectures and other talks in connection with these. The first such session was held in 1954. By 2015, the total number of such sessions has reached 62. At the sixth lecture (1959), a paper entitled "Tsunami Countermeasures for the Sanriku Coast" (Sasaki, 1959) was one of the first publications released during the initial period of the society's tsunami research. In this paper, an author affiliated with the Iwate Prefecture Civil Engineering Department discussed methods for designing coastline structures based on historical tsunami and other events that have occurred along the Sanriku coast. The conclusion alluded to the uncertainty of tsunami phenomena, and stated that open spaces should be left behind coastal dykes as well as mentioning the necessity for a process to evacuate people in cases where structures are unable to hold back a tsunami, which we now understand as similar to the current approach adopted in tsunami countermeasures. Subsequently as well, papers on tsunami have continued to be published, increasing to the 1,000 compilations that have currently been released. This number has increased since the 1990s, and research has been particularly enthusiastic since 2000. This pace was significantly influenced by the increase in tsunami research due to the disasters associated with the 2004 Sumatra earthquake tsunami and the 2011 off the Pacific coast of the Tohoku earthquake tsunami as well as the increase in tsunami research on account of the Japanese government's promotion of measures to counter tsunami occurring

along the Nankai Trough since 2003 (Central Disaster Management Council, 2003) (Fig. 1.1.1-1). In addition, tsunami research results have frequently been presented at Earthquake Engineering Symposium, which have been hosted by the Japan Society of Civil Engineers Earthquake Engineering Committee.

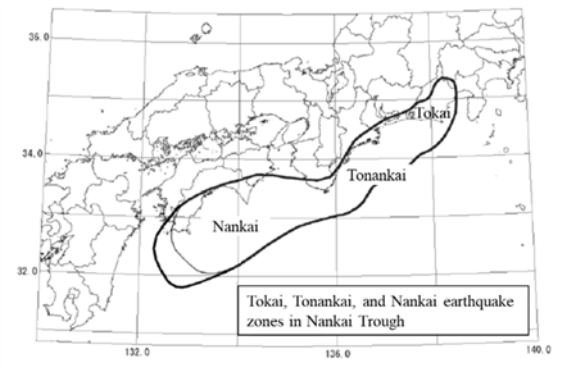

Figure 1.1.1-1 Example of tsunami source region of Nankai Trough by Central Disaster Management Council (2003)

1.1.2. The Nuclear Civil Engineering Committee and the Tsunami Evaluation Subcommittee

(1) Prior to the 2011 Tohoku earthquake

The Nuclear Civil Engineering Committee was established for the purposes of conducting research on issues related to civil engineering technology pertaining to the use of nuclear power and contributing to the promotion of scholarship and technology. The Tsunami Evaluation Subcommittee was launched in 1999 to conduct research on tsunami.

Two turning points led to this development. One was the compilation by the seven relevant government ministries and agencies of a guide on tsunami countermeasures (National Land Agency et al., 1998) to be used for disaster administration, an endeavor that was prompted by the 1993 Hokkaido Nansei-oki earthquake and tsunami. The guide indicated the need to take into consideration not only the largest historical tsunami, but also the largest supposed earthquake tsunami. The second point was that standardized methods had not yet been compiled for assessing tsunami with respect to nuclear power plants. After approximately two years of deliberations, the results of technological progress and knowledge developed about tsunami sources and numerical calculations were compiled, thereby consolidating methods for configuring design tsunami for nuclear power facilities. These results were released in a publication entitled “Tsunami Assessment Method for Nuclear Power Plants in Japan” (Japan Society of Civil Engineers, 2002).

These results served as the foundation for “Chapter 4. Tsunami Height Assessment”, which was published in the Japan Electric Association’s Nuclear Power Plant Aseismic Design

Guidelines (Japan Electric Association, 2008). An English version was also prepared and released (JSCE, 2006). These guidelines were also referenced and quoted in reports released by the International Atomic Energy Agency (IAEA) and the Nuclear Regulatory Commission in the United States (IAEA, 2011; NRC, 2009), and have been recognized to a certain extent internationally as well (Fig. 1.1.2-1).

Since then, reviews have also been advanced on probabilistic assessments of tsunami height (Japan Society of Civil Engineers, 2011a) and changes in submarine topography due to tsunami (Fujii et al., 2009; Ikeno et al, 2009; Fujita et al., 2010) along with other issues.

(2) After the 2011 Tohoku earthquake

After the 2011 Tohoku earthquake, the Japan Society of Civil Engineers set up 10 committees established to conduct their work for a fixed period of time, among these were committees that would address particular topics, in addition to the society's permanent committees. Expert knowledge was accumulated, compiled into many proposals and published. For example, a committee studying tsunami estimation and disaster reduction took into account the lessons learned from the damage wrought by the massive tsunami triggered by the 2011 Tohoku earthquake and proposed methods of incorporating these lessons over the short and long-term to counter disaster from massive tsunami (Japan Society of Civil Engineers, 2012).

After the tsunami damage to nuclear power plants from the 2011 Tohoku earthquake, the Nuclear Civil Engineering Committee held a session to report the results of tsunami research on November 2, 2011, at which a report was presented on the direction for tsunami configuration that takes into account the Great East Japan Earthquake as well as methods for configuring tsunami height (Japan Society of Civil Engineers, 2011b).

A committee was established to research the special topic of nuclear safety technology, which the Nuclear Civil Engineering Committee was central to such deliberations, and proposed a new framework for earthquake and tsunami resistant design as well as a risk management system (Japan Society of Civil Engineers, 2013). Specifically, the proposal stated: "A new concept of 'anti-catastrophe' is proposed in addition to the conventional concept of 'safety' for performance vis-à-vis an earthquake or tsunami. The assurance of 'anti-catastrophe' is important for handling events or other situations that exceed the standard ground motion or standard tsunami". This approach is in accordance with the concept of defense in depth, which is the basis for ensuring nuclear safety, and, furthermore, the proposal broadly took into consideration a general ease of understanding such information. This publication is a compilation of relevant tsunami assessment technology with a view towards contributing towards this framework as well.

Following the 2011 Tohoku earthquake, the Tsunami Evaluation Subcommittee collected and analyzed information about this tsunami disaster. For example, the height of traces of tsunami

obtained from surveys and the results of calculations of tsunami based on many proposed tsunami source models were compared for this tsunami (Kurita et al., 2013). Useful results were obtained for methods for configuring uncertainty in probabilistic tsunami hazard analysis, such as the variance of calculation results for the run-up height records of historical tsunami increases according to the distance of such traces from the coastline. After taking into account the results obtained from these reviews of the 2011 Tohoku earthquake, research results, which had been compiled since 2002, were added to put together this publication.

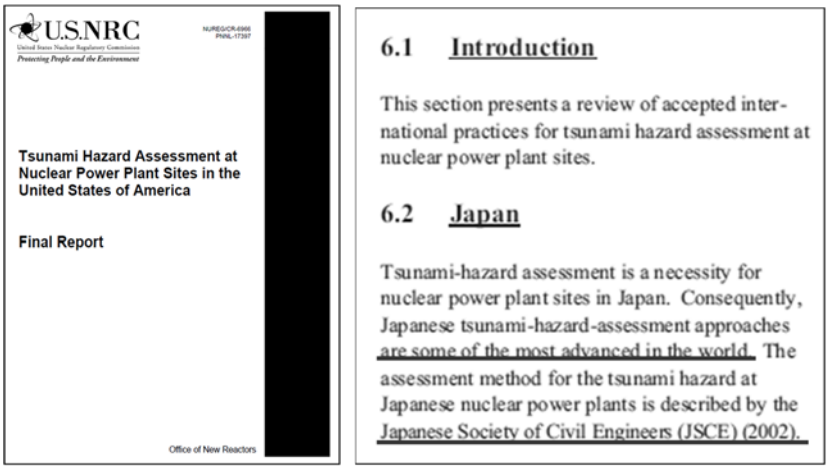
U.S.NRC
United States Nuclear Regulatory Commission
Protecting People and the Environment

NUREG/CR-6966
PNNL-17397

Tsunami Hazard Assessment at Nuclear Power Plant Sites in the United States of America

Final Report

Office of New Reactors

6.1 Introduction

This section presents a review of accepted international practices for tsunami hazard assessment at nuclear power plant sites.

6.2 Japan

Tsunami-hazard assessment is a necessity for nuclear power plant sites in Japan. Consequently, Japanese tsunami-hazard-assessment approaches are some of the most advanced in the world. The assessment method for the tsunami hazard at Japanese nuclear power plants is described by the Japanese Society of Civil Engineers (JSCE) (2002).

Figure 1.1.2-1 Report of tsunami hazard assessment by U.S.NRC and page quoted from tsunami evaluation assessment by JSCE in it.

1.1.3. Atomic Energy Society of Japan

Since the accident at the Fukushima Daiichi Nuclear Power Station, the Atomic Energy Society of Japan (“AESJ”), a group of experts specializing in the nuclear field, has progressively contributed to resolution of the accident and other aspects, and continued to fulfill its responsibility. Within that context, the AESJ launched an accident investigation committee, which published the results of its efforts in a final report (AESJ, 2014; hereinafter “AESJ Report”). The AESJ Report consolidates analyses of the Fukushima Daiichi accident as well as the conditions of other stricken nuclear power plants. Moreover, deliberations were conducted both inside and outside the AESJ to put together the fundamental causes of the accident as well as proposals.

This report classifies the fundamental causes into direct factors and contextual factors. It further breaks down the direct factors into measures to counter the direct impact of a tsunami in cases where the design basis is exceeded, measures to counter a severe accident arising as a result of such exceedance, and measures for accident mitigation and avoidance during an emergency, and the report

points out that these three measures have not been sufficient. In addition, as to the contextual factors, the report notes problems concerning the awareness and stance taken by stakeholders in relation to the assurance of nuclear safety.

The recommendations, which were developed through an examination of these fundamental causes, are comprised into 50 items classified into five categories (Fig. 1.1.3-1). The focus here is on the content related to tsunami countermeasures in recommendations I and II, and summaries are given.

Recommendation I “Basic Items of Nuclear Safety” touches upon first clarifying the goals of nuclear safety and the necessity for systematizing such goals, and states that the way to realize such goals requires achieving a greater understanding of defense in depth, which has been previously recommended, and enhancing its application.

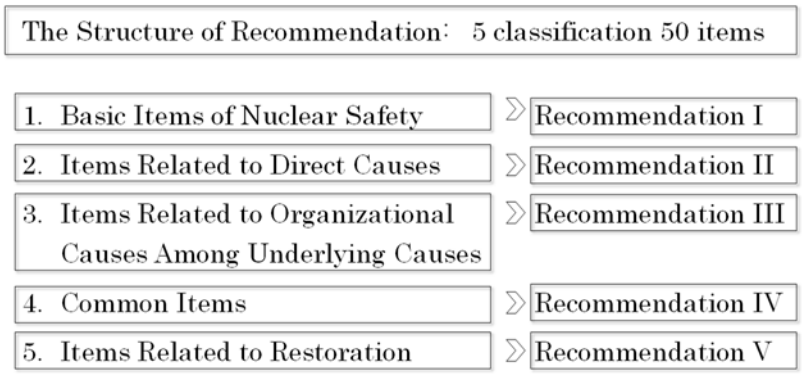

Figure 1.1.3-1 Recommendations of the AESJ Investigation Committee (AESJ, 2014)

Recommendation II “Items related to Direct Causes” (Fig. 1.1.3-2) discusses the necessity of all-encompassing assessments of many external events, including earthquakes, in terms of “1. Strengthening measures against external events”. More specifically, the recommendation calls for first understanding the vulnerabilities of a nuclear power plant and specifying the responses by conducting a comprehensive assessment of anticipated external events, including not only earthquakes and tsunamis, but also fires and other such events, and for addressing the vulnerabilities where an extensive loss of safety function may simultaneously occur in response to an external event resulting in a critical situation (cliff-edge measures). Under “4. Enhancement of the nuclear safety assessment technology”, the report discusses how the utilization of probabilistic risk assessment technology should be incorporated, which is able to consider a variety of uncertainties in order to increase the quality of predictions, and the utilization of numerical calculation techniques, which employ the latest computer performance for analysis of natural phenomena and other events.

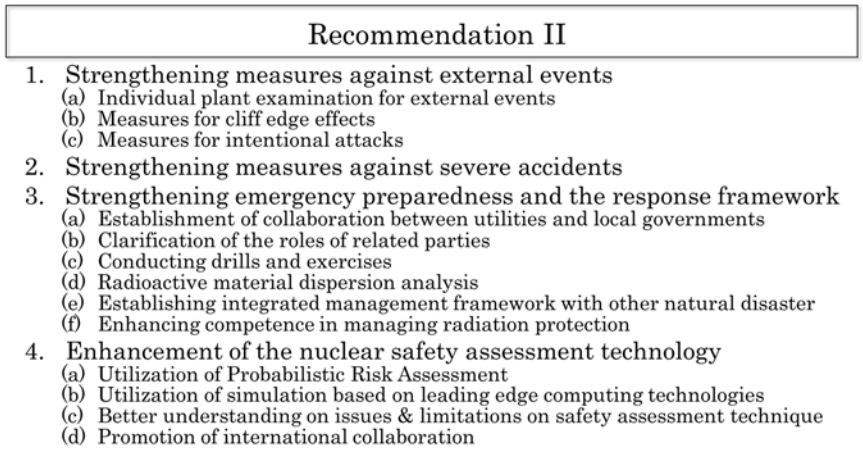

Figure 1.1.3-2 Composition of Recommendation II of the AESJ Investigation Committee (AESJ, 2014)

1.1.4. JSME Japan Society of Mechanical Engineers

The Japan Society of Mechanical Engineers (JSME) launched two task forces immediately after the 2011 Tohoku earthquake, conducted investigations of the damage from the perspective of mechanical engineering, and compiled the results. Furthermore, the JSME put together proposals from its broad perspective (Japan Society of Mechanical Engineers, 2013). The focus here is on the content related to tsunami, and an overview is given.

The proposals comprised four issues: “I. System integration of large systems”, “II. Design-based approach and addressing the ‘beyond’ ”, “III. Issues pertaining to risk communication”, and “IV. Continuing research and its development into standards and criteria”.

Issue I points out the presence of weaknesses found in gaps in specialized knowledge about nuclear power plants and other large facilities, and proposes as a countermeasure that a methodology for system integration be systematized into the “science of design”.

Issue II points out that a lesson learned is to properly explain to society in advance the risk of any exceedance in cases where an “estimated value” is set for planning or design of man-made structures and to obtain society’s acceptance of this risk of exceedance as an “acceptable risk”, and proposes that such procedures be followed in formulating any “estimated values”.

Issue III states the need for accurately predicting the inherent risks and benefits during the manufacturing planning stage, announcing these risks and benefits to society and obtaining society’s understanding in advance, as well as the need for risk communication during the preceding stage beginning with design in issue II. To this end, it is proposed that engineers study the essential knowledge for PRA standards and other risk management methodologies.

Issue IV proposes continuing research as well as incorporating the results of such investigations

and research into standards, criteria, manuals and so on, and, furthermore, developing as well as training researchers and engineers.

1.1.5. Ministry of Land, Infrastructure, Transport and Tourism

After the 2011 Tohoku earthquake, the Ministry of Land, Infrastructure, Transport and Tourism compiled the “Guide to Configuring Estimates of Tsunami Inundation” (Ministry of Land, Infrastructure, Transport and Tourism, 2012), “Guidelines on Tsunami Resistant Design of Breakwaters” (Ministry of Land, Infrastructure, Transport and Tourism, 2013a), and “Guidelines on Tsunami Resistant Design of Seawalls (Parapets) in Ports” (Ministry of Land, Infrastructure, Transport and Tourism, 2013b). These publications each presented the approach of estimating tsunami inundation along the coast where significant damage was sustained due to the tsunami resulting from the 2011 Tohoku earthquake as well as such techniques and their utilization, along with the basic concepts for tsunami resistant design of breakwaters and seawalls at port facilities.

The first guide assumed the largest class of tsunami and proposed the approach of “protecting human life no matter what” by minimizing damage through multiple layers of defense comprised of many tangible and intangible measures, and detailed such methods. The latter two guidelines took into consideration the social impact of tsunami on human life, property, etc., and called for the appropriate setting of contextual safety goals for ports with respect to such facilities and seawalls in keeping with tsunami size and frequency. With respect to both designs, the proposal is for design to be undertaken in a manner that addresses design-basis tsunami after taking into consideration movements, such as Level 2 ground motion, as described in the “Technical Standards and Commentaries for Port and Harbour Facilities in Japan” (Ports and Harbours Association of Japan, 2007; English version - The Overseas Coastal Area Development Institute of Japan, 2009) and to aim for a “resilient structure” to the extent possible that would not collapse easily even if struck by a tsunami exceeding the design-basis tsunami in order to enhance the effectiveness of structures in minimizing damage. In this way proposals have been made that aim to minimize damage through multiple layers of defense comprised of multiple countermeasures as well as the need for a design to counter a tsunami exceeding the design tsunami after taking into consideration the effects of seismic vibration on facilities that provide tangible countermeasures, which are one type of countermeasure.

1.1.6. Trends around the World

(1) IAEA

In 2011, the IAEA published a detailed safety guide entitled “Meteorological and Hydrological Hazards in Site Evaluation for Nuclear Installations” (IAEA, 2011). This

publication is a compilation of guidance and recommendations on climate and hydrological disasters striking nuclear power facilities, and addresses tsunami as well as storm surge, wind-generated waves, seiches, floods and other events. In addition, basic approaches to countermeasures and other concepts are discussed as well as the “dry site” concept as a measure to counter general flood damage not limited to tsunami.

(2) United States

The United States has experienced damage from tsunami along its Pacific coast. In 2009, the NRC released “Tsunami Hazard Assessment at Nuclear Power Plant Sites in the United States of America (NUREG/CR-6966)” (NRC, 2009). This publication provides an overview of methods for assessing tsunami in general. In addition to earthquakes, descriptions are given of factors giving rise to tsunami, including submarine landslides, slope failure and volcanic phenomena. In addition, descriptions are given of the effects of tsunami on a nuclear power plant, explaining run-up overflow, descending water levels, scouring, sedimentation, tsunami force, debris and methods for assessing the effects of these. Furthermore, in 2016 two volumes were published: “Tsunami Hazard Assessment: Best Modeling Practices and State-of-the-Art Technology (NUREG/CR-7223)” and “Tsunami Hazard Assessment Based on Wave Generation, Propagation, and Inundation Modeling for the U.S. East Coast (NUREG/CR-7222)”. The former is a broad compilation of the latest methods for tsunami assessment, and the latter describes methods for tsunami assessment along the eastern coast of the United States, including specific examples. In addition, a probabilistic tsunami hazard analysis was conducted at the Diablo Canyon Power Plant in the United States (PG&E, 2010). In addition to earthquakes, consideration was also given to submarine landslides as a factor giving rise to tsunami.

1.2. Future direction and role of this publication

Here, the course taken in research on tsunami countermeasures in Japan is considered in looking back on close to 20 years of tsunami countermeasures for nuclear power plants, and the role of this publication is discussed in improving the safety of nuclear power plants in the future.

Research on tsunami countermeasures since the end of World War II has been confirmed since the late 1950s and early 1960s, and discussed tangible countermeasures by means of structures as well as intangible countermeasures by means of evacuations and other such methods, ever since such research was first conducted. Later, seawalls and other tangible countermeasures have been implemented in regions damaged by massive tsunami occurring around the Japan Trench or Nankai Trough. The tsunami heights estimated when implementing these countermeasures principally referenced the heights of historical tsunamis. In the latter 1990s, a shift was proposed from historical

tsunami to supposed tsunami for tsunami heights to be used in configuring tsunami countermeasures. Following this, in 2002, the “Tsunami Assessment Method for Nuclear Power Plants in Japan” was developed, which compiled methods for evaluating water levels using probable tsunami based on seismological and other knowledge as well as data on historical tsunamis. This method contributed to the evolution of methods for configuring tsunami water levels for nuclear power plants in Japan. The massive tsunami resulting from the 2011 Tohoku earthquake significantly exceeded the tsunami heights configured based on data at the time using this method, and four nuclear power plants, Onagawa, Fukushima Daiichi, Fukushima Daini and Tokai, experienced inundations of seawater due to the effects of the tsunami inside their sites or buildings. Of these nuclear power plants, three locations were successfully shut down safely, but the tsunami caused a situation at the Fukushima Daiichi Nuclear Power Station where a large quantity of radioactive materials was released.

Following this, the Japan Society of Civil Engineers and other academic societies presented recommendations from their respective perspectives. As stated in Appendix Sections 1.1.2 to 1.1.4, what the recommendations presented by the Japan Society of Civil Engineers, JSME and AESJ have in common is the importance they place on countermeasures pertaining to tsunami that exceed design scale. The Japan Society of Civil Engineers proposes this in terms of “anti-catastrophe” performance, and the JSME provides proposals in terms of “responding to ‘beyond’ ”. The AESJ states that the previously proposed defense in depth should be better understood and its application enhanced. In addition, the Ministry of Land, Infrastructure, Transport and Tourism has put forth proposals to appropriately configure design tsunami for ports and other structures along coastlines as well as aiming for a “resilient structure” that increases the effectiveness of minimizing damage even with respect to a tsunami exceeding the design tsunami.

Taking the aforementioned into consideration, it is important that the concept of defense in depth be kept in mind for natural external forces such a tsunami with respect to nuclear power plants, that safety targets be appropriately configured and multiple configurations made of the design scale as well as on a scale exceeding such settings for natural external forces, and that countermeasures be constructed commensurate with these respective scales. This will make it possible to maintain the “anti-catastrophe” performance that allows for a “response to address the ‘beyond’” in addition to safety as concerns external forces in terms of the design scale. The content detailed here is still conceptual, so it is necessary, in the near future, to specifically systematize this concept by taking into consideration the special characteristics of nuclear power plants, and it is essential that collaborative work be conducted in various fields toward this end.

One sort of collaboration with respect to tsunami is the release of the publication “Tsunami Resistant Engineering for Nuclear Safety”, which was compiled by the Japan Association for Earthquake Engineering. This publication brings together knowledge of experts in the fields of earthquake engineering, nuclear engineering, civil engineering and other areas to systematize

comprehensive technologies for ensuring the safety of nuclear power plants against tsunami, and it is hoped that this publication will be used and developed in the future.

The elemental technologies pertaining to tsunami assessment compiled in this publication, in addition to their use in safety assessments and other examinations of nuclear power plants, play an important role in quantitatively assessing the effects of tsunami, which is necessary for a framework for safety assessments that will be systematized in the future. In addition, it goes without saying that it is important that the framework for safety assessments and the elemental technologies in this publication be constantly updated through continuous research and investigation based on the latest research results and other findings in the endeavor to improve safety.

[Appendix 1 References]

Atomic Energy Society of Japan's Investigation Committee on the Nuclear Accident at the Fukushima Daiichi Nuclear Power Plant (2014): Full Picture of the Fukushima Daiichi Nuclear Power Station Accident and Proposals for Tomorrow: Final Report of the Society's Accident Investigation, 448p.
http://dl.hieng.ir/bot/165287498_1488715197.pdf (Accessed on August 2016)

Central Disaster Management Council (2003): The Report of Tonankai and Nankai Earthquake, 50p. (in Japanese).
http://www.bousai.go.jp/kaigirep/chuobou/9/ (Accessed on April 2016)

Committee on Specific Topics Concerning Civil Engineering Technology for Nuclear Safety (2013): Proposal on Optimal Aseismicity and Tsunami Resistant Performance of Nuclear Power Plants (Civil Engineering Perspective).
http://committees.jsce.or.jp/2011quake/node/158 (Accessed on April 2016)

Fujii, N., M. Ikeno, T. Sakakiyama, M. Matsuyama, M. Takao and K. Mukaihara (2009): Hydraulic Experiment on Flow and Topography Change in Harbor due to Tsunami and Its Numerical Simulation, Journal of Japan Society of Civil Engineers B2, Vol. 56, pp. 291-295 (in Japanese).

Fujita, N., K. Inagaki, N. Fujii, M. Takao and T. Kaneto (2010): Study on Field Applicability of Estimation Model for Topography Change due to Tsunamis, Annual Journal of Civil Engineering in the Ocean, Vol. 26, pp. 213-218 (in Japanese).

Geospatial Information Authority of Japan, Ministry of Agriculture, Fisheries Agency, Ministry of Transport, Japan Meteorological Agency, Ministry of Construction, and the Fire and Disaster Management Agency (1998): Guide to Strengthening Tsunami Countermeasures in Regional Disaster Prevention Plans (in Japanese).
http://tsunami-dl.jp/document/022 (Accessed on August 2016)

IAEA (2011): Meteorological and Hydrological Hazards in Site Evaluation for Nuclear Installations, Draft Safety Guide, DS417, 2011.
http://www-pub.iaea.org/MTCD/publications/PDF/Pub1506_web.pdf
(Accessed on August 2016).

Ikeno, M., T. Yoshii, M. Matsuyama and N. Fujii (2009): Calculation of Suspended Sediment Pickup based on Tsunami Experiments and Proposal of Pickup Equation, Journal of Japan Society of Civil Engineers B2, Vol. 65, pp. 506-510 (in Japanese).

Japan Electric Association (2008): Nuclear power plant seismic design technical guidelines, JEAG4601-2008, 222p. (in Japanese).

Japan Society of Civil Engineers, Tsunami Evaluation Subcommittee, Nuclear Civil Engineering Committee, JSCE (2002): Tsunami Assessment Method for Nuclear Power Plants in Japan, 72p. (in Japanese).
http://committees.jsce.or.jp/ceofnp/node/5 (Accessed on April 2016)

Japan Society of Civil Engineers, Tsunami Evaluation Subcommittee, Nuclear Civil Engineering Committee (2006): Tsunami Assessment Method for Nuclear Power Plants in Japan, 2006.
http://committees.jsce.or.jp/ceofnp/system/files/JSCE_Tsunami_060519.pdf
(Accessed on August 2016)

Japan Society of Civil Engineers, Tsunami Evaluation Subcommittee, Nuclear Civil Engineering Committee, (2011): Methods for Probabilistic Tsunami Hazard Analysis.
http://committees.jsce.or.jp/ceofnp/node/39 (Accessed on August 2016)

Japan Society of Mechanical Engineers (2013): Lessons Learned from the Great East Japan Earthquake Disaster, Report of the JSME Research Committee on the Great East Japan Earthquake Disaster, 122p.
https://www.jsme.or.jp/jsme/uploads/2016/08/Great-East-Japan-Earthquake-Disaster-Full-Text.pdf (Accessed on August 2016)

Kurita, T., M. Matsuyama, and D. Uchino (2013): Uncertainty of Numerical Tsunami Simulation Evaluated in Comparison with the Field Survey Results of the 2011 Tohoku Earthquake Tsunami, Journal of Japan Society of Civil Engineers B2, Vol. 69, No. 2, pp. I-216 - I-220 (in Japanese).

Ministry of Land, Infrastructure, Transport and Tourism (2011): Basic guidelines on promotion of tsunami disaster prevention area (in Japanese).
http://www.mlit.go.jp/common/000188287.pdf (Accessed on August 2016)

Overseas Coastal Area Development Institute of Japan (2009): Technical Standards and Commentaries for Port and Harbour Facilities in Japan, 998p.

Pacific Gas and Electric Company (2010): Methodology for Probabilistic Tsunami Hazard Analysis: Trial Application for the Diablo Canyon Power Plant Site, 182p.

Ports and Harbours Bureau, Ministry of Land, Infrastructure, Transport and Tourism (2013a): Tsunami design guidelines for breakwaters, 35p. (in Japanese).
http://www.mlit.go.jp/kowan/kowan_tk5_000018.html (Accessed on August 2016)

Ports and Harbours Bureau, Ministry of Land, Infrastructure, Transport and Tourism (2013b): Tsunami design guidelines for tsunami wall in harbours, 35p. (in Japanese).
http://www.mlit.go.jp/kowan/kowan_tk5_000018.html (Accessed on August 2016).

Sasaki, S. (1959): Countermeasures against tsunami disaster at Sanriku Coastal Area, Proceedings of The 6th Coastal Engineering Conference, pp. 18-28 (in Japanese).

U.S. Nuclear Regulatory Commission (2009): Tsunami Hazard Assessment at Nuclear Power Plant Sites in the United States of America - Final Report (NUREG/CR-6966), 84p.
http://www.nrc.gov/reading-rm/doc-collections/nuregs/contract/cr6966/
(Accessed on August 2016)

U.S. Nuclear Regulatory Commission (2016a): Tsunami Hazard Assessment Based on Wave Generation, Propagation, and Inundation Modeling for the U.S. East Coast (NUREG/CR-7222), 133p.
https://www.nrc.gov/reading-rm/doc-collections/nuregs/contract/cr7222/
(Accessed on August 2016)

U.S. Nuclear Regulatory Commission (2016b): Tsunami Hazard Assessment: Best Modeling Practices and State-of-the-Art Technology (NUREG/CR-7223), 117p.
http://www.nrc.gov/reading-rm/doc-collections/nuregs/contract/cr7223/
(Accessed on August 2016)

Chapter 2. Examination of Tsunami Source Configuration

2.1. Basic matters for tsunami source configuration

2.1.1. Earthquake source region and ground physical properties

(1) Initiation location of past earthquakes

Large past tsunamis, which have occurred around Japan, have been concentrated along plate boundaries and the eastern margin of the Japan Sea, and it has been extremely rare for a tsunami to occur in the East China Sea side of Kyushu or the Japan Sea side of southwestern Japan. Earthquakes having a magnitude of 9 or greater, which have occurred around the world since the 20th century, have initiated in subduction zones. According to Figure 1 in Rajendran (2013), the source regions of interplate earthquakes of M8.5 or greater, which have occurred between 1906 and 2012, have not overlapped with each other.

(2) Seismogenic layer

Around the Japanese Archipelago, earthquakes have occurred in a variety of patterns, but the locations where both interplate and intraplate earthquakes occur have been found to be limited. The region where interplate earthquakes occur along a plate boundary is called the seismogenic zone, and Pacheco et al. (1993) stated that such a region corresponds to one where stable slip occurs, and believed that thrust-type (shallow dipping reverse fault-type) earthquakes occurred along a plate boundary within this region. However, it is known that there is coupling to a certain extent even near trench axes and deep transition zones, and consideration has also been given to including these in tsunami source models.

Lay et al. (2012) analyzed differences in behavior in terms of depth along plate boundaries where megathrust earthquakes have occurred in order to explain differences in the characteristics of seismic wave radiation between large and medium-sized earthquakes. After classifying the inclination of the dip angle into four regions, the authors presumed the rupture domains of large earthquakes in recent years as shown in Table 2.1.1-1 based on their analyses of tsunami and seismic waves.

Even when looking at inland crustal earthquakes, it has been pointed out that there is a seismogenic layer where failure does not progress beyond a specific depth. The cause of this lower limit to the seismogenic layer is believed to be because the rupture pattern in rock changes due to temperature and pressure, in other words due to depth (Ito, 2008). Consequently, when earthquakes are greater than a specific magnitude, fault width reaches a maximum.

The thickness of this seismogenic layer varies depending upon location.

Table 2.1.1-1 Rupture domains of interplate megathrust faults (Lay et al., 2012)

Domain	Rupture Characteristics
A - near trench domain	• From the trench down to about 15 km depth below sea level • Either aseismic deformation or large coseismic displacements in tsunami earthquakes • Tsunami earthquakes or anelastic deformation and stable sliding occur
B - central megathrust domain	• From 15 to 35 km depth • Large slip occurs with minor short-period seismic radiation
C - downdip domain	• From 35 to 55 km depth • Moderate slip occurs with significant coherent short-period seismic radiation
D - transition domain	• Depth of 30-45 km in several subduction zones, typically involving subduction of relatively young plates with shallow dip angles • Slow slip events, low frequency earthquakes (LFEs), and seismic tremor can occur

(3) Rigidity modulus of medium near hypocenters

When data for P wave velocity structure and the velocity ratio between P waves and S waves are used to estimate rigidity corresponding to location and depth, the results given in Table 2.1.1-2 have been found.

Of these, in cases where “the fault plane covers depths both shallower and deeper than 20 km”, it is also possible to take into account the distribution of seismic moment to calculate rigidity in cases where a seismic model is used that takes into account slip heterogeneity.

Crust 1.0 (Laske et al., 2013) is a data set of crustal structures around the globe.

Table 2.1.1-2 Rigidity modulus of medium near hypocenters

Region	Basis	Rigidity modulus
Intraplate region in southwest Japan, the eastern margin of the Japan Sea, and shallow plate boundary (when the entire fault plane exists at a depth of 20 km or less)	Adopt the intermediate value of the range below: Vp=6.0km/s Vp/Vs=1.6-1.7 ρ=2.7-2.8g/cm^3 lead to μ=3.36×10^{10}-3.94×10^{10} N/m^2	3.5×10^{10} N/m^2 (3.5×10^{11} dyne/cm^2)
Intraplate region of oceanic plate, and deep plate boundary (when the entire fault plane exists at a depth of 20 km or more)	Adopt the intermediate value of the range below: Vp=8.0-8.1km/s Vp/Vs=1.75-1.80 ρ=3.2-3.5g/cm^3 lead to μ=6.31×10^{10}-7.50×10^{10} N/m^2	7.0×10^{10} N/m^2 (7.0×10^{11} dyne/cm^2)
Medium depth of plate boundary(fault plane covers depths both shallower and deeper than 20 km)	Adopt intermediate values between shallow and deep regions	5.0×10^{10} N/m^2 (5.0×10^{11} dyne/cm^2)

(4) Plate relative motion and boundary shape

In Figure 2.1.1-1, general values are given based on Seno (2005) for the relative movement velocity of plates around the Japan Archipelago. In addition to this, Loveless and Meade (2010) calculated the relative movement of blocks subdividing the area around the Japan Archipelago. Both of these are generally consistent with each other.

Bird (2003) proposed a model for plate relative movement around the world (PB2002), dividing plate boundaries according to type. The areas between the Kuril-Kamchatka Trench and Japan Trench, Nankai Trough and Ryukyu Trench as well as the Izu-Ogasawara Trench have been divided into subduction zones (SUB). The eastern margin of the Japan Sea is regarded as an oceanic convergent boundary (OCB), and, although there is a converging boundary, it is distinguished from a subduction zone. The definitions of these two types are given in Table 2.1.1-3.

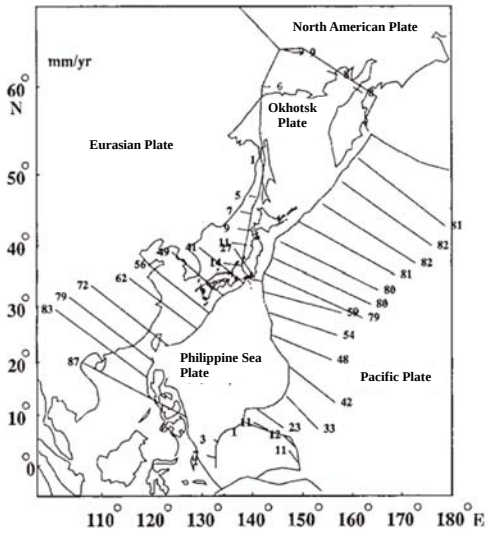

(Unit: mm/year)

Figure 2.1.1-1 Approximate value of plate relative motion velocity around the Japanese archipelago (Seno, 2005 ©Tokyo Geographical Society)

Table 2.1.1-3 Classification condition of plate boundary type SUB and OCB (Bird, 2003)

Class	Condition
SUB	• Plate boundary steps with a convergent (component of) velocity • Having a Benioff zone of intermediate to deep earthquakes and/or a parallel volcanic arc with Quaternary activity
OCB	• Lying entirely within seafloor whose age is known from linear magnetic anomalies to be less than 180 Ma, and/or at water depths exceeding 2000 m • Relative velocity has an azimuth above ±20 deg. of the azimuth of the plate boundary step

In order to create models of tsunami sources based on interplate earthquakes, data on depth distribution along plate boundaries are necessary. In addition to various references concerning plate boundary shape, the following available sources provide such data.

- National Research Institute for Earth Science and Disaster Resilience: Japan Seismic Hazard Information Station (J-SHIS)

  http://www.j-shis.bosai.go.jp/
- United States Geological Survey (USGS): Slab Models for Subduction Zones

  http://earthquake.usgs.gov/data/slab/
- Headquarters for Earthquake Research Promotion, Earthquake Research Committee (2004): Long-Term Assessment of Seismicity Around the Sea of Hyuganada and the Southwest Islands Trench

- Ministry of Education, Culture, Sports, Science and Technology's Research and Development Bureau and the Japan Agency for Marine-Earth Science and Technology (2013): Project for Assessment and Research on Multi-Segment Ruptures in Eastern Sea, Southeastern Sea and South Sea Earthquakes: Report of Survey, Observation and Research Results to Assess Multi-Segment Ruptures in Eastern Sea, Southeastern Sea and South Sea Earthquakes (2008~2012)
- Cabinet Office (2012): Investigative Commission on Models of Megathrust Earthquakes in the Nankai Trough (Second Report)

(5) Interplate coupling and earthquake magnitude

In recent years, supercycle earthquakes (Sieh et al., 2008) have been suggested, which are thought to occur in inherent periods longer than the periods of time for which information has been obtained from archives and mechanical records.

Nishimura (2012a) has aligned plate boundaries where strong coupling has been estimated based upon geodetic observations and areas where megathrust earthquakes have occurred since the 20th century. Moreover, the current state of knowledge taking into account advances made in geodetic interplate coupling research has been compiled below.

- Mean degree of coupling specific to a subduction zone
  - Large: Cascade, Chile, Sumatra and Nankai Trough
  - Medium: Kamchatka, Aleutian, Alaska, Mexico, Central America, Colombia, Peru and Japan Trough
  - Small: Subduction zones in the Western Pacific (New Zealand, Tonga, Izu-Ogasawara, Mariana, etc.)
- Source regions of megathrust earthquakes (moment magnitude ("M_W") up to 9), which have occurred in the past, have been estimated to have coupling ranging from medium to strong, and they do not uniformly have a strong coupling. Megathrust earthquakes are unknown in subduction zones where coupling is estimated to be weak.
- The breadth of coupling regions (including partial coupling) ranges up to a maximum of 300 km. The occurrence of megathrust earthquakes is known in Chile, Alaska and the Japan Trough, which all have coupling of a larger scale.
- There are also many subduction zones, such as the Aleutians and other areas, where there is a significant change in the degree of coupling in the strike direction of the subduction zone.
- Although it is difficult to explain interplate coupling in terms of single parameters such as plate relative velocity or the date of the subducting plate, attempts to explain the existence of any degree of coupling have been effective when multiple elements are combined (see

for example Scholz and Campos, 1995).

Scholz and Campos (1995), which has been mentioned in this context, has been updated by Scholz and Campos (2012). Scholz and Campos (2012) estimates seismological interplate coupling based upon earthquake history and geodetic interplate coupling based upon GPS data, and finds that, excluding a small number of exceptions, both coincide with a difference of less than 10%. Based on this, the coupling coefficient for Honshu (along the Japan Trench) is 0.54~0.65, 1.0 for the Nankai Trough and 0 for the Ryukyu trench, and there is a connection between the coupling coefficient and the force in a normal direction acting between the plates.

Wang and Bilek (2014) presented the following views regarding the relationship between plate boundary surface shape and earthquake magnitude.

- All observed megathrust earthquakes have occurred in sea regions where smooth topography has been subducting. Plate boundaries accompanied by topography, where there is very significant undulation, creeps, and megathrust earthquakes have not occurred in such areas.
- Subducting seamounts are typical examples of terrain with significant undulation. Regions where seamounts are subducting are accompanied by medium to small earthquakes, and no evidence has been obtained that large earthquakes have occurred. The termination on the southern end of the fracture of 2011 Tohoku earthquake (the 2011 off the Pacific coast of the Tohoku Earthquake) occurred not at a location where the Philippine Plate was the foot wall, but in an area where seamounts were subducting.

2.1.2. Scaling law and stress drop

(1) Scaling law for earthquake magnitude

As shown in main volume 4.2.1.1 of the main text, there are at least three approaches, which are described below, with respect to the scaling law for fault parameters related to M_W.

1) Method where limits are not set on fault length L, fault width W or slip amount D

$\log M_0$ (N·m) = 1.5 M_W + 9.1, $M_0 = \mu LDW$

M_0: Seismic moment, μ: Rigidity of medium around hypocenter,

L: Fault length, W: Fault width, D: Slip amount

So, if M_W increases by 0.1, then M_0 will be $10^{0.15}$. In cases where no limit is set for either L, W, or D, if M_W increases by 0.1, then L, W, and D will all be $10^{0.05}$=1.12.

2) Method setting a limit only on fault width W (L model)

When W reaches the upper limit, if M_W increases by 0.1, then both L and D will be $10^{0.075}$=1.19.

3) Method setting a limit on mean slip amount D and fault width W (W model)

When D or W reaches the upper limit, if M_W increases by 0.1, then both L will be $10^{0.15}$=1.41.

These three relationships correspond to the scaling laws for the three stages presented by Irikura and Miyake (2011) and Murotani et al. (2015), which will be discussed later. According to the scaling laws for the three stages, as the fault length increases, there is a shift in the relationship from 1)->2)->3). 3) is a state where slip amount is saturated with respect to fault length and has been substantiated by a variety of data in recent years.

(2) Static stress drop

The extent of the release in stress before and after fault motion is referred to as stress drop. In particular, the difference in shear stress prior to fault motion beginning and after its completion is called static stress drop. Because static stress drop corresponds to slip amount per characteristic length that is targeted, the greater the static stress drops, the greater the slip amount per fault length and fault area is.

In accordance with the underlying assumptions, static stress drop is expressed according to various methods as shown below. In the configuration of fault parameters for a tsunami, the formula for circular faults put forth by Eshelby (1957) is often used unless the link in comparison to fault with is particularly long and massive.

$$\Delta\sigma=(7/16)\, M_0/(S/\pi)^{1.5}$$

where, $\Delta\sigma$: Stress drop, M_0: Seismic moment, S: Fault area.

This results in a relationship where mean slip amount D is proportional to $S^{0.5}$, and, of the relationships discussed in main volume 4.2.1.1 of the main volume, this corresponds to “1) Method where limits are not set on fault length L, fault width W or slip amount D”.

(3) Knowledge about stress drop and scaling laws as concerns interplate earthquakes

Murotani et al. (2013) analyzed fault models for interplate earthquakes around the world, and proposed the following scaling law for M_W =6.7 ~ 9.2 earthquakes.

$$S=1.34\times10^{-10}M_0^{2/3}$$

$$D=1.66\times10^{-7}M_0^{1/3}$$

$$S_a=2.81\times10^{-11}M_0^{2/3}=0.2S$$

where, S refers to the fault area (km^2), M_0 seismic moment (N·m), D mean slip amount (m), and

S_a the asperity area. When rigidity is calculated using the above formula, it is found to be μ=4.5×10^{10}(N/m^2), and stress drop according to the formula for circular fracture surface is $\Delta\sigma$=1.57(MPa). When standard deviation is taken into consideration for the parameters, stress drop is within a range of 1.57/1.91=0.82~1.57×1.91=3.00 (MPa), which is almost equivalent to the range of M_W ±0.2. Moreover, the range of 0.5×standard deviation for stress drop according to Murotani et al. (2013) is 1.57/1.91$^{0.5}$=1.14~1.57×1.91$^{0.5}$=2.17 (MPa), which is almost equivalent to the range of M_W ±0.1.

The Cabinet Office (2012) analyzed fault models for six case studies of trench-type megathrust earthquakes around the world and found that the value for mean stress drop was 1.2MPa, and the value adding standard deviation to the mean value was 2.2MPa, and the value subtracting standard deviation from the mean value was 0.7MPa. Moreover, when earthquakes smaller than M_W=8.0 are included, taking into account that the value of the mean stress drop for trench-type earthquakes is 3.0MPa and that 3.0MPa was used for the mean stress drop in the Central Disaster Management Council's review of tsunami associated with trench-type earthquakes, this has been applied to the principle fault for megathrust earthquakes in the Nankai Trough (areas that are deeper than the 10 km depth of the plate boundary surface).

This stress drop of 3.0 MPa has often been used in recent years as the stress drop for interplate earthquakes viewed conservatively. However, even when viewed from the relationship described by Murotani et al. (2013), it is the maximum stress drop within the scope of standard deviation for the parameters.

(4) Heterogeneity of slip amount distribution on fault planes

It is known that fault motion during an earthquake is not uniform and that there are significant localized areas of slip amount on fault surfaces. Somerville et al. (1999) statistically analyzed source parameters for 15 intraplate earthquakes that occurred between 1971 and 1995, and obtained the scaling laws shown in Table 2.1.2-1. This relationship has been used as the standard for heterogeneous models with regard to strong motion prediction. The heterogeneity of this fault motion also affects tsunami. Since Satake (1989), research has been conducted to find the heterogeneity of fault motion using inversion of the tsunami shape. With this method, the fault plane is subdivided into several small faults, and the calculation tsunami shape at the observation point when unit slip amount is given for each of these is regarded as Green's function. The least-square method is used to determine weighting (slip amount of each small fault) so that the superposition weighted to each Green's function conforms to the observed tsunami shape. Annaka et al. (1999) proposed a method that introduces run-up height records of tsunami into the evaluation function and reflects nonlinearity in shallow sea areas. In cases where the size of the

fault studied is large, a method has also been used where the time variation of displacement for each small fault is included in the inversion object (see for example Satake et al., 2013).

For the tsunami source models for probable maximum tsunamis that reflect heterogeneity in slip distribution, the characteristic models indicated in appendix volume 2.2 and 2.3 have often been used, but methods have also been proposed that represent slip distribution more randomly. These are based on the method for preparing random source models proposed by Mai and Beroza (2002), and, by deploying slip distribution and other elements on fault planes into wavenumber regions and setting the correlation distance, complex tsunami source models have been prepared that have patches for large slip with respect to large earthquakes. Goda et al. (2014) and Fukutani et al. (2015) applied this to tsunami having their source along the Japan Trench, and Yasuda et al. (2015) to tsunami associated with the Nankai Trough to assess the impact that uncertainty in slip distribution has on tsunami water levels.

Table 2.1.2-1 Scaling laws for heterogeneous source models (Somerville et al., 1999)

Rupture Area vs. Seismic Moment	$A(\mathrm{km}^2) = 2.23 \times 10^{-15} \times M_0^{2/3}(\mathrm{dyne \cdot cm})$
Average Slip vs. Seismic Moment	$D(\mathrm{cm}) = 1.56 \times 10^{-7} \times M_0^{1/3}(\mathrm{dyne \cdot cm})$
Combined Area of Asperities vs. Seismic Moment	$A_a(\mathrm{km}^2) = 5.00 \times 10^{-16} \times M_0^{2/3}(d\mathrm{yne \cdot cm})$
Area of Largest Asperity vs. Seismic Moment	$A_l(\mathrm{km}^2) = 3.64 \times 10^{-16} \times M_0^{2/3}(\mathrm{dyne \cdot cm})$
Radius of Largest Asperity vs. Seismic Moment	$r_l(\mathrm{km}) = 1.08 \times 10^{-8} \times M_0^{1/3}(\mathrm{dyne \cdot cm})$
Average Number of Asperities	2.6
Area of Fault Covered by Asperities	0.22
Average Asperity Slip Contrast	2.01
Hypocentral Distance to Center of Closest Asperity vs. Moment	$R_A(\mathrm{km}) = 1.35 \times 10^{-8} \times M_0^{1/3}(\mathrm{dyne \cdot cm})$
Slip Duration vs. Seismic Moment	$T_R(\mathrm{sec}) = 2.03 \times 10^{-9} \times M_0^{1/3}(\mathrm{dyne \cdot cm})$
Corner Spatial Wavenumber Along Strike	$\log K\, C_x(\mathrm{km}^{-1}) = 1.72 - 0.5M_w$
Corner Spatial Wavenumber Down Dip	$\log K\, C_y(\mathrm{km}^{-1}) = 1.93 - 0.5M_w$

*Units added to Somerville et al. (1999)

2.2. Earthquakes supposed along plate boundaries

2.2.1. Knowledge gained from 2011 Tohoku earthquake

Here, points are deduced and consolidated from knowledge about 2011 Tohoku earthquake that may serve as reference for methods of configuring probable maximum tsunami.

(1) Earthquake magnitude and fracture zone expansion

Of the regional divisions shown in Figure 2.2.1-1, significant slip was observed during 2011 Tohoku earthquake in regions along the trench in the southern area off the coast of Sanriku and along the trench off the coast of Boso from the northern area off the coast of Sanriku. The regions off the coast of Ibariki Prefecture, off the coast of Fukushima Prefecture, off the coast of Miyagi Prefecture and in the central area off the coast of Sanriku have also been regarded as source regions. The earthquake magnitude, which was M_W=9.0, and the breadth of the fracture zone (length of approximately 450 km and width of approximately 200 km) significantly exceeded what had previously been assumed. The following points have been cited as distinguishing features of this earthquake.

- Rupture occurred that extended across the typical interplate thrust earthquake region and tsunami earthquake region near trench axes.
- Rupture extended to the region near trench axis where it had not been known that tsunami earthquakes had occurred in the past.
- Significant deviation was seen in slip amount in both the strike direction and dip angle direction.

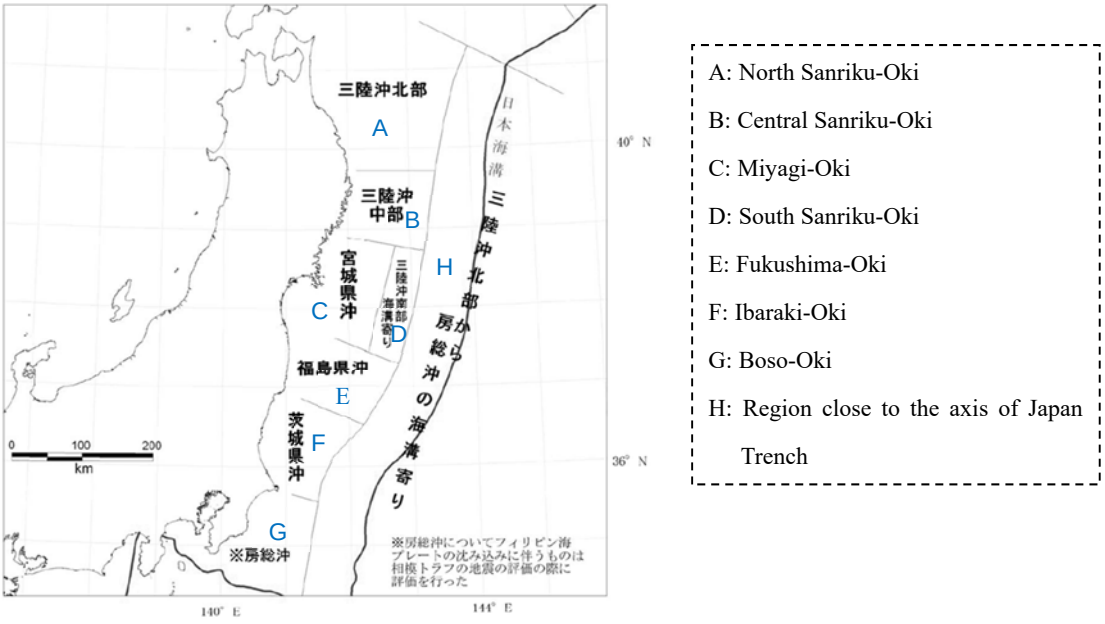

A: North Sanriku-Oki
B: Central Sanriku-Oki
C: Miyagi-Oki
D: South Sanriku-Oki
E: Fukushima-Oki
F: Ibaraki-Oki
G: Boso-Oki
H: Region close to the axis of Japan Trench

Figure 2.2.1-1 Segmentation of seismic activity area from Sanriku-Oki to Boso-Oki (HERP, 2011)

(2) Significant slip near trench axes

It has commonly been estimated, using multiple methods, that approximately a slip of 50 meters occurred near the trench axis. The model, which was prepared by the Geospatial

Information Authority of Japan and Japan Coast Guard (2011) that reproduces crustal movements is shown in Figure 2.2.1-2, and indicates that there is a maximum of approximately 56 meters of slip amount.

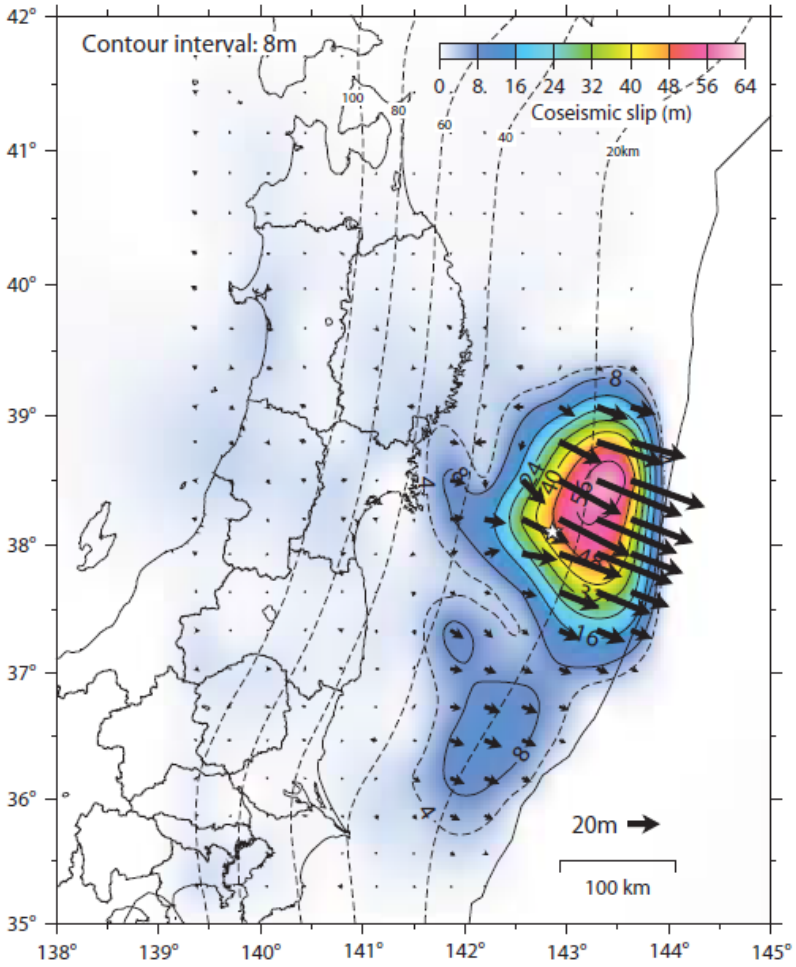

Data : F3 final solution of GNSS by GSI(fixed point is 'Fukue' in Kyushu) and seafloor geodetic observation (SGO) data by JCG

Period : From March 10th to March 12th, 2011.

The star shows the epicenter location of the main shock. The moment magnitude is 9.0 when rigidity modulus is assumed to be 40 GPa. The dashed lines show depth of the plate boundary. The vectors show slip distribution on the plate boundary.

Figure 2.2.1-2 Slip amount distribution of 2011 Tohoku earthquake to explain ground and seafloor crustal movements (Geospatial Information Authority of Japan and Japan Coast Guard, 2011)

(3) Analysis of cumulative stress

It has been pointed out that accumulated strain was released over a broad range across the region where 2011 Tohoku earthquake initiated. Also, it has been pointed out that near trench axes where coupling had conventionally been regarded as very small, there is the possibility of stress accumulation and coupling to a certain extent.

Hasegawa et al. (2012) stated that the strain, which had accumulated across a range extending from the central area off the coast of Sanriku to off the coast of Fukushima, almost completely released due to the change in the stress state before and after 2011 Tohoku earthquake occurred. The Japan Agency for Marine-Earth Science and Technology (2013), based on borehole surveys conducted by the Agency's Deep-sea Drilling Vessel Chikyu, found that the stress state in the source region of the Pacific coast of the Tohoku region changed from a compressed state to an expanded one.

(4) Data acquired prior to the earthquake and response to phenomena during the earthquake

According to Zhao et al. (2011), the large slip area during 2011 Tohoku earthquake corresponded to the high velocity region along the plate boundary. Also, the high velocity region formed asperity where there was significant coupling between plates corresponding to subduction of seamounts and other features, and, in this region, the core of the megathrust earthquake formed due to the accumulation of stress over a long period of time.

According to Nishimura (2012b), the region of significant slip during the earthquake generally corresponds to places where there was considerable slip deficit as estimated based on GPS data prior to the earthquake. However, the distribution of slip deficit changed over time due to the impact of postseismic deformation and other effects. Koketsu et al. (2012) stated that regions where there was significant back slip were related to the cycle of megathrust earthquakes.

Based on such knowledge, it is possible that regions where significant stress dissipates during an earthquake may be related using information obtained in between earthquake strikes.

(5) Time variation of the rupture

Using tsunami shape inversion, it has been found that an interplate earthquake (M_W=8.8) such as that of the Jogan earthquake model serves as a trigger for tsunami earthquakes such as that experienced in 1896 (Satake et al., 2012). According to Satake et al. (2013), slip up to a maximum of 25 meters occurred within 2.5 minutes after fracture initiated in the depths of the plate boundary off the coast of Miyagi Prefecture. Also, near trench axes, slip up to a maximum of 69 meters occurred 3 to 4 minutes after fracture initiated. Moreover, near the trench axis off the coast of Sanriku, slip measuring 10 meters occurred around 4 minutes after fracture initiated. Whether or not consideration is given to such time delays results in differences in tsunami shape.

With such a megathrust earthquake, the fracture zone is broad, so consideration needs to be given to the development of fracture over time in order to reproduce phenomena.

For earthquakes off the Pacific coast of the Tohoku region which have significant slip amount, tsunami inversion has provided solutions of several minutes for rise time.

Based on the earthquake ground motion data, it has been estimated rise time has been around 30 seconds, which is longer than that for an ordinary M7 class earthquake (several seconds). The rise times estimated using tsunami and earthquake inversion are given below.

- Tsunami (solution for individual small faults)
  - Satake et al. (2013): 30 ~ 150 seconds
    *Based on inversion where the time windows are 30sec × 5.
  - Japan Nuclear Energy Safety Organization (2011): 60 ~ 300 seconds
- Earthquake ground motion
  - Inversion of high frequency GPS data: Rise time in regions where there is 40~60 m of slip amount is 30~40 seconds, and there is not much correlation with fracture propagation velocity (Yue and Lay, 2011).
  - Reproduction of earthquake ground motion: Rise time of 20 ~ 30 seconds (Kawabe and Kamae, 2012)

In assessments of strong motion, it is often assumed that rise time $\simeq$ fault width/(fracture propagation velocity × 2) (see for example the Headquarters for Earthquake Research Promotion, 2009). When based on this assumption, then:

If rupture propagation velocity is 2.8km/s and fault width is 50km, then rise time will be 8.9 seconds

If rupture propagation velocity is 2.8km/s and fault width is 100km, then rise time will be 17.9 seconds.

From this, it may be seen that there are cases where the rise time found based on the simple relationship between rupture propagation velocity and fault width and the actual rise time deviate.

(6) Contribution of horizontal crustal movement to tsunami generation

Satake et al. (2013) stated that, because the slope of sea bottom was steep around the trench axis, the wave making effect resulting from horizontal crustal movement affects tsunami amplitude, and the wave making effect resulting from horizontal crustal movement increases the maximum amplitude of tsunami by 30 to 60%, and approximately 20 to 40% of this maximum amplitude was a contribution resulting from horizontal crustal movement. Accordingly, near trenches where the slope of sea bottom is large and the dip angle of the fault is small, the wave generation effect resulting from horizontal crustal movement may not be disregarded. The wave

generation effect produced by horizontal crustal movement may be considered using the method proposed by Tanioka and Satake (1996) (see Section 6.1.2.2 of the main volume).

2.2.2. Region-specific features of tsunami sources (sea areas associated with subduction of the Pacific plate)

(1) Sea area along the Kuril-Kamchatka Trench

Figure 2.2.2-1 by the Central Disaster Management Council (2006) shows the tsunami source region in the northern area extending from the Kuril-Kamchatka Trench to the Japan Trench. In the sea area along the Kuril-Kamchatka Trench, earthquakes occur continuously and uniformly along the trench as shown in Figure 2.2.2-2, and the segment divisions are comparatively distinct, and earthquakes have occurred at relatively short intervals. Based on tsunami inversion, it has been found that the Kuril earthquake that occurred in 1918 corresponds to the previous earthquake in 2006 (Ministry of Education, Culture, Sports, Science and Technology's Research and Development Bureau and the Hokkaido University Graduate School of Science, 2012).

Most of the past large earthquakes have been interplate earthquakes, but reverse fault earthquakes within plates have also occurred such as the 1994 earthquake off the eastern side of Hokkaido.

In addition, the Central Disaster Management Council (2006) has confirmed, based on the results of tsunami deposit surveys from the Nemuro to Tokachi regions in Hokkaido, that massive tsunamis have occurred dozens of times over the past approximately 6,500 years. The earthquakes corresponding to tsunami deposits at intervals of approximately 500 years are called "500-year interval earthquakes", and are believed to be interplate earthquakes that have occurred repeatedly across the region extending from off the coast of Nemuro to off the coast of Tokachi, with the most recent occurrence in the early 17th century. With regard to tsunami source models for re-creating the area flooded, the Central Disaster Management Council (2006) assessed the moment magnitude at M_W=8.6, and Ioki and Tanioka (2016) used additional data to assess the moment magnitude at M_W=8.8. According to the slip deficit distribution which the Geospatial Information Authority of Japan (2012) estimated using GNSS data, relatively strong coupling has been observed off the coast of both Kushiro and Nemuro.

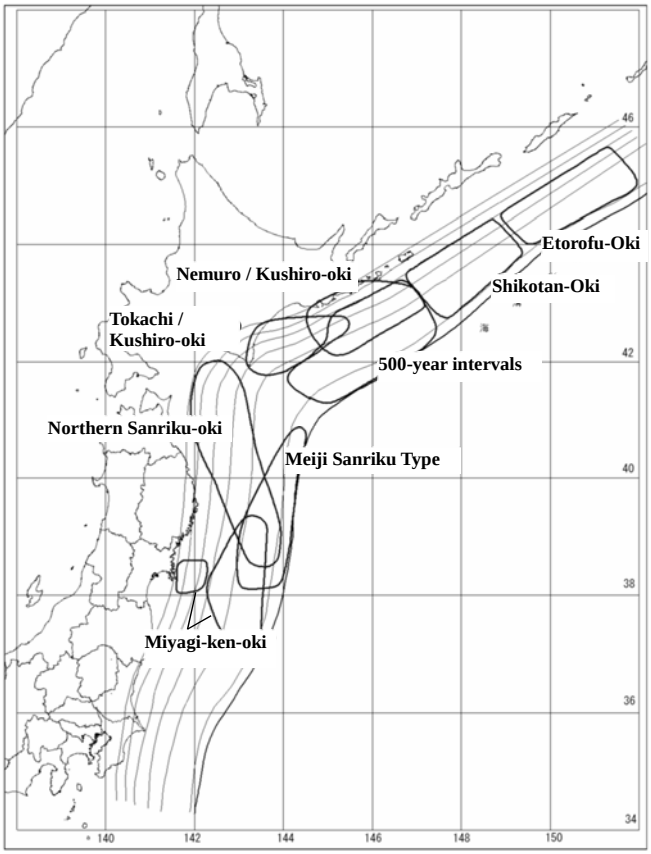

Figure 2.2.2-1 Map of tsunamigenic zones along the Kuril Trench - the northern area along the Japan Trench (Central Disaster Management Council, 2006)

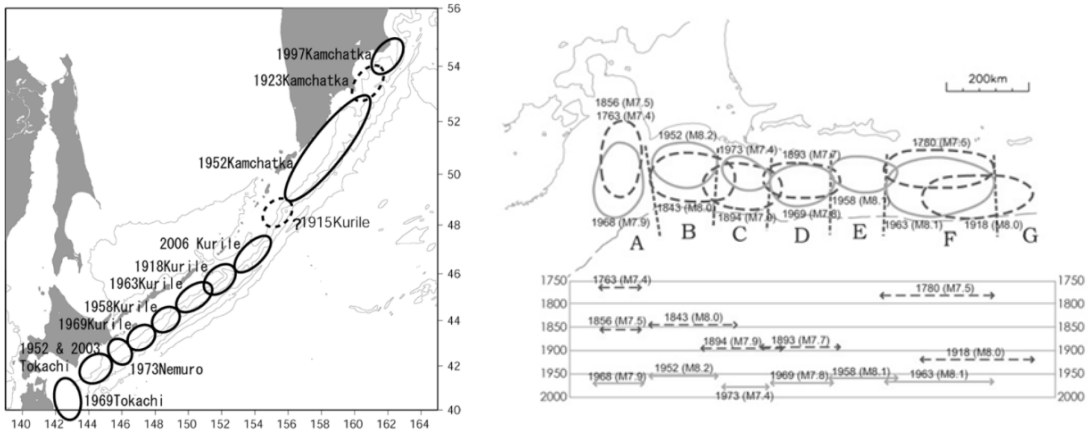

Figure 2.2.2-2 Source regions of the large earthquakes along the Kuril Trench (HERP, 2004)

According to DeMets (1992) the area from the Bussol Strait to the southeastern part of Hokkaido forms a forearc sliver and is believed to move in a rotating motion in comparison to the surrounding area. Both Liu et al. (2013) and the Ministry of Education, Culture, Sports, Science and Technology (2008) suggested, based on the relationship between regions where earthquakes have occurred in the past and a three-dimensional crustal heterogeneous structure of the area where the island arcs meet of the Japan Trench and the Kuril-Kamchatka Trench produced using seismic wave tomography, that the low velocity region corresponding to spallation of the lower crust in the Hidaka collision zone serves as a fracture barrier. Kasahara et al. (1997) confirmed that, in the region off the coast of the southern Kuril Islands, there are tectonic lines known as the Nosappu fracture zone and the Iturup fracture zone, and that there is a distinguishing feature along these boundaries as the geomagnetic linear sequence and normal fault systems differ. Also, because the sediment thickness differs on both sides and discontinuity in the underground structures is seen in the Nosappu fracture zone, these are regarded as factors resulting in the structure of this ancient oceanic plate dominating the current seismicity barrier.

(2) Region close to the axis of Japan Trench

In the vicinity of the Japan Trench, 2011 Tohoku earthquake occurred as well as tsunami earthquakes, such as the 1896 Meiji Sanriku tsunami, and intraplate normal fault earthquakes, such as the 1933 Showa Sanriku tsunami. Aida (1977) proposed a normal fault earthquake model for the 1611 Keicho Sanriku tsunami, but Tsuji (1994), Watanabe (1998) and the Headquarters for Earthquake Research Promotion (2011) indicated the possibility that this was a tsunami earthquake.

Off the coast of Miyagi Prefecture in the southern area along the Japan Trench, there are earthquakes that have occurred in areas very close to the land (e.g. the 1978 earthquake off the coast of Miyagi Prefecture) and earthquakes that have occurred offshore (e.g. the 1897 earthquake off the coast of Miyagi Prefecture).

A series of earthquakes that occurred off the eastern side (off the coast of Shioya) of Fukushima Prefecture in 1938 are the only large earthquakes recorded off the coast of Fukushima Prefecture. In these earthquakes, there were reverse fault earthquakes as well as normal fault earthquakes. Off the coast of the Boso Peninsula, the 1677 earthquake tsunami occurred, which is believed to have been a tsunami earthquake in the vicinity of the Japan Trench.

Ye et al. (2012) reported that, in the depths along the plate boundary in the central area off the coast of Sanriku, there is a low seismicity region where strain is released by aseismic slip (SLSR: Sanriku-oki low seismicity region), and that the SLSR corresponds to the northern limit of the large slip of 2011 Tohoku earthquake. Also, Uchida and Matsuzawa (2011) showed that coupling was weak in the depths of the plate boundary in the central area off the coast of Sanriku

based on an analysis of coupling rates in the source region of 2011 Tohoku earthquake using data on small repetitive earthquakes.

Off the coast of the Boso Peninsula, from the vicinity of Mito into a southeasterly direction, the Northeast edge of the Philippine Plate abuts the Pacific Plate. According to the Japan Agency for Marine-Earth Science and Technology (2011) and Shinohara et al. (2011), propagation of the fracture of 2011 Tohoku earthquake to the south stopped in the region where the plate on the subducting Pacific Plate changes from the North American Plate to the Philippine Plate.

Based on a numerical simulation of the relationship between the extent of flooding onto the Sendai and Ishinomaki plains and the extent of flooding estimated from surveys of tsunami deposits, Satake et al. (2013) stated that there is a high possibility that the 869 Jogan earthquake was not solely a tsunami earthquake. The Headquarters for Earthquake Research Promotion (2011) found that Jogan earthquakes have recurrence intervals of approximately 600 years, including the earthquakes similar to 2011 Tohoku earthquake.

Namegaya and Satake (2012) estimated the moment magnitude of the Jogan earthquake at 8.7 if the ratio between the tsunami inundation distance and the tsunami deposit distribution, which were obtained from 2011 Tohoku earthquake, were factored in, and the inundation range during the Jogan earthquake was broader than the distribution range of tsunami deposits. Sugawara et al. (2013) compared the area of the Sendai plain flooded by the 869 tsunami and 2011 Tohoku tsunami, and showed that both overlapped for the most part.

(3) Sea area along the Izu-Ogasawara Trench

In the area ranging from the Izu-Ogasawara Trench to the Mariana Trench, no earthquakes have occurred which have been accompanied by noteworthy tsunami. Near the point where there is a triple junction of plates, an earthquake off the coast of the Boso Peninsula occurred in 1953, and, south of there, an earthquake in the waters close to Hachijo Island occurred in 1972. The earthquake that occurred off the coast of Saipan in 1990 (M_W=7.4) and the one in the waters near Chichijima (Peel Island) in 2010 (M_W=7.4) were both intraplate normal fault earthquakes. A classification of interaction between plates worked out by Abe (1978) placed the sea area ranging from Izu to the Mariana trench as a stable type in which few earthquakes occur.

Okal et al. (2013) used ISC seismic time series data and WWSSN data to determine the sources and mechanisms for the period during which there are no CMT catalogs (which became available after 1976). Based on this, it was estimated that, an M8 inter-plate thrust fault earthquake has occurred once in every 320 years in this sea area.

Fujioka et al. (2002) indicated the geological regional division of the Izu-Ogasawara Trench partitioned according to tectonic lines.

2.2.3. Region-specific features of tsunami sources (sea area associated with subduction of the Philippine Plate)

(1) Sea area along the Sagami Trough

In the northwestern part of Sagami Bay, relatively large tsunamis have occurred in comparison to earthquake magnitudes. The Central Disaster Management Council (2013) found that M8 class earthquakes occurring on the upper surface of the Philippine Plate along the Sagami Trough are believed to have occurred every 200 to 400 years, and, of these, earthquakes equivalent to or greater than the 1703 Genroku earthquake, which caused significant upheaval on the edge of the Boso Peninsula, have occurred at intervals between 2,000 and 3,000 years.

The Central Disaster Management Council (2013) conducted an inversion analysis using crustal movements and tsunami heights from the 1703 Genroku earthquake and the 1923 Kanto earthquake to create a fault model that takes into account slip heterogeneity. As for earthquake magnitude, the 1703 Genroku earthquake was M_W=8.5 and the 1923 Kanto earthquake M_W=8.2.

(2) Sea area along the Nankai Trough

In the sea area along the Nankai Trough, large earthquakes have repeatedly occurred, and the average recurrence interval has been between 120 and 160 years. The history of these earthquake occurrences may be explained using a time-predictable model.

In the sea area along the Nankai Trough, the division of fault segments is clear. Although combinations of these segments have changed depending upon the earthquake, they have occurred in the Tonankai and Nankaido during almost the same period of time. The pattern of occurrence has been that Tonankai occurs first, then Nankaido occurs.

The Headquarters for Earthquake Research Promotion (2013) showed that the pattern with which these anticipated earthquakes have occurred is as shown in Figure 2.2.3-1. The Cabinet Office (2012) applied a fracture propagation velocity of 2.5 km/s and a rise time of 60 seconds to a model for megathrust earthquakes along the Nankai Trough.

	Depth	Estimated rupture area						M_W based on a scaling law
		Z	A	B	C	D	E	
Patterns in which the Tokai and Nankai regions interlock	Shallow							8.8
	Medium	■	■	■	■	■	■	
	Deep							
	Shallow							9.0*1
	Medium	■	■	■	■	■	■	
	Deep	■	■	■	■	■	■	
	Shallow	■	■	■	■	■	■	9.0
	Medium	■	■	■	■	■	■	
	Deep							
	Shallow	■	■	■	■	■	■	9.1*2
	Medium	■	■	■	■	■	■	
	Deep	■	■	■	■	■	■	
	Shallow							8.7
	Medium		■	■	■	■	■	
	Deep							
	Shallow		■	■	■	■	■	8.9
	Medium		■	■	■	■	■	
	Deep							
	Shallow							8.8
	Medium	■	■	■	■	■		
	Deep							
	Shallow	■	■	■	■	■		9.0
	Medium	■	■	■	■	■		
	Deep							
	Shallow							8.7
	Medium		■	■	■	■		
	Deep							
	Shallow		■	■	■	■		8.9
	Medium		■	■	■	■		
	Deep							
	Shallow		■	■	■	■		8.4
	Medium							
	Deep							
Patterns in which two earthquakes in the Tokai / Nankai area occur with time lag	Shallow							8.7,8.3
	Medium	■	■	■	■	■	■	
	Deep							
	Shallow							8.5,8.3
	Medium		■	■	■	■	■	
	Deep							
	Shallow							8.7,8.2
	Medium	■	■	■	■	■		
	Deep							
	Shallow							8.5,8.2
	Medium		■	■	■	■		
	Deep							

*1 : Cabinet Office (2011) Strong ground motion model
*2 : Cabinet Office (2011) Tsunami simulation model

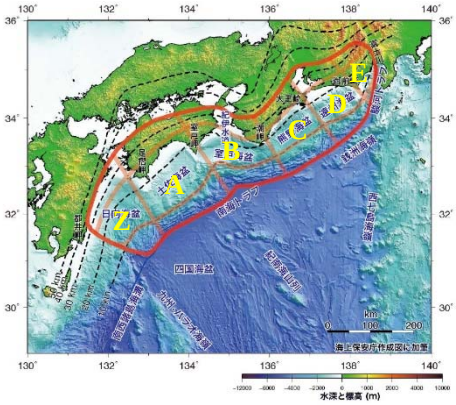

Figure 2.2.3-1. Patterns of supposed earthquakes along the Nankai Trough (HERP, 2013)

(3) Sea area along the Ryukyu Trench

Large earthquakes have repeatedly occurred in the Sea of Hyuganada. Moreover, the distribution of sources of past tsunamis in the area around Nansei Islands to the south is shown in Figure 2.2.3-2. Kato (1987) reported that the 1771 Yaeyama tsunami caused the significant run-up height of more than 25 meters on Ishigaki Island. As for the cause, Matsumoto and Kimura (1993) pointed out the existence of large depressed geological formations, which were found based upon precise geological surveys and sonic profiling surveys, and indicated the possibility of submarine landslide occurring due to an earthquake. Nakamura (2009) reported that this could be explained in terms of a reverse fault earthquake where the fault width was less than 50 km, and stated that the event was a tsunami earthquake with M_W=8.0.

According to Goto et al. (2010) as well as Goto and Shimabukuro (2012), there are tsunami rocks and ancient documents which contains records of tsunami in the southern area. On the other hand, currently, no records have been discovered with respect to the northern to central areas, which range from the Okinawa Islands to the Amami Islands. Taking such data into account, the authors reported that there is a distinctive difference between both areas.

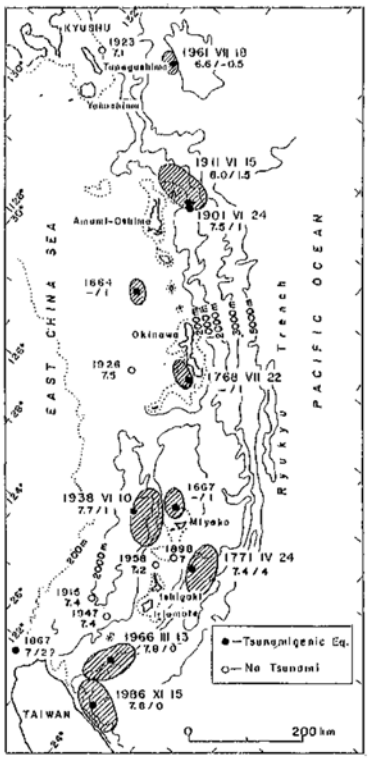

Figure 2.2.3-2 Source distribution of past tsunamis around Nansei Islands occurred after 1664 (Hatori, 1988)

*Numbers beside the tsunami source regions are the occurrence date, M_{JMA}, and m of Imamura and Iida scale.

In the northern area of the Ryukyu Trench, there is a relative displacement where the upper layer moves toward the sea area, and it has been suggested that the degree of coupling is low compared to that of the sea area along the Nankai Trough. Yamamoto et al. (2013) reported that the Kyushu-Palau ridge (KPR) corresponds to an area of distinctly low velocity in the depths of the Philippine Plate. The 1968 Sea of Hyuganada earthquake and the 1707 Hoei earthquake did not extend to the KPR, so it is possible that the KPR forms a barrier to fracture propagation during earthquakes. As for this interpretation, Wallace et al. (2012) stated that, for a megathrust earthquake to occur, it is necessary that the range of the smooth weak boundary surface be broad,

but a geographical configuration where there are large undulations such as seamounts would prevent such a formation.

According to Yokose et al. (2010), the Ryukyu Trench is divided into northern, central and southern areas along the Tokara Channel and Miyako Depression. Based upon an analysis of GPS data, the northern, central and southern areas move laterally with respect to each other. Wu et al. (2010) used stress inversion to find the distribution of crustal stress in the area around the Ryukyu Trench. As a result, they reported that the stress state undergoes distinct changes along the Tokara Channel, the reason for which is believed to be subducting of the thick crust of the Amami submarine plateau.

2.2.4. Region-specific features of tsunami sources (far-field tsunamis)

(1) From offshore Chile to offshore Peru

Large earthquakes have occurred in the region ranging from offshore Chile to offshore Peru at intervals of several decades or more in each demarcated region. The April 2014 earthquake (M_W=8.2) occurred at a location covering a seismic gap, which is called the Iquique Gap. At 7:54 on September 17, 2015 (Japan Standard Time), an earthquake, having its source off the coast of central Chile, occurred (Illapel earthquake, M_W=8.3), and the accompanying tsunami also reached the coast of Japan. According to the Japan Meteorological Agency (2015), the maximum height of the tsunami recorded was 0.8 meters at Kuji Bay, Japan.

In southern Chile, earthquakes have occurred at intervals of about 130 years. Of these, the 1960 Chile earthquake tsunami was the largest earthquake ever recorded (M_W=9.5). Cisternas et al. (2006) and Shishikura (2013) stated that the 1575 earthquake was the only comparable event that occurred prior to 1960, and reported that, over the past 2,000 years, earthquakes equivalent to the one which occurred in 1960 have occurred on average at intervals of 300 years.

Melnick et al. (2009) divided the source regions of past earthquakes systematically at promontory points, and reported that petrological discontinuity may act as a barrier to fractures. Matsumoto et al. (2010) reported that, although many earthquakes have occurred along active transform faults and sea trenches north of 46° S, there have been very few earthquakes that have occurred in the vicinity of 46° 30’S, suggesting a connection at the point at the triple junction of plates off the coast of Chile where earthquakes have not occurred and ridges are subducting. In addition, they reported that there is a gap on land in the volcanic zone along the vicinity of 46° 30’S, which is the point of the triple junction of plates off the coast of Chile.

(2) North American Cascadia subduction zone

Based on the reproducibility of tsunami height, Satake and Wang (1998) estimated that the slip amount during the 1700 North American Cascadia subduction zone earthquake was approximately 7 meters. According to Satake et al. (1996), the entire segment of approximately 900 km ruptured during the 1700 earthquake. The current seismic gap as presented by Hatori (1998) is smaller than the 1700 rupture zone.

Scholz (2014) divided the area into four fracture patterns based on research conducted by Goldfinger et al. (2012) on the seismicity of the Cascadia subduction zone through the Holocene, and proposed fault models for several rupture patterns.

(3) Alaska ~ Aleutian ~ Kamchatka

The major tsunamis that have occurred from Alaska through the Aleutian to the Kamchatka region are shown in Table 2.2.4-1.

Table 2.2.4-1 Source regions of major tsunamis (M_W=8.5 or greater) occurred in North Pacific and maximum tsunami height in Japan

Source Region	Year	Magnitude	Tsunami height in Japan
Alaska	1964	M_W=9.2, M_t=9.1	0.75m: Ofunato, Iwate Pref.
Aleutian	1957	M_W=8.6, M_t=9.0	0.48m: Kushimoto, Wakayama Pref.
	1965	M_W=8.7, M_t=8.6	0.55m: Kushimoto, Wakayama Pref. 1.06m (double amplitude): Hiroo, Hokkaido
Kamchatka	1923 (Feb.)	M_W=8.6, M_t=8.8	0.5m: Kushimoto, Wakayama Pref.
	1952	M_W=9.0, M_t=9.0	3.0m: Miyako and Kamaishi, Iwate Pref. etc.

* M_W: Abe (1989), MacInnes et al. (2010), Tanioka (2013), M_t: Based on Abe (1989). Tsunami height: Hatori (1965), Watanabe (1998), Tsuji et al. (1998)

In addition, the 1946 Aleutian earthquake (M_S=7.4 and M_W=8.2) was reported to be a typical tsunami earthquake. Also, during this tsunami, the earthquake caused submarine landslide, giving rise to a large tsunami having a local focus along the coastline nearby.

Based on estimates of subsidence during earthquake using samples of peat and peat-silt couplets taken on land, Shennan et al. (2007) reported that, with the exception of 1964, megathrust earthquakes have occurred at intervals of approximately 600 years (intervals of a minimum of 180 years when estimation error is taken into account) over the past 3,800 years. Also, they reported that the largest interval was approximately 1,000 years between 1964 and the previous event.

The largest earthquake off the coast of Kamchatka was the 1952 earthquake, and Johnson and Satake (1999) have proposed a tsunami source model based on tsunami inversion.

Tanioka (2013) compiled the results of surveys and other investigations on tsunami deposits and reported that tsunamis exceeding 5 meters along the coastline have occurred once every 100 to 400 years.

(4) Off the coast of Sumatra to the Andaman Sea

Rajendran (2013) reported, based upon surveys of tsunami deposits and other investigations, that megathrust earthquakes have repeatedly occurred at intervals of approximate 500 years in the subduction zone between Sumatra and Andaman. Tanioka et al. (2006) presented a tsunami source model (M_W=9.2) for 2004 earthquake off the island of Sumatra, which was the largest of these. The mean fracture propagation velocity is 1.7 km/s.

Tang et al. (2013) reported, based on an analysis using the P-wave velocity structure, that there is a thick oceanic crust in the area of the boundary along the region where the 2004 and 2005 earthquakes occurred, and that it is possible this acted as a barrier to fracture propagation.

According to Koyama et al. (2012), the Indo-Australian Plate runs diagonally into the Burma Microplate, and the Burma Microplate runs into the Sunda Microplate, which is located to the east, in a north-northeasterly direction at a rate of approximately 37 mm/year. The Andaman Ridge is expanding in a north-northwest direction, and the area between the Burma-Nicobar Trench and the Andaman Ridge as well as two transform faults, the large Sumatra fault and the Sagaing fault which are considered an extension of this, are heading north as the Burma Microplate. Curray (2005) reported that the Andaman Sea is an extensible back-arc basin that began to open up during the Cenozoic era resulting from an expansion that progressed in a vertical direction to the trench due to lateral displacement of a sliver (Burma Plate) formed during the Eocene epoch.

(5) Southeast Asia ~ Oceania

The heights of all of the tsunamis along the Japanese coast that have occurred in the past in the sea area between Southeast Asia and Oceania have been low. The largest earthquake magnitude in the past 100 years for the same area is either the M_W=8.5 (M_S=8.2), which occurred in Indonesia's Banda Sea in 1938, or the M_S=8.3 earthquake, which occurred off the southeast coast of Mindanao island in the Philippines in 1924.

Bautista and Oike (2000) estimated, based on records of earthquakes that have remained at churches in the Philippines, the epicenter and M_S distribution of 485 earthquakes between 1608 and 1895. Of these, the largest was M_S8.0. Accordingly, in the area around the Philippines, the magnitude of earthquakes over the past 400 years or so has been M_W=8.5 (M_S=8.3) at the largest.

In other words, during a period that is almost equivalent to the period for which highly reliable historical data is available with respect to the area around Japan, the greatest magnitude of an earthquake in the past around the Philippines has been M_W =8.5.

Kawata et al. (1998) presented the results of calculations of tsunami assumed to occur in the subduction zone of the Pacific Rim. Even in a case where a M_W =9.0 earthquake is assumed in the sea area of southeast Asia, the water level along the coast of Japan will not rise above the water height resulting from a Chile tsunami anticipated off the coast of Chile.

According to knowledge about the seismicity of the New Guinea Trench presented by Okal (1999), earthquakes have continuously occurred in an approximately 550-kilometer section ranging from 134.75°E to 139.75°E. Here, the 1996 Irian Jaya (Biak) earthquake ruptured a segment extending approximately 300 km.

2.2.5. Case studies of standard fault model configuration methods, etc.

(1) Case assuming an interplate megathrust earthquake

A case study is presented for configuration of a standard fault model in a case where a M_W=9 class interplate earthquake is assumed in the sea area along the Nankai Trough and the area ranging from the Kuril-Kamchatka Trench to the Japan Trench.

The methods presented by the Cabinet Office (2012) and by Sugino et al. (2014) are typical of the methods for creating a characterized fault model for megathrust earthquakes along plate boundary. Overviews of both methods are given in Figure 2.2.5-1.

The approach to parameter configuration has been compiled into a flowchart and shown in Figure 2.2.5-2.

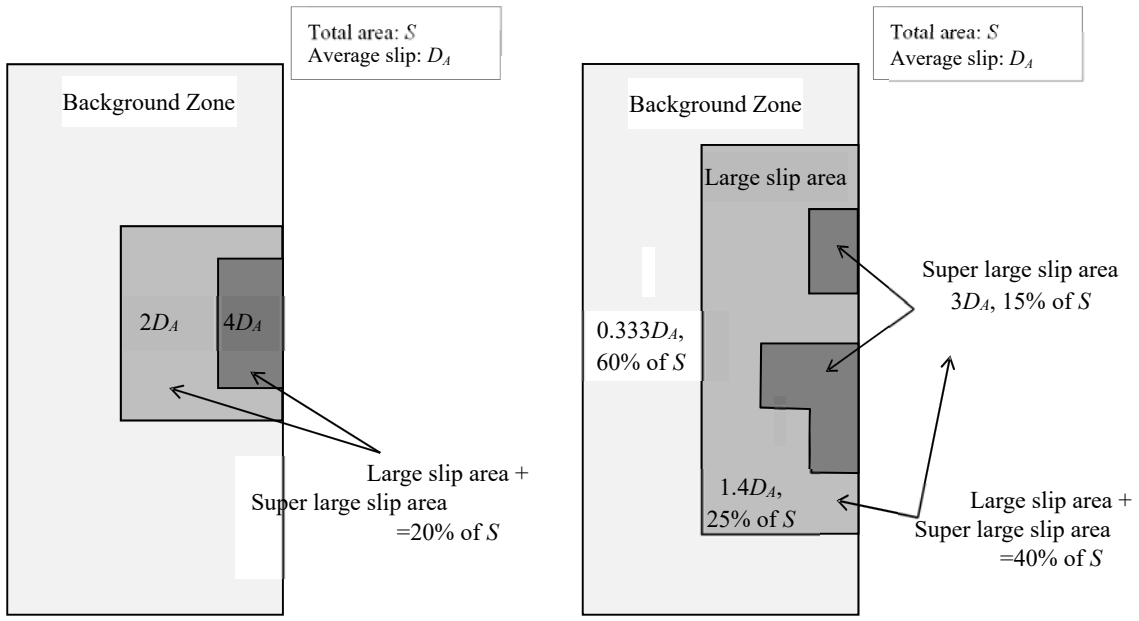

(1) Cabinet Office (2012) (2) Sugino et al. (2014) (for M_W=8.9 or larger)

Figure 2.2.5-1 Fault modeling methods by the Cabinet Office (2012) and by Sugino et al. (2014)

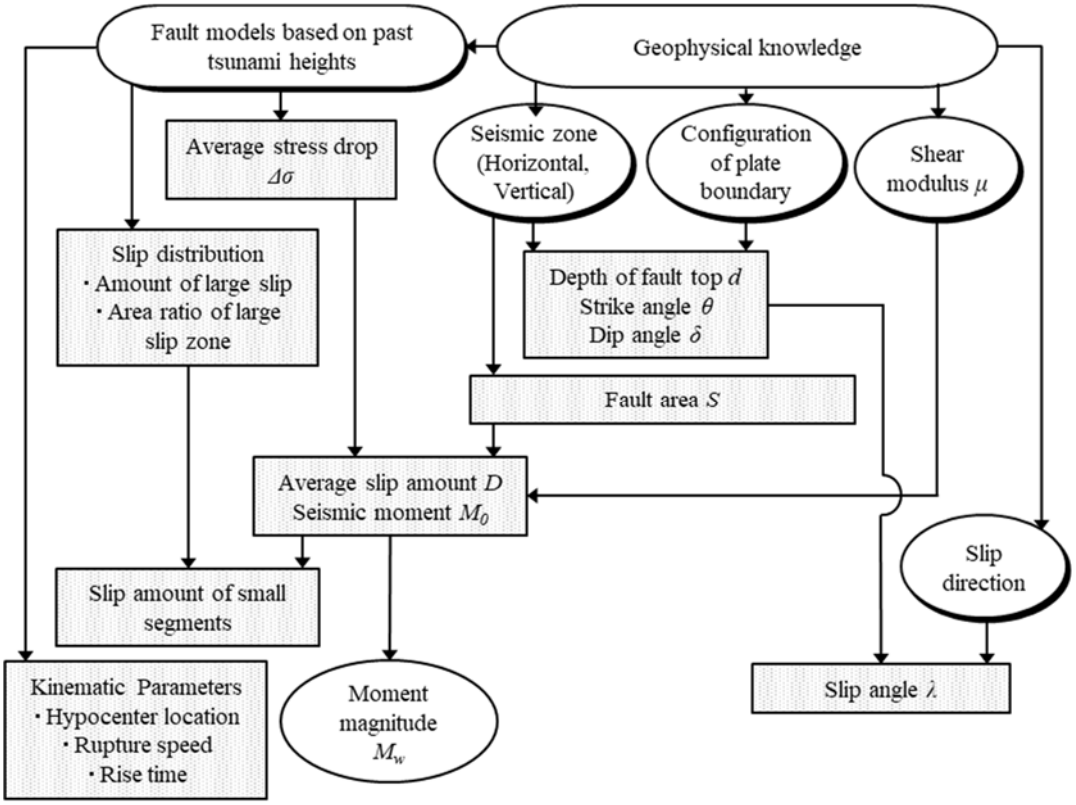

Figure 2.2.5-2 Parameter setting flowchart when assuming interplate megathrust earthquake

* The rectangles represent the fault parameters necessary for tsunami calculation, and the shaded items represent the items necessary before parameter setting.

(2) Case where configuration of each specific sea area is based upon fault models of past tsunami

The Japan Society of Civil Engineers (2002) presented a method for configuring standard fault models using fault models based on past tsunami heights. An example for the sea area along the Japan Trench and the Kuril-Kamchatka Trench (southern area) is shown below.

A flowchart for the configuration of the fault parameters is shown in Figure 2.2.5-3. Based on fault models that best explain the run-up height records of past tsunamis which are shown in Figure 2.2.5-4 and Table 2.2.5-1, consideration is given to maximum M_W in the past as indicated in Figure 2.2.5-5 to apply the most appropriate scaling law that reflects the earthquake initiation pattern.

Of the sea area divisions in Figure 2.2.5-5, 3 and 8 are sea areas where tsunami earthquakes are assumed and 4 is a sea area where an intraplate normal fault earthquake is assumed, and the others correspond to typical interplate earthquakes.

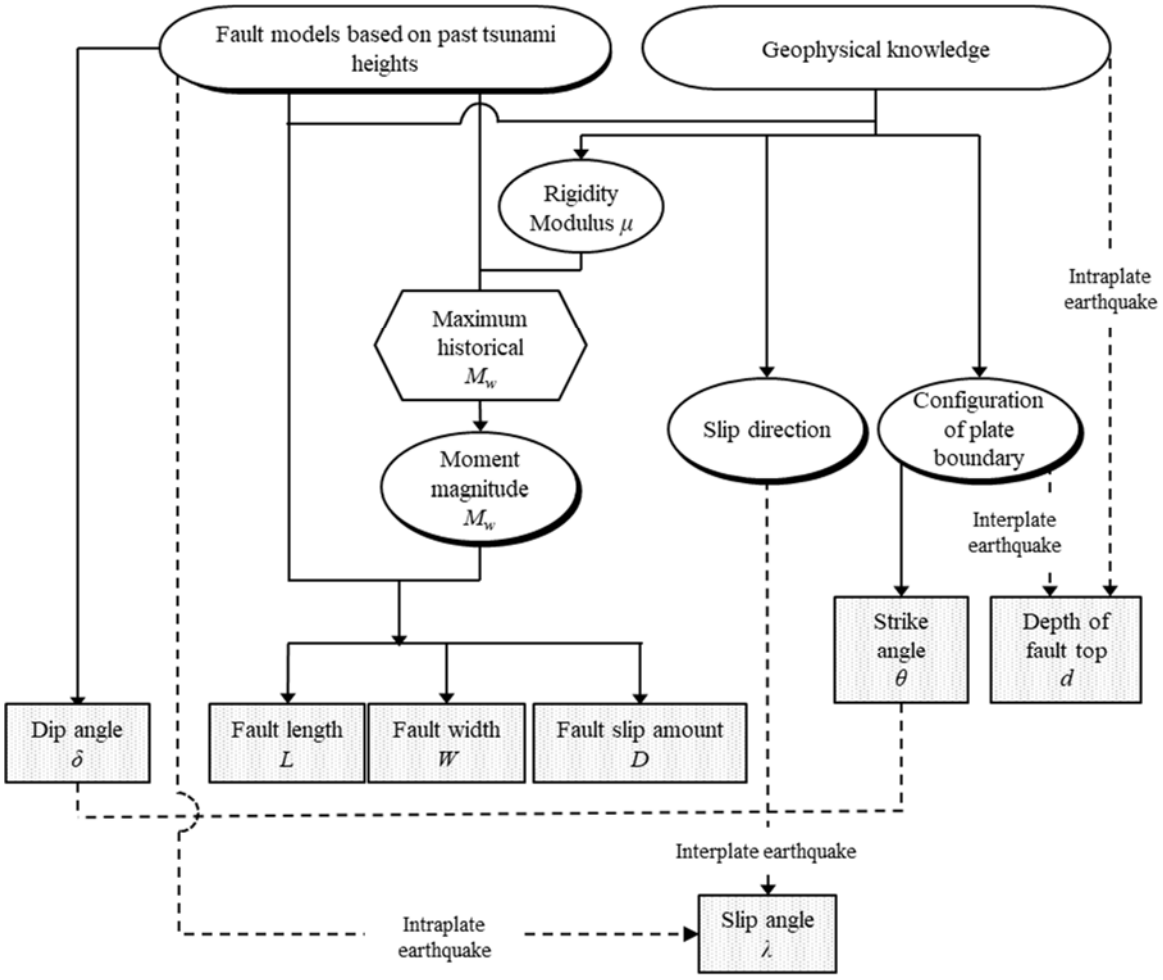

Figure 2.2.5-3 Parameter setting flowchart for standard fault model along the Japan Trench and the Kuril-Kamchatka Trench (southern area)

* Different flows between interplate and intraplate earthquakes are indicated by dashed lines. The rectangles represent the fault parameters necessary for tsunami calculation, and the shaded items represent the items necessary before parameter setting.

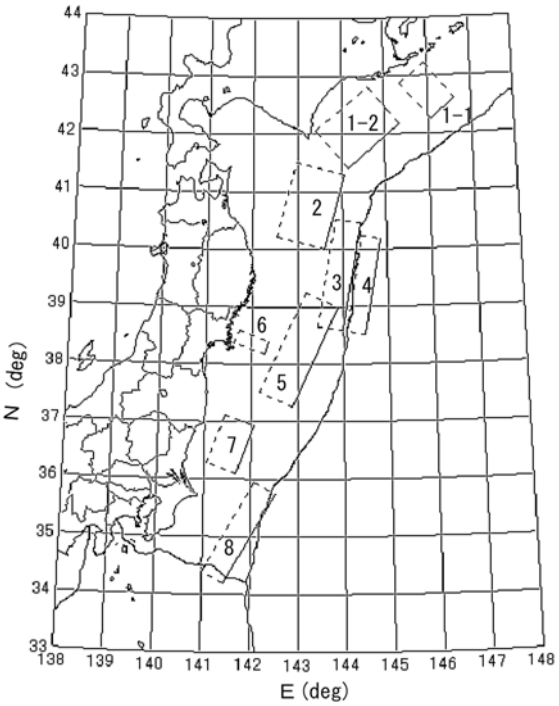

Figure 2.2.5-4 Position of fault models based on past tsunami heights

*The figure was drawn with "SEIS-PC for Windows95" by Ishikawa and Nakamura (1997)

Table 2.2.5-1 Fault parameters of fault models based on past tsunami heights

No.	Length L (km)	Width W (km)	Slip amount D (m)	Dip angle δ (deg.)	Slip angle λ (deg.)	rigidity μ $\times 10^{10}$ (N/m^2)	M_0 $\times 10^{20}$ (N·m)	M_W	past tsunami
1-1	60	100	2.2	27	115	5.0	6.6	7.81	1973
1-2	130	100	3.5	20	115	5.0	22.8	8.17	1952
2	150	100	6.0	20	80	5.0	45.0	8.37	1968
3	210	50	9.7	20	75	3.5	35.6	8.30	1896
4	185	50	6.6	45	270	7.0	42.7	8.354	1933
5	210	70	4.0	15	85	5.0	29.4	8.246	1793
6	26	65	2.0	20	85	7.0	2.4	7.52	1978
7	100	60	2.3	10	85	5.0	6.9	7.83	1938
8	200	50	6.5	20	95	3.5	22.8	8.17	1677

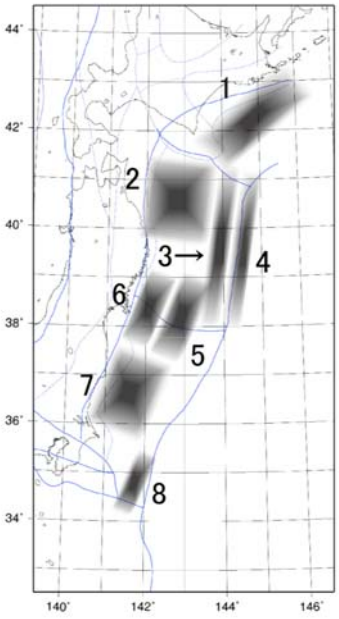

Segment	Past Max. Mw	Historical tsunami
1	8.2	1952
2	8.4	1968
3	8.3	1896
4	8.6	1611
5	8.2	1793
6	7.7	1978
7	7.9	1938
8	8.2	1677

Figure 2.2.5-5 Sea area segmentation and past maximum M_W

Table 2.2.5-2 Example of parameter setting procedure for standard fault model near the Japan Trench and the Kuril-Kamchatka Trench (southern area)

<table>
<tr><th></th><th>Typical interplate thrust earthquake</th><th>Tsunami earthquake</th><th>Intraplate normal fault earthquake</th></tr>
<tr><td>Scaling law</td><td colspan="3">Width should have an upper limit</td></tr>
<tr><td>Fault length</td><td colspan="3">A suitable scaling law is applied to the fault models based on past tsunami heights which is set in the vicinity of expected positions</td></tr>
<tr><td rowspan="2">Fault width</td><td colspan="3">A suitable scaling law is applied to the fault models based on past tsunami heights which is set in the vicinity of expected positions</td></tr>
<tr><td>Width should have an upper limit when the depth exceeds 50 km</td><td colspan="2">Upper limit of the width is 50km</td></tr>
<tr><td>Slip Amount</td><td colspan="3">A suitable scaling law is applied to the fault models based on past tsunami heights which is set in the vicinity of expected positions</td></tr>
<tr><td>Depth of upper edge of the fault plane</td><td colspan="2">Depth is to be determined on the basis of the depth of the upper surface of the subducting plate</td><td>Depth is set to zero</td></tr>
<tr><td>Strike angle</td><td colspan="3">Strike direction is set according to the strike direction of the upper surface of the subducting plate</td></tr>
<tr><td>Dip angle</td><td colspan="3">Same as the fault models based on past tsunami heights</td></tr>
<tr><td>Slip angle</td><td colspan="2">Slip angle is decided on the basis of the strike and slip direction</td><td>Same as the fault models based on past tsunami heights</td></tr>
<tr><td>Shear modulus</td><td colspan="3">3.5×10^{10} (N/m^2) when depth is less than 20 km
7.0×10^{10} (N/m^2) when depth is more than 20 km
5.0×10^{10} (N/m^2) when the fault model extends over both regions</td></tr>
</table>

2.3. Earthquakes anticipated along the eastern margin of the Japan Sea

(1) Knowledge about past tsunamis, etc. on the eastern margin of the Japan Sea

On the eastern margin of the Japan Sea, a distinct plate boundary has not formed, but M=7.5 class earthquakes have occurred in a region of narrow width, which is the eastern margin of the Japan Sea. The upper limit of the size of earthquakes that have occurred in the surrounding area is M7.2. Moreover, multiple references have indicated a seismic gap for large earthquakes off the coast of Akita.

On the basis of the characteristics and strike of active faults, Okamura (1998) has broadly classified the eastern margin of the Japan Sea into a northeastern area (depth of 2,000m or less north of the Shakotan Peninsula), central area (eastern margin of the Japan Basin from west of the Tsugaru Peninsula to northwest of the Shakotan Peninsula), and southern area (eastern margin of the Yamato Basin from the area around Sado Island to northwest of the Oga Peninsula).

Flank collapse is regarded as the most likely cause of the 1741 Oshima-Ōshima Island tsunami. Satake and Kato (2000) as well as Satake (2000) used numerical elevation data for land and submarine topography to re-create the original sector from the collapsed topography to the north of Oshima-Ōshima Island, and conducted numerical simulations of tsunami based on this reproduction.

There is an approach that holds that the active fault distribution and aftershock distribution (corresponding for the most part to the tsunami source region) do not coincide based upon a comparison of aftershock distribution and the results of investigations of active faults conducted subsequent to the 1993 earthquake off the southwest coast of Hokkaido (Okamura, 1993). On the other hand, the Ministry of Land, Infrastructure, Transport and Tourism et al. (2014) configured probable maximum tsunamis based upon active fault distribution.

The Japan Coast Guard's Hydrographic Department (2001) reported that the Shirabeshi Seamount and other submarine volcanic edifices are distributed in the gap between the 1940 earthquake off the coast of Shakotan and the 1993 earthquake off the coast of Southwest Hokkaido, and, between the source region of the 1983 earthquake in the central part of the Japan Sea and the 1993 earthquake off the southwest coast of Hokkaido, there is the Matsumae Plateau, which is a horst that formed when volcanic edifices and the Japan Sea expanded, including Oshima-Ōshima and Oshima-Koshima, separating the source regions of both. Also, Kyuroku Island is located on the southern edge of the source region of the 1983 earthquake in the central part of the Japan Sea, and, in the sea area ranging from the 1940 earthquake off the coast of Shakotan to the 1983 Nihonkai Chubu earthquake, the source region is divided by the seafloor where it is predicted that the crustal structure is different from the volcanic edifices, horst and other surrounding areas.

(2) Magnitude of earthquakes on the eastern margin of the Japan Sea as considered based on crustal structures

1) Data used

Here, the models of inland earthquakes from around the world have been collected and analyzed in order to clarify the relationship between crustal structure and earthquake magnitude with respect to inland-type earthquakes that occur within the Earth's crust.

The collected data is given below. In particular data was extracted from documentary records when models were collected from a common standpoint with respect to large inland earthquakes.

•Earthquake magnitude and fault models:

- The fault specifications that Murotani et al. (2015) used for reviewing the scaling laws pertaining to inland mega-fault systems
- The highly reliable data, which was extracted by Hashimoto (2007) from the objects analyzed by Stirling et al. (2002) concerning scaling laws, that includes data on subsurface fault length (adopted also in Murotani et al., 2015)
- Fault model that can explain run-up height of past tsunami on the eastern margin of the Japan Sea as adopted by the Japan Society of Civil Engineers (2002) (since 1900) (Figure 2.3-1)
- Data added for this review to the aforementioned models:
- Specifications of large earthquakes that Hanks and Bakun (2002) added when considering scaling laws for inland earthquakes, but parameters have been revised for those where width has been assumed when estimating earthquake magnitude.
- Foremost large inland earthquakes that have occurred in recent years
- 2001 China Kunlun (Kokoxili) earthquake
- 2001 India Bhuj (Gujarat) earthquake

•Data on crust thickness

- Crust 1.0, a global model at 1x1 degrees of the crust structure which was developed by Laske et al. (2013) has been used.

•Epicenter locations

- Epicenter locations are mainly based upon USGS Earthquake Search. Values found in documentary records have been used for those locations for which there is no data in the USGS Earthquake Search.

Historical tsunami	M_W	S (km^2)	L (km)	W (km)	D (m)	d (km)	θ (deg.)	δ (deg.)	λ (deg.)	μ ($\times 10^{10}$ N/m^2)	M_0 ($\times 10^{20}$ Nm)	Ref.
1940 Shakotan-Oki	7.70	4050	135	30	3.2	0	347	40	90	3.5	4.54	Japan Society of Civil Engineers (2002)
1964 Niigata	6.93	900	45	20	3.3	1	202	60	90	3.5	1.04	Noguera and Ku. Abe (1992)
		300	20	15	3.0	1	189	60	90	3.5	0.32	
	7.51	813	32.5	25	5.3	0	200	60	52	3.5	1.51	Kato and Ando (1995)
		813	32.5	25	2.9	0	200	60	90	3.5	0.82	
1983 Nihonkai -Chubu	7.74	1200	40	30	7.6	0	22	40	90	3.5	3.19	Aida (1984) Model-10
		1800	60	30	3.05	0	355	25	80	3.5	1.92	
1993 Hokkaido Nansei-Oki	7.84	2250	90	25	5.71	10	188	35	80	3.5	4.50	Takahashi et al. (1995) DCRC-26 model
		650	26	25	4.00	5	175	60	105	3.5	0.91	
		458	30.5	15	12	5	150	60	105	3.5	1.92	

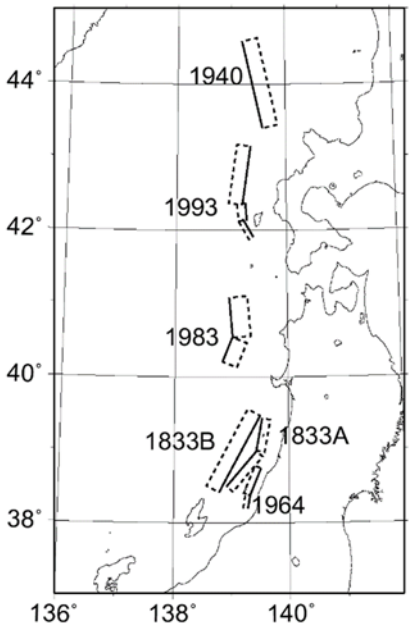

Figure 2.3-1 Fault models based on the past tsunami heights on the eastern margin of the Japan Sea (the Japan Society of Civil Engineers, 2002)

2) Relationship between crust thickness and M_W as well as fault length

When the relationship between crust thickness and M_W as well as fault length for the consolidated intraplate earthquakes from around the world is plotted, the arrangement is created

as shown in Figure 2.3-2 and Figure 2.3-3.

- In areas where crust thickness is less than approximately 40 km, no earthquake exceeding M_W= 8 has occurred.
- The upper limit of fault thickness appears to be conditioned upon crust thickness. Generally, 7.5 times the crust thickness is the upper limit.

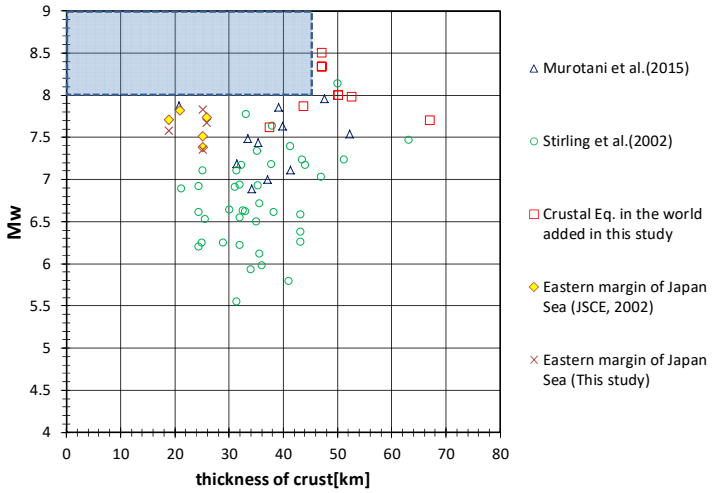

Figure 2.3-2 Relationship between crustal thickness and M_W at the epicenter position of the crustal earthquake in the world

*Crustal thickness is the sum of the upper, middle and lower crust

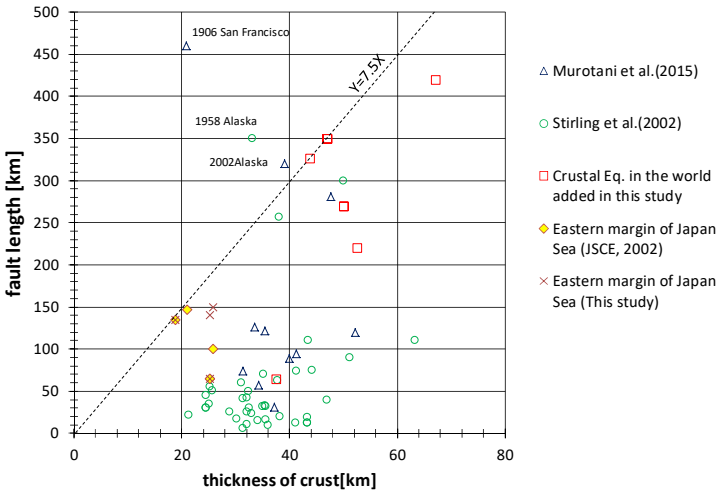

Figure 2.3-3 Relationship between crustal thickness and fault length at the epicenter of earthquake in the world crust

*Crustal thickness is the sum of the upper, middle and lower crust

3) Crustal structure of the eastern margin of the Japan Sea

Kodaira (2013) and No et al. (2014) reported that the 1983 Nihonkai Chubu earthquake

occurred in the boundary between island arc crust and transition crust, and this fault reached as far as the vicinity of the Mohorovicic discontinuity. The earthquake source fault reaches a depth of up to 20 km. This event differs from an upper intra-crustal fault resulting from an ordinary active inland fault, and its characteristics are believed to appear in areas where plates collide on the eastern margin of the Japan Sea.

According to Ichijo et al. (2010), Hasegawa (2002), Shiba and Uetake (2011), Nakahigashi et al. (2012) and Nakahigashi et al. (2013), the same tendency has been observed even in areas where large earthquakes occurred in the past on the eastern margin of the Japan Sea besides the 1983 Nihonkai Chubu earthquake.

2.4. Earthquakes anticipated at submarine active faults

2.4.1. Basis for standard fault model configuration and other specifics

(1) Knowledge about past tsunamis, etc. in sea area around Southwest Japan

In the area around Southwest Japan, no large tsunami has occurred with the exception of two, the 1792 tsunami resulting from the Mt. Mayuyama collapse and the 1596 tsunami in Beppu Bay. Of these, Abe (1999) reported that, although the scale of the 1596 tsunami in Beppu Bay was abnormally large compared to the size of the earthquake, its cause has not been able to be identified.

On the Japan Sea side, there have been cases where small tsunamis have occurred due to M7 class earthquakes that struck in locations close to the coastline.

There is a legend about a megathrust earthquake tsunami that occurred in 1026 (3rd year of the Manju era) off the coast of what is currently Masuda City in Shimane Prefecture that caused damage to the coastal area. Based upon excavation and research conducted along the Masuda River, a position has been stated that, although tsunami deposits and unique sand layers have been discovered which indicate carbon isotopes dating to approximately 1,000 years ago, there are no entries about tsunami in major historical records of the time (Minoura et al., 1993). In the future, as the collection of data advances with regard to whether or not there were any tsunamis and, if there were, what were the causes, tsunami height distributions, etc., there is the possibility that such tsunami may serve as material for review in order to configure standard fault models.

(2) Scaling laws for mega-fault systems

Of the data on inland crustal earthquakes that Takemura (1998) followed that served as the basis for scaling laws applied to submarine active faults and the eastern margin of the Japan Sea by Japan Society of Civil Engineers (2002), the longest fault length was 85 km associated with

the 1891 Nobi earthquake, and even longer fault lengths are extrapolated areas. Here, case studies are presented of reviews conducted in recent years of scaling laws for mega-fault systems.

1) Murotani et al. (2015)

- Reference data:
  - Of the earthquakes in mega-fault systems exceeding a length of 80 km that have occurred inland around the world and medium-sized earthquakes that have occurred in recent years, 11 were selected for analysis conducted using seismic tsunami shapes and surveys conducted of surface earthquake faults. In cases where there are multiple analysis results, the mean was selected.
  - Furthermore, of reliable data selected by Hashimoto (2007) from a database provided by Stirling et al. (2002), 40 earthquakes were added for which the subsurface fault lengths were obtained.
- Results :
  - The ratio of the earthquake source fault length and the surface fault length is almost 1:1.
  - The maximum displacement observed on the Earth's surface (Dsurf) is generally 2 ~ 3 times the mean slip amount at the earthquake source fault.
  - Dsurf and the maximum slip amount at the earthquake source fault is a proportional relationship of almost 1:1.
  - Dsurf saturates 10 m when the length of the earthquake source fault is roughly 100 km. When width W=18 km, then S=1.0×10^{17} M_0, and a scaling relationship has been proposed where slip amount saturates here.

2) Shaw and Scholz (2001)

Shaw and Scholz (2001) analyzed the parameters of intraplate and interplate earthquakes around the world, and reported that, when the ratio of L/W exceeds ten-fold, then slip amount reaches an upper limit. However, W is fixed at 15 km and corresponds to the thickness of the seismogenic layer. Moreover, the following relational expression has been derived.

$$D = \alpha \cdot (L/2) \qquad (L \leq 2W)$$

$$D = \alpha \cdot \left(1/\left[1/L + 1/2W\right]\right) \qquad (L > 2W)$$

3) Manighetti et al. (2007)

Manighetti et al. (2007) proposed a scaling law for slip amount in relation to earthquakes that occur in multiple segments. The smaller the number of segments, the quicker slip amount saturates over total length. Also, the greater the number of segments, the smaller the saturated slip amount. The number of interlocking segments depends on the strength of the barrier between

segments, and this strength is reported to vary depending upon the maturity of the fault.

4) The Headquarters for Earthquake Research Promotion's treatment of mega-fault systems in "Methods for Long-Term Assessment of Active Faults"

Taking into account research conducted by Manighetti et al. (2007), the "Methods for Long-Term Assessment of Active Faults" (Headquarters for Earthquake Research Promotion, 2010) states: "With respect to active mega-fault systems where the length exceeds 100 km, the possibility that the amount of displacement during activity may be saturated has been indicated…., so, in cases where length is not greater than four times the width of the fault plane, earthquake magnitude is estimated based upon the L-M formula provided by Matsuda (1975), and, in cases exceeding this length, a model has been configured where multiple demarcated segments rupture so that the length does not exceed four times". In other words, in cases where length exceeds four times the width of the fault plane, a model has been provided that arranges models, which apply the scaling relationship for each demarcated sector into many parts, in a series.

2.4.2. Case studies of standard fault model configuration methods, etc.

The Ministry of Land, Infrastructure, Transport and Tourism et al. (2014) also created models for submarine active faults other than in the eastern margin of the Japan Sea. Models have been configured for 60 faults (including submarine active faults in the eastern margin of the Japan Sea) throughout the entire Japan Sea.

2.4.3. Tsunami source configuration methods for probable maximum tsunami

(1) Configuration method for slip angle based on relationship between regional stress field and fault plane angle

1) Examination policy

With regard to cases where data has been obtained about the location, strike and length of submarine active fault, methods are to be examined for estimating the static fault parameters necessary for numerical simulations of tsunami.

The oceanic crust far away from the coastline is relatively stable, and no large earthquakes have occurred in this area in the past. On the other hand, in sea areas relatively close to the coastline, seismic activity has been reported in the past that includes large earthquakes, and there is also the possibility of such activity in the future. This examination will focus on the upper

intraplate earthquakes that occur at submarine active fault relatively close to the coastline. On the sea bottom in coastal waters, crustal structures have structures similar to those on land and hypocenter distribution and stress fields are also believed to be connected with those in land areas, so utilizing knowledge and data about inland crustal earthquakes, consideration will be given to that which makes it possible to configure tsunami source models for probable maximum tsunamis.

2) Occurrence patterns of inland crustal earthquakes

Along with the size of an earthquake, the width of the fault plane increases, but it has been pointed out that an upper limit is reached at a certain width depending on location. Fracture zones for shallow earthquakes are limited to seismogenic layers, and the scaling law for fault parameters changes before and after the upper limit for the fault width.

When the fracture of one rectangular fault extends across all layers of seismogenic layer thickness H_e, fault width W takes a value commensurate with dip angle δ and is expressed using the following equation.

$$W = \frac{H_e}{\sin\delta} \qquad \text{(2.4.3.1)}$$

According to Ito et al. (1995) and the Fukuoka Regional Headquarters of the Japan Meteorological Agency (1998), the maximum depth of inland crustal earthquakes is believed to be between 15 and 20 km.

Using the earthquake mechanism analyses detailed in the Japan Meteorological Agency's Seismological Bulletin of Japan, the fracture surfaces were identified for 31 examples of earthquakes having a hypocenter depth of less than 20 km and a magnitude of 5.0 or greater as reported by the Japan Meteorological Agency and occurred inland in southwestern Japan between 1973 and August 1998. The frequency distribution of dip angle is given in Figure 2.4.3-1, and these earthquakes occurred generally at high angles (45 ~ 90°).

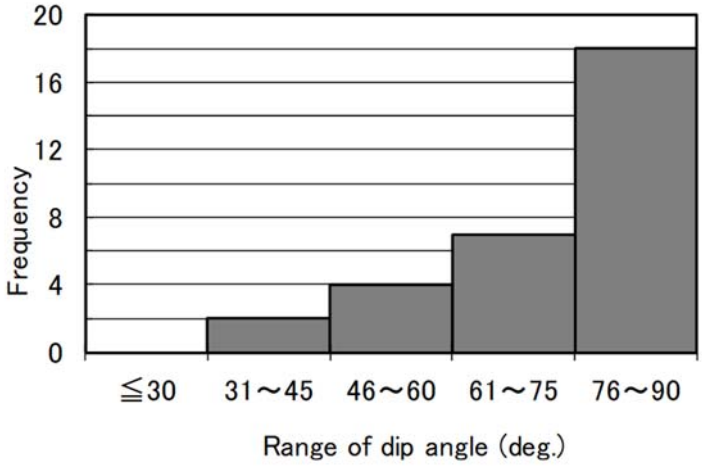

Figure 2.4.3-1 Frequency distribution of dip ales of shallow inland earthquakes occurred in Southwest Japan

According to the analysis of the earthquake mechanisms provided by Global CMT, the orientation of the P and T axes is uniform for each region and does not depend upon earthquake type. In other words, with regard to earthquakes of M_W=5.0 or greater, fault motion corresponds well with wide-area stress field.

(2) Configuration methods for slip angle based on the relationship between regional stress field and fall plane angle

The dip angle and other characteristics of faults may be configured based upon surveys. In cases where data is not well-defined, the following may serve as a guide, which is based upon a variety of knowledge.

- Depth of fault upper edge: 0 ~ 5km
- Dip angle: 45 ~ 90° (for southwestern Japan) and 30 ~ 60° (Chuetsu region)
- Slip angle: Range found based upon regional stress field and dip angle

Of these, the range found based upon regional stress field and dip angle may be configured based upon the principle shown in Figure 2.4.3-2.

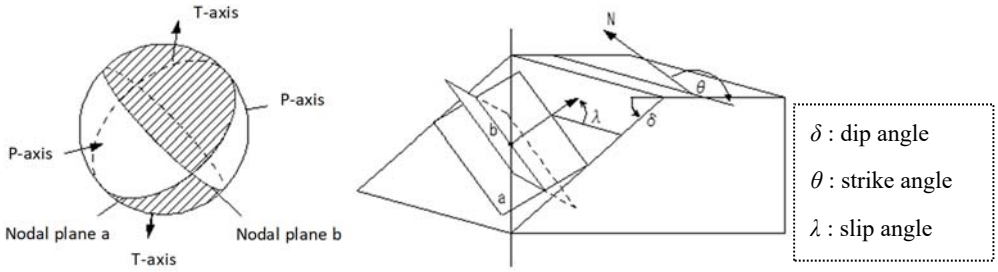

Figure 2.4.3-2 Schematic diagram of the relationship between focal mechanism and fault motion

* Based on the principle of the focal mechanism, the slip angle can be geometrically estimated from the stress field around the active fault and the strike and dip angles of the fault.The principal pressure (P) axis and the principal tension (T) axis intersect with the two node faces at 45°, and the slip vector coincides with the normal vector of the auxiliary plane (the node which is not the actual fault plane) (JSCE, 2002).

The orientation of the P axis is believed to be within a range of 90° ~ 120° for southwestern Japan and 110° ~ 140° for the Chuetsu Region (both are clockwise from the north).

Although there are descriptions pertaining to the azimuth angle of the P axis, trends have also been seen regarding dip (dip angle) of the P axis. An analysis of earthquakes less than *M*=5.0 and a depth of 30 km that have occurred in Southwest Japan and are based on analyses of such mechanisms by various institutions is given in Figure 2.4.3-3. It is found that the plunge of the P and T axes is within 32° and their principal axes are almost horizontal.

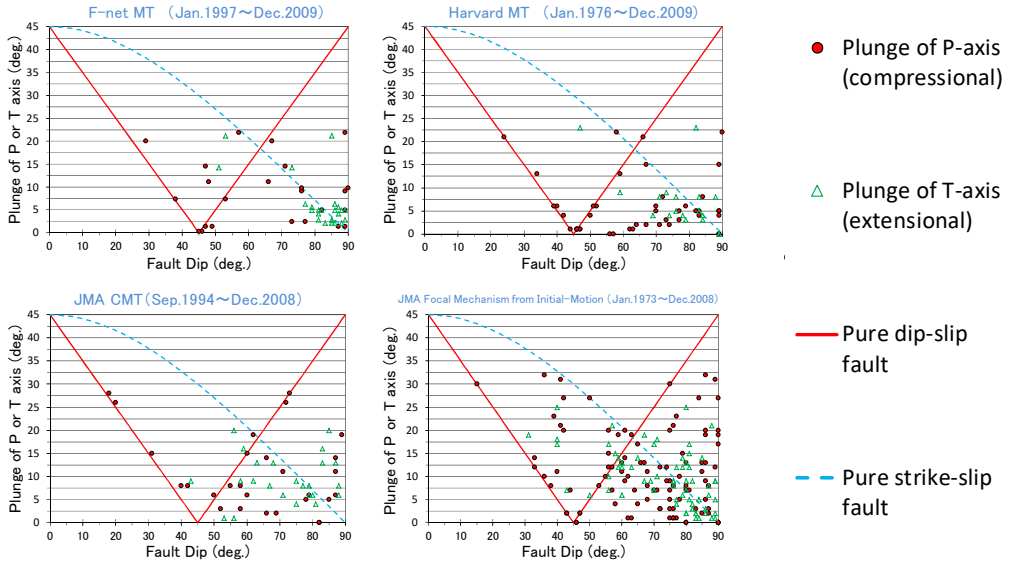

Figure 2.4.3-3 Distribution of P and T axes of upper crustal earthquake occurred in Southwest Japan

(3) Basic fault parameter configuration methods for probable maximum tsunami

1) Procedure based on relationship between fault length and moment magnitude

A flowchart for the fault parameter configuration method for a tsunami anticipated at submarine active fault (Koba et al., 2001) is shown in Figure 2.4.3-4.

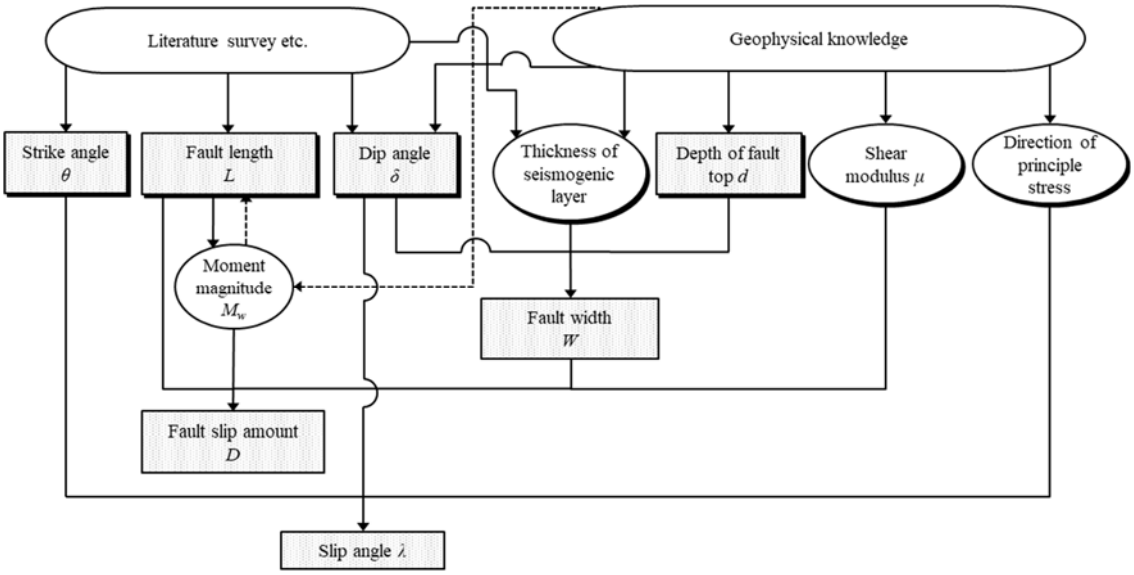

Figure 2.4.3-4 Tsunami standard fault model setting flowchart assumed for submarine active fault (Procedure based on relationship between fault length and moment magnitude)

*The rectangles express the fault parameters necessary for tsunami calculation, and the grayed items express information needed prior to setting the parameters. In cases where the moment magnitude is set prior to the fault length, the fault length is computed from the moment magnitude along the flow indicated by the broken line.

Cases where dip angle and other parameters are well-defined based on surveys of active faults or other data may be treated as definitive.

The methods for configuring the parameters have been compiled in Table 2.4.3-1. The depth of the upper edge of faults assuming a shallow earthquake is given as 0 km. Also, from the aforementioned range of 15 ~ 20 km, the thickness of the seismogenic layer has been limited to 15 km, a depth where slip amount increases.

Based on the principles of earthquake mechanisms, slip angle may be estimated geometrically from the strike and dip angles and the stress field in the area around the fault. A conceptual diagram is shown in Figure 2.4.3-5. The principle axis of pressure (P axis) and the principle axis of tension (T axis) incline 45° from the two nodal planes a and b, and the slip vector

coincides with the direction of the normal line of the auxiliary plain (nodal plane b, which is not an actual fault plane). The orientation of the stress access may be estimated by referencing analyses of earthquake mechanisms of past earthquakes as well as previous case studies showing regional stress field in regions of Japan (see for example Tsukahara, 1999).

Similar to what was done regarding the eastern margin of the Japan Sea, those relationship equations provided by Takemura (1998) that are given below and express the relationship between fault length and earthquake magnitude are applied for the scaling law.

i) When fault width has reached the upper limit

$$\log L(km) = 0.75M_w - 3.77, L \propto D, W = const. \quad \text{.....(2.4.3.2)}$$

ii) When fault width has not reached the upper limit

$$W = \frac{2}{3}L, L \propto W \propto D \quad \text{.....(2.4.3.3)}$$

where, L represents fault length and D slip amount. Also, M_W is moment magnitude and is connected to fault parameters using the following relationship.

$$\log M_0(N \cdot m) = 1.5M_w + 9.1 \quad \text{.....(2.4.3.4)}$$

$$D = \frac{M_0}{\mu LW} \quad \text{.....(2.4.3.5)}$$

where, μ represents rigidity.

In cases where fault length and seismogenic layer thickness are given, then

- when fault width has reached the upper limit: equations (2.4.3.1), (2.4.3.2), (2.4.3.4), and (2.4.3.5)
- when fault width is below the upper limit: equations (2.4.3.3), (2.4.3.4), and (2.4.3.5) are applied, and, if the relationship of both fields is connected continuously, then fault width and slip amount may be computed.

Table 2.4.3-1 Method of setting basic fault parameters of tsunami assumed for submarine active fault (Procedure based on the relationship between fault length and moment magnitude)

Parameter	Setting procedure
Length (L)	Fault length is to be set on the basis of the results of an active faults survey. When determining the length from M_W, it follows the scaling law.
Width (W)	Width is set on the basis of the thickness of seismogenic layer and dip angle.
Dislocation (D)	$D = M_0 / \mu LW$ Where, $\log M_0$ (Nm) = 1.5 M_W + 9.1 .
Depth of upper edge of the fault plane (d)	0 km
Strike angle (θ)	On the basis of the result of active faults survey
Dip angle (δ)	On the basis of the earthquake focal mechanism solutions, or set from 45° to 90°
Slip angle (λ)	Determined by strike direction, dip angle and direction of principle stress axis.
Shear modulus (μ)	3.5×10^{10}(N/m^2)
Scaling law	1) $W <$ "thickness of the seismogenic layer" / sinδ $W = 2L / 3$ $L \propto W \propto D$ 2) $W >$ "thickness of the seismogenic layer" / sinδ $W =$ "thickness of the seismogenic layer" / sinδ $\log L$ (km) = 0.75 M_W - 3.77 (Takemura's formula) $L \propto D$

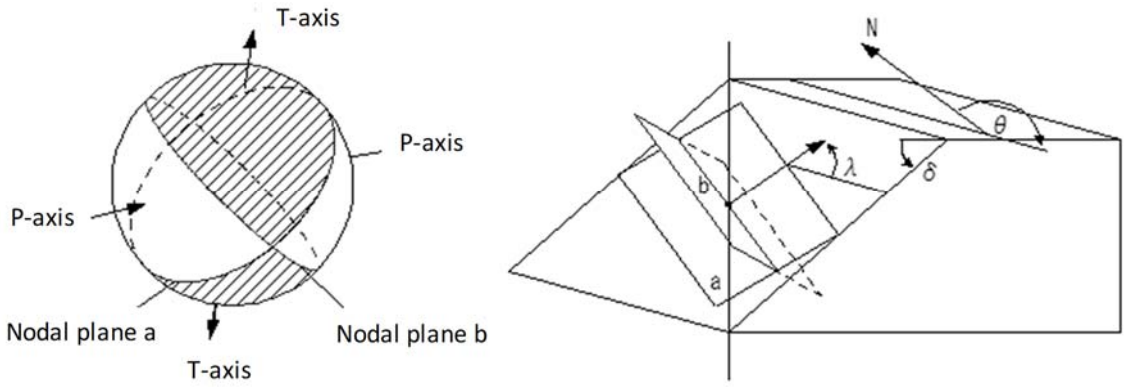

Figure 2.4.3-5 Schematic diagram of the relationship between focal mechanism and fault motion (Drawing based on Sato (1989))

2) Procedure based on relationship between fault area and moment magnitude

The procedure based upon the relationship between fault area and moment magnitude is applied to fault models assuming slip heterogeneity. For more specific details, refer to case studies of such applications presented in appendix volume 6.

Differences from the procedure based on the relationship between fault length and moment magnitude are given below.

First, in cases where fault length and seismogenic layer thickness are given, the equation for when the fault width reaches the upper limit (2.4.3.1) is applied and the equation for when the fault width is below the upper limit (2.4.3.3) is applied to compute fault area *S*.

$$S = L \cdot W$$

Next, the following scaling laws are used to compute M_0 based upon fault area *S*.

$$M_0 = (S / 2.23 \times 10^9)^{3/2} \times 10^{-7} \qquad (M_w < 6.5)$$

$$M_0 = (S / 4.24 \times 10^5)^2 \times 10^{-7} \qquad (6.5 \le M_w < 7.7)$$

(Irikura and Miyake, 2001)

$$M_0 = 1.575 \times \mathrm{S} \times 10^{11} \qquad (7.7 \le M_w)$$

(Prepared based upon Ministry of Land, Infrastructure, Transport and Tourism et al. (2014))

A flowchart of the fault parameter configuration method based upon the relationship between fault area and M_W is shown in Figure 2.4.3-6.

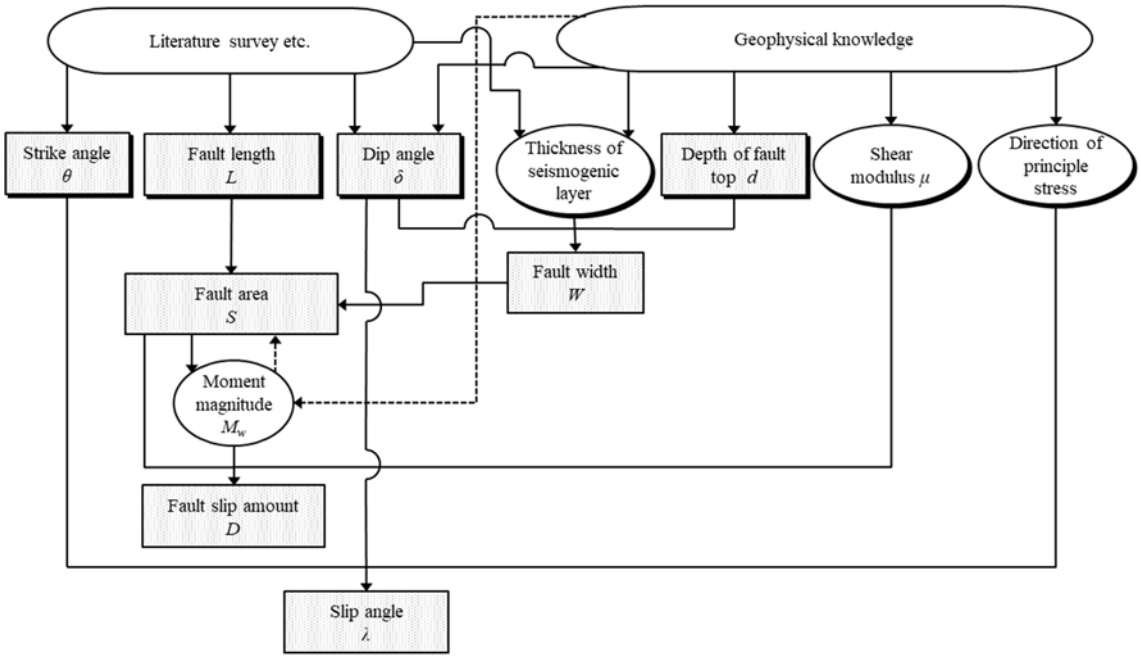

Figure 2.4.3-6 Tsunami standard fault model setting flowchart assumed for submarine active fault (Procedure based on relationship between fault area and moment magnitude)

*The rectangles express the fault parameters necessary for tsunami calculation, and the grayed items express information needed prior to setting the parameters. In cases where M_W is set prior to the fault length, the fault length is computed from M_W along the flow indicated by the broken line. Cases where dip angle and other parameters are well-defined based on surveys of active faults or other data may be treated as definitive. Matters related to slip heterogeneity and kinematic fault parameters have been omitted.

[Appendix 2 References]

Abe, Ka. (1978): Chapter 3 Modern seismology, H. Kanamori ed., Iwanami Course Earth Science 8 Physics of earthquake, Iwanami Shoten, pp. 89-167 (in Japanese).

Abe, Ka. (1989): Quantification of tsunamigenic earthquakes by the Mt scale, Tectonophysics. Vol. 166, pp. 27-34.

Abe, Ka. (1999): Quantification of Historical Tsunamis by the Mt Scale, Zisin (Journal of the Seismological Society of Japan, 2nd ser.), Vol. 52, pp. 369-377 (in Japanese with English abstract).

Aida, I. (1984): A Source Model of the Tsunami Accompanying the 1983 Nihonkai-Chubu Earthquake, Bulletin of the Earthquake Research Institute, University of Tokyo, Vol. 59, pp. 93-104 (in

Japanese with English abstract).

Aida, I. (1997): Simulation of Large Tsunamis Occurring in the Past off the Coast of the Sanriku District, Bulletin of the Earthquake Research Institute, University of Tokyo, Vol. 52, pp. 71-101 (in Japanese).

Annaka, T., K. Ohta, H. Motegi, I. Yoshida, M. Takao and H. Soraoka (1999): A study on the tsunami inversion method based on shallow water theory, Proceedings of Coastal Engineering, JSCE, Vol. 46, pp. 341-345 (in Japanese).

Bautista, M.L.P. and K. Oike (2000): Estimation of the magnitudes and epicenters of Philippine historical earthquakes, Tectonophysics, Vol. 317, pp. 137-169.

Bird, P. (2003): An updated digital model of plate boundaries, Geochemistry, Geophysics, Geosystems, Vol. 4, 1027.

Cabinet Office, Government of Japan (CAO) Study meeting on the huge earthquake model of the Nankai Trough (2nd report) (in Japanese).
http://www.bousai.go.jp/jishin/nankai/model/pdf/20120829_2nd_report01.pdf
(Accessed on Aug. 2016)

Central Disaster Management Council Expert study group on trench type earthquakes around Japan Trench / Kuril Trench Trench (2006): Report of expert study group on trench type earthquakes around Japan Trench / Kuril Trench Trench (in Japanese).

Central Disaster Management Council Investigation meeting for earthquake model directly under the capital city (2013): Report on seismic source fault model, seismic intensity distribution and tsunami height of M7 class earthquake directly under the capital and M8 class earthquake along the Sagami Trough (in Japanese).

Cisternas, M., B.F. Atwater, F. Torrejon, Y. Sawai, G. Machuca, M. Lagos, A. Eipert, C. Youlton, I. Salgado, T. Kamataki, M. Shishikura, C.P. Rajendran, J.K. Malik, Y. Rizal and M. Husni (2005): Predecessors of the giant 1960 Chile earthquake, Nature, Vol. 437, pp. 404-407.

Cisternas, M., B. Atwater, T. Kamataki, Y. Sawai and M. Shishikura (2006): Repeated paleo-giant-earthquake caused in source area of the 1960 Chilean earthquake, Historical Earthquakes, No. 21, pp. 87-91 (in Japanese with English abstract).

Curray, J.R. (2005): Tectonics and history of the Andaman Sea region, Journal of Asian Earth Sciences, Vol. 25, pp. 187-232.

DeMets, C. (1992): Oblique convergence and deformation along the Kuril and Japan trenches, Journal of Geophysical Research, Vol. 97, pp. 17615-17625.

Eshelby, J. D. (1957): The determination of the elastic field of an ellipsoidal inclusion and related problems, Proceedings of the Royal Society of London, Series A, Mathematical and Physical Sciences, Vol. 241, pp. 376-396.

Fujioka, K., M. Kido and M. Yuasa (2002): Tectonic framework of Izu-Bonin Arc, NSF-IFREE

MARGINS Subduction Factory Workshop, Hawaii.

Fukuoka Meteorological Observatory (1998): Earthquake and tsunami in Kyushu and Yamaguchi Prefecture, Memoirs of the Fukuoka Meteorological Observatory, No. 53, 435p. (in Japanese).

Fukutani, Y., A. Suppasri, and F. Imamura (2015): Stochastic analysis and uncertainty assessment of tsunami wave height using a random source parameter model that targets a Tohoku-type earthquake fault, Stochastic Environmental Research and Risk Assessment, Vol. 29, pp. 1763-1779.

Geospatial Information Authority of Japan (GSI) (2012): Slip deficit rate along the Chishima (Kuril) Trench, Report of The Coordinating Committee for Earthquake Prediction, Japan, Vol. 88, pp. 463-468 (in Japanese).

Geospatial Information Authority of Japan (GSI) and Japan Coast Guard (JCG) (2011): Slip distribution model during 2011 Tohoku earthquake on plate boundary based on both land GPS observation and ocean bottom crustal movement observation (in Japanese). http://www.gsi.go.jp/common/000060854.pdf (Accessed on Aug. 2016).

Goda, K., P. M. Mai, T. Yasuda and N. Mori (2014): Sensitivity of tsunami wave profiles and inundation simulations to earthquake slip and fault geometry for the 2011 Tohoku earthquake, Earth, Planets and Space, Vol. 66, 105.

Goldfinger, C., C. H. Nelson, A. E. Morey, J. E. Johnson, J. R. Patton, E. Karabanov, J. Gutiererez-Pastor, A. T. Eriksson, E. Gracia, G. Dunhill, R. J. Enkin, A. Dallimore and T. Vallier (2012): Turbidite event history— Methods and implications for Holocene paleoseismicity of the Cascadia Subduction Zone, U.S. Geological Survey Professional Paper 1661-F, 170p.

Goto, K., T. Kawana and F. Imamura (2010): Historical and geological evidence of boulders deposited by tsunamis, southern. Ryukyu Island, Japan. Earth-Science Reviews, Vol.102, pp.77-99.

Goto, K. and A. Shimabukuro (2012): Interdisciplinary study of the 1771 Meiwa Tsunami, Science Journal Kagaku, Vol. 82, No. 2, pp. 208-214.

Hanks, T.C. and W.H. Bakun (2002): A bilinear source-scaling model for M-logA observations of continental earthquakes, Bulletin of the Seismological Society of America, Vol. 92, No. 5, pp. 1841-1846.

Hasegawa, A. (2002): Chapter 3 Crustal structure and seismic activity in Northeast Japan, Active faults and earthquake tectonics in the eastern margin of the Japan Sea, Tokyo University Publishing, pp. 27-43 (in Japanese).

Hasegawa, A., K. Yoshida, Y. Asano, T. Okada, T. Iinuma and Y. Ito (2012): Change in stress field after the 2011 great Tohoku-Oki earthquake, Earth and Planetary Science Letters, Vol. 355-356, pp. 231-243.

Hashimoto, T. (2007): The surface length of earthquake fault and the moment magnitude, Abstracts, Japan Geoscience Union Meeting, S145-013.

Hatori, T. (1965): On the Alaska tsunami of March 29, 1964, as observed along the coast of Japan, Bulletin of the Earthquake Research Institute, Vol. 43, pp. 399-408.

Hatori, T. (1988): Tsunami Magnitudes and Source Areas along the Ryukyu Islands, Zisin (Journal of the Seismological Society of Japan, 2nd ser.), Vol. 41, pp. 541-547 (in Japanese with English abstract).

Hatori, T. (1998): Magnitude Scale of Tsunamis Generated from the South-East Alaska to Western North America, Zisin (Journal of the Seismological Society of Japan, 2nd ser.), Vol. 51, pp. 203-210 (in Japanese with English abstract).

Ichijo, K., Y. Murai, T. Takanami, R. Miura, Y. Machida, Y. Nishimura and Y. Nakamura (2010): Seismic activity around the source area of the 1940 Shakotan-Hanto-oki earthquake deduced from ocean bottom seismographic observation, Research meeting of the University of Tokyo Earthquake Research Institute, Improvement of Research on Imaging and Monitoring of Lithospheric Short Wavelength Heterogeneity - Toward Elucidation of Spatiotemporal Changes in Seismogenic Zone Structure - (in Japanese).

Ioki, K. and Y. Tanioka (2016): Re-estimated fault model of the 17th century great earthquake off Hokkaido using tsunami deposit data, Earth and Planetary Science Letters, Vol. 433, pp. 133-138.

Irikura, K. and H. Miyake (2001): Prediction of strong ground motions for scenario earthquakes, Journal of Geography (Chigaku Zasshi), Vol. 110, No. 6, pp. 849-875 (in Japanese with English abstract).

Irikura, K. and H. Miyake (2011): Recipe for predicting strong ground motion from crustal earthquake scenarios, Pure and Applied Geophysics, Vol. 168, pp. 85-104.

Ishikawa, Y. and K. Nakamura (1997): SEIS-PC for Windows95, Abstracts, Japan Earth and Planetary Science Joint Meeting, 78p. (in Japanese).

Ito, K., Y. Umeda, S. Ohmi, A. Ohigashi and K. Matsumura (1995): Changes in the thickness of the seismogenic layer and the 1995 Hyogo-ken Nanbu earthquake, Programme and abstracts, the Seismological Society of Japan, No. 2, 40p. (in Japanese).

Ito, K. (2008): Seismogenic layer and active faults and subsurface structure in the Kinki region, Kansai branch of the Japan Society of Applied Geological Societies FY2008 general meeting and research presentation special lecture (in Japanese).

Japan Nuclear Energy Safety Organization (JNES) Seismic Safety Division (2011): Cross-check analysis on the results of numerical simulation for past tsunami caused by 2011 Tohoku earthquake conducted by nuclear operators, Earthquake · Tsunami 3-4, Opinions on Earthquake · Tsunami Opinion Hearing (Part 3) (in Japanese).
http://dl.ndl.go.jp/view/download/digidepo_6011652_po_3-4.pdf?contentNo=8&alternativeNo= (Accessed on Aug. 2016).

Johnson, J. M. and K. Satake (1999): Asperity distribution of the 1952 great Kamchatka earthquake and its relation to future earthquake potential in Kamchatka, Pure and Applied Geophysics, Vol. 154, pp. 541-553.

Japan Coast Guard (JCG) (2001): Submarine topography and active structure in the eastern margin of the Japan Sea, Report of The Coordinating Committee for Earthquake Prediction, Japan, Vol. 66, pp. 100-104 (in Japanese).

Japan Agency For Marine-Earth Science and Technology (JAMSTEC) (2011): Tohoku earthquake, subsurface structure in the southernmost focal region, JAMSTEC website (in Japanese). http://www.jamstec.go.jp/donet/j/topics/201103tohoku_2/index.html (Accessed on Aug. 2016).

Japan Agency For Marine-Earth Science and Technology (JAMSTEC) (2013): Stress state change in the source region of the Tohoku earthquake revealed by drilling survey of Deep-sea Scientific Drilling Vessel "Chikyu", Press release (in Japanese). http://www.jamstec.go.jp/j/about/press_release/20130208/ (Accessed on Aug. 2016).

Japan Meteorological Agency (JMA) (2015): About the earthquake that occurred off central Chile around 07:54 September 27, 207 (7th report), press release (in Japanese). http://www.jma.go.jp/jma/press/1509/18i/kaisetsu201509181700.pdf (Accessed on Aug. 2016).

Kasahara, J., T. Sato, K. Mochizuki and K. Kobayashi (1997): Paleotectonic structures and their influence on recent seismo-tectonics in the south Kuril subduction zone, The Island Arc, Vol. 6, pp. 267-280.

Kato, T. and M. Ando (1995): Reconsideration of fault models, 1964 Niigata earthquake, Programme and abstracts, the Seismological Society of Japan, 72p.

Kato, Y. (1987): Run-up Height of Yaeyama Seismic Tsunami (1771), Zisin (Journal of the Seismological Society of Japan, 2nd ser.), Vol. 40, No. 3, pp. 377-381 (in Japanese with English abstract).

Kawabe, H. and K. Kamae (2012): Characterized Source Modeling of the 2011 Tohoku Earthquake, Programme and abstracts, the Seismological Society of Japan, Fall Meeting, 62p.

Kawata, Y., N. Koike, S. Kado and M. Inoue (1998): Far Field Tsunami Potential along Japanese Coastal Region, Proceedings of Coastal Engineering, Vol. 45, pp. 336-340.

Koba, M., T. Annaka, K. Inagaki, H. Tanaka and H. Soraoka (2001): Tsunami source model configuration method assumed for submarine active fault, Proceedings of Coastal Engineering, vol. 48, pp. 326-330 (in Japanese).

Kodaira, S. (2013): 2-2 Survey of crustal structure of marine area by multi-channel etc., Result report of the priority investigation of strain concentration area, National Research Institute for Earth Science and Disaster Resilience (in Japanese).

Koketsu, K., Y. Yokota, N. Kato and T. Kato (2012): Backslip Migration and Weakening at the Last Stage of a Seismic Supercycle, Programme and abstracts, the Seismological Society of Japan, Fall Meeting, 29p.

Koyama, J., M. Tsuduki and K. Yomogida (2012): Megathrust Earthquakes in Oblique Subduction Zones Part 1: The Sagami Trough, Geophysical Bulletin of Hokkaido University, No. 75, pp. 161-174.

Laske, G., G. Masters., Z. Ma and M. Pasyanos (2013): Update on CRUST1.0 - A 1-degree global model of earth's crust, Geophysical Research Abstracts, Vol. 15, EGU2013-2658.

Lay, T., H. Kanamori, C. J. Ammon, K. D. Koper, A. R. Hutko, L. Ye, H. Yue, and T. M. Rushing (2012): Depth-varying rupture properties of subduction zone megathrust faults, Journal of Geophysical Research, Vol. 117, B04311.

Liu, X., D. Zhao and S. Li (2013): Seismic heterogeneity and anisotropy of the southern Kuril arc: insight into megathrust earthquakes, Geophysical Journal International, Vol. 194, pp. 1069-1090.

Loveless, J. P. and B.J. Meade (2010): Geodetic imaging of plate motions, slip rates, and partitioning of deformation in Japan, Journal of Geophysical Research, Vol. 115, B02410.

MacInnes, B. T., R. Weiss, J. Bourgeois and T. K. Pinegina (2010): Slip distribution of the 1952 Kamchatka great earthquake based on near-field tsunami deposits and historical records, Bulletin of the Seismological Society of America, Vol. 100, issue 4, pp. 1695-1709.

Mai, P. M., and G.C. Beroza (2002): A spatial random field model to characterize complexity in earthquake slip, Journal of Geophysical Research, Vol. 107, pp. ESE10-1-ESE10-21.

Manighetti, I., M. Campillo, S. Bouley and F. Cotton (2007): Earthquake scaling, fault segmentation, and structural maturity, Earth and Planetary Science Letters, Vol. 253, Issues 3-4, pp. 429-438.

Matsuda, T. (1975): Magnitude and Recurrence Interval of Earthquakes from a Fault, Zisin (Journal of the Seismological Society of Japan, 2nd ser.), Vol. 28, pp. 269-283 (in Japanese with English abstract).

Matsumoto, T. and M. Kimura (1993): Detailed Bathymetric Survey in the Sea Region of the Estimated Source Area of the 1771 Yaeyama Earthquake Tsunami and Consideration of the Mechanism of Its Occurrence, Zisin (Journal of the Seismological Society of Japan, 2nd ser.), Vol. 45, pp. 417-426 (in Japanese with English abstract).

Matsumoto, T., A. Doi, S. Kise and N. Abe (2010): Tectonics of Chile Triple Junction based on marine geophysical data, the 30th Polar Region Geoscience Symposium "Solid Earth Dynamics Explored from Polar Regions" (in Japanese).

Melnick, D., B. Bookhagen, M. R. Strecker and H.P. Echtler (2009): Segmentation of megathrust rupture zones from fore-arc deformation patterns over hundreds to millions of years, Arauco peninsula, Chile, Journal of Geophysical Research, Vol. 114, B01407.

Ministry of Education, Culture, Sports, Science and Technology-Japan (MEXT) (2008): Estimation of three-dimensional crustal inhomogeneous structure of plate boundary and its surrounding area, Study on trench type earthquake including Tonankai / Nankai earthquake - FY 2008 report, pp. 52-88 (in Japanese).

Ministry of Land, Infrastructure, Transport and Tourism (MLIT), Cabinet Office, Government of Japan (CAO) and Ministry of Education, Culture, Sports, Science and Technology-Japan (MEXT) - Study meeting on large-scale earthquake in the Sea of Japan (2014): Report by the Study Group on Large Scale Earthquakes in the Sea of Japan (in Japanese).

Minoura, K., T. Nakata and T. Matsui (1993): A Trace of the Manjyu Tsunami, Abstracts, the 100th Annual Meeting of the Geological Society of Japan, Vol. 100, 684p.

Murotani, S., K. Satake and Y. Fujii (2013): Scaling relations of seismic moment, rupture area, average slip, and asperity size for M~9 subduction-zone earthquakes, Geophysical Research Letters, Vol. 40, pp. 5070-5074.

Murotani, S., S. Matsushima, T. Azuma, K. Irikura and S. Kitagawa (2015): Scaling Relations of Source Parameters of Earthquakes Occurring on Inland Crustal Mega-Fault Systems, Pure and Applied Geophysics, Vol. 172, pp. 1371-1381.

Nakahigashi, K., M. Shinohara, E. Kurashimo, T. Yamada, A. Kato, T. Takanami, K. Uehira, Y. Ito, T. Iidaka, T. Igarashi, H. Sato, R. Hino, K. Obana, Y. Kaneda, N. Hirata, T. Iwasaki and T. Kanazawa (2012): Seismic structure of the source region of the 2007 Chuetsu-oki earthquake revealed by offshore-onshore seismic survey: Asperity zone of intraplate earthquake delimited by crustal inhomogeneity, Tectonophysics, Vol. 562-563, pp. 34-47.

Nakahigashi, K., M. Shinohara, T. Yamada, K. Uehira, K. Mochizuki and T. Kanazawa (2013): Seismic structure of the extended continental crust in the Yamato Basin, Japan Sea, from ocean bottom seismometer survey, Journal of Asian Earth Sciences, Vol. 67-68, pp. 199-206.

Nakamura, M. (2009): Fault model of the 1771 Yaeyama earthquake along the Ryukyu trench estimated from the devastating tsunami, Geophysical Research Letters, Vol. 36, L19307.

Namegaya, Y. and K. Satake (2012): Re estimation of magnitude of the AD 869 Jogan earthquake inferred from tsunami deposit distribution and computed inundation distances, Programme and abstracts, the Seismological Society of Japan, Fall Meeting, 32p.

Nishimura, T. (2012a): The 197th meeting of The Coordinating Committee for Earthquake Prediction (CCEP) (Nov, 21, 2012) Material (in Japanese).

Nishimura, T. (2012b): Crustal deformation of northeastern Japan based on geodetic data for recent 120 years, Journal of the Geological Society of Japan, vol. 118, No. 5, pp. 278-293.

No, T., T. Sato, S. Kodaira, T. Ishiyama, H. Sato, N. Takahashi, Y. Kaneda (2014): The source fault of the 1983 Nihonkai-Chubu earthquake revealed by seismic imaging, Earth and Planetary Science Letters, Vol. 400, pp. 14-25.

Noguera, E. and Ku. Abe (1992): Numerical experiment of the 1964 Niigata earthquake tsunami on a fine grid space, Programme and abstracts, the Seismological Society of Japan, No. 1, 81p.

Okal, E. A. (1999): Historical seismicity and seismotectonic context of the great 1979 Yapen and 1996 Biak, Irian Jaya Earthquakes, Pure and Applied Geophysics, Vol. 154, No. 3/4, pp. 633-675.

Okal, E. A., D. Reymond and S. Hongsresawat (2013): Large, pre-digital earthquakes of the Bonin-Mariana subduction zone, 1930-1974, Tectonophysics, Vol. 586, pp. 1-14.

Okamura, Y. (1993): Submarine geological survey of the source area of the 1993 Hokkaido Nansei Oki Earthquake by R/V Hakurei maru, Chishitsu News, No. 471, pp. 13-18.

Okamura, Y. (1998): A trial to estimate reverse fault and crustal shortening in the eastern margin of the Japan Sea, Chikyu monthly, Vol. 20, No. 8, pp. 460-465 (in Japanese).

Pacheco, J. F., L.R. Sykes and C.H. Scholz (1993): Nature of seismic coupling along simple plate boundaries of the subduction type, Journal of Geophysical Research, Vol. 98, No. B8, pp. 14133-14159.

Rajendran, K. (2013): On the recurrence of Great subduction zone earthquakes, Current Science, Vol. 104, No. 7, pp. 880-892.

Research and Development Bureau, Ministry of Education, Culture, Sports, Science and Technology-Japan (MEXT) and Graduate School of Science, Hokkaido University (2012): Research on earthquakes such as off Nemuro, etc. (FY 2011) Result report (in Japanese).

Satake, K. (1989): Inversion of tsunami waveforms for the estimation of heterogeneous fault motion of large submarine earthquakes: The 1968 Tokachi-oki and 1983 Japan Sea earthquakes, Journal of Geophysical Research, Vol. 94, No. B5, pp. 5627-5636.

Satake, K., K. Shimazaki, Y. Tsuji and K. Ueda (1996): Time and size of a giant earthquake in Cascadia inferred from Japanese tsunami records of January 1700, Nature, Vol. 379, pp. 246-249.

Satake, K. and K. Wang (1998): Coseismic Fault slip of the 1700 Cascadia Earthquake and its Implications to Seismic Coupling, Programme and abstracts, the Seismological Society of Japan, No. 2, 54p.

Satake, K. (2000): Examining the fault motion below the seabed from tsunami and deep ocean survey, Chikyu monthly, Extra edition No. 31, pp. 99-109 (in Japanese).

Satake, K. and Y. Kato (2000): Volume and Tsunami Origin of the 1741 Oshima Oshima flank collapse, Abstracts, Japan Earth and Planetary Science Joint Meeting, Vb-020 (in Japanese).

Satake, K., Y. Fujii, T. Harada and Y. Namegaya (2012): Time and space distribution of coseismic slip of the 2011 Tohoku earthquake as inferred from tsunami waveform data triggering of tsunami earthquake by deeper interplate earthquake, Programme and abstracts, the Seismological Society of Japan, Fall Meeting, 32p.

Satake, K., Y. Fujii, T. Harada and Y. Namegaya (2013): Time and Space Distribution of Coseismic Slip of the 2011 Tohoku Earthquake as Inferred from Tsunami Waveform Data, Bulletin of the

Seismological Society of America, Vol. 103, No. 2B, pp. 1473-1492.

Sato, R. (1989): Handbook of Seismic Fault Parameters in Japan, Kajima Institute Publishing, 390p. (in Japanese).

Scholz, C. H. and J. Campos (1995): On the mechanism of seismic decoupling and back arc spreading at subduction zones, Journal of Geophysical Research, Vol. 100, No. B11, pp. 22103-22115.

Scholz, C. H. and J. Campos (2012): The seismic coupling of subduction zones revisited, Journal of Geophysical Research, Vol. 117, B05310.

Scholz, C. H. (2014): Holocene Earthquake History of Cascadia: A Quantitative Test, Bulletin of the Seismological Society of America, Vol. 104, No. 4, pp. 2120-2124.

Seno, T. (2005): Plate Motions in the World, Journal of Geography (Chigaku Zasshi), Vol. 114, No. 3, pp. 350-366 (in Japanese with English abstract).

Shaw, B. E. and C. H. Scholz (2001): Slip-length scaling in large earthquakes: Observations and theory and implications for earthquake physics, Geophysical Research Letters, Vol. 28, pp. 2995-2998.

Shennan, I., A. Long and N. Barlow (2007): Recurrent Holocene paleoseismicity and associated land/sea-level changes in south central Alaska, USGS Earthquake Hazards Program Final Report, 06HQGR0033.

Shiba, Y. and T. Uetake (2011): Rupture Process of the 1964 MJMA 7.5 Niigata Earthquake Estimated from Regional Strong-Motion Records, Bulletin of the Seismological Society of America, Vol. 101, No. 4, pp. 1871-1884.

Shinohara, M., T. Yamada, K. Nakahigashi, S. Sakai, K. Mochizuki, K., Uehira, Y. Ito, R. Azuma, Y. Kaiho, T. No, H. Shiobara, R. Hino, Y., Murai, H. Yakiwara, T. Sato, Y. Machida, T. Shinbo, T. Isse, H. Miyamachi,, K. Obana, N. Takahashi, S. Kodaira, Y. Kaneda, K. Hirata, S., Yoshikawa, K. Obara, T. Iwasaki, and N. Hirata (2011): Aftershock observation of the 2011 off the Pacific coast of Tohoku Earthquake by using ocean bottom seismometer network, Earth, Planets and Space, Vol. 63, pp. 835-840.

Shishikura, M. (2013): History and postseismic deformation of the 1960 Chile earthquake (M_w= 9.5), Report of The Coordinating Committee for Earthquake Prediction, Japan, Vol. 89, pp. 417-420 (in Japanese).

Sieh, K., D. H. Natawidjaja, A. J. Meltzner, C. C. Shen, H. Cheng, K. S. Li, B. W. Suwargadi, J. Galetzka, B. Philibosian and R. L. Edwards (2008): Earthquake supercycles inferred from sea-level changes recorded in the corals of west Sumatra, Science, Vol. 322, pp. 1674-1678.

Somerville, P., K. Irikura, R. Graves, S. Sawada, D. Wald, N. Abrahamson, Y. Iwasaki, T. Kagawa, N. Smith, and A. Kowada (1999): Characterizing crustal earthquake slip models for the prediction of strong ground motion, Seismological Research Letters, Vol. 70, No. 1, pp. 59-80.

Stirling, M. W., D. Rhoades and K. Berryman (2002): Comparison of earthquake scaling relations derived from data of the instrumental and preinstrumental era, Bulletin of the Seismological

Society of America, Vol. 92, pp. 812-830.

Sugawara, D., F. Imamura, K. Goto and Y. Minoura (2013): Jogan tsunami and Tohoku earthquake tsunami, Analyzing the Great East Japan Earthquake 2 - Earthquake Disaster and Humanities, Towns and Records, Akashi Shoten, pp. 179-188 (in Japanese).

Sugino, H., Y. Iwabuchi, N. Hashimoto, K. Matsusue, K. Ebisawa, H. Kameda and F. Imamura (2014): The characterized tsunami source model regarding the Inter-plate Earthquake Tsunami, Journal of Japan Association for Earthquake Engineering, Vol. 14, Issue 5, pp. 1-18 (in Japanese with English abstract).

Takahashi, T., T. Takahashi and N. Shuto (1995): Analysis of the Hokkaido Nansei oki Earthquake by the tsunami numerical simulation, Abstracts, Japan Earth and Planetary Science Joint Meeting, 370p. (in Japanese).

Takemura, M. (1998): Scaling Law for Japanese Interplate Earthquakes in Special Relations to the Surface Faults and the Damages, Zisin (Journal of the Seismological Society of Japan, 2nd ser.), Vol. 51, pp. 211-228 (in Japanese with English abstract).

Tang, G., P. J. Barton, L. C. McNeill, T. J. Henstock, F. Tilmann, S. M. Dean, M. D. Jusuf, Y. S. Djajadihardja, H. Permana, F. Klingelhoefer and H. Kopp (2013): 3-D active source tomography around Simeulue Island offshore Sumatra: Thick crustal zone responsible for earthquake segment boundary, Geophysical Research Letters, Vol. 40, pp. 48-53.

Tanioka, Y., Yudhicara, T. Kususose, S. Kathiroli, Y. Nishimura, S. Iwasaki and K. Satake (2006): Rupture process of the 2004 great Sumatra-Andaman earthquake estimated from tsunami waveforms, Earth, Planets and Space, Vol. 58, pp. 203-209.

Tanioka, Y. (2013): Summary of great earthquakes occurred along the Alaska-Aleutian-Kamchatka subduction zone, Report of The Coordinating Committee for Earthquake Prediction, Japan, Vol. 89, pp. 425-428 (in Japanese).

The Headquarters for Earthquake Research Promotion, Earthquake Research Committee (2004): Long-Term Evaluation of Seismic Activity along the Kuril Trench (Second Edition) (in Japanese).
http://jishin.go.jp/main/chousa/04dec_chishima2/index.htm (Accessed on Aug. 2016)

The Headquarters for Earthquake Research Promotion, Earthquake Research Committee (2009): Strong ground motion prediction method of earthquakes occurred by specified earthquake faults ("Recipe") (in Japanese).
http://jishin.go.jp/main/chousa/09_yosokuchizu/g_furoku3.pdf (Accessed on Aug. 2016).

The Headquarters for Earthquake Research Promotion, Earthquake Research Committee (2010): "Long-Term Evaluation Method of Active Fault" Report (Preliminary Version) (in Japanese).
http://www.jishin.go.jp/main/choukihyoka/katsu_hyokashuho/honpen.pdf
(Accessed on Aug. 2016)

The Headquarters for Earthquake Research Promotion, Earthquake Research Committee (2011): Long-Term Evaluation of Earthquake Activity from Sanriku-Oki to Boso Oki (Second Edition) (in Japanese).
http://www.jishin.go.jp/main/chousa/11nov_sanriku/ (Accessed on Aug. 2016)

The Headquarters for Earthquake Research Promotion, Earthquake Research Committee (2013): Long term evaluation of seismic activity of the Nankai Trough (Second Edition). http://jishin.go.jp/main/chousa/13may_nankai/index.htm (in Japanese, accessed on Aug. 2016).

Tsuji, Y. (1994): Tsunami earthquake that occurred in history, Chikyu monthly, Vol. 16, No. 2, pp. 73-85 (in Japanese).

Tsuji, Y., K. Ueda and K. Satake (1998): Japanese Tsunami Records from the January 1700 Earthquake in the Cascadia Subduction Zone, Zisin (Journal of the Seismological Society of Japan, 2nd ser.), Vol. 51, pp. 1-17 (in Japanese with English abstract).

Tsukahara, H. (1999): Current crustal stress field in the Japanese archipelago, Chikyu monthly, Vol. 21, No. 10, pp. 660-666 (in Japanese).

The Tsunami Evaluation Subcommittee, The Nuclear Civil Engineering Committee, JSCE (Japan Society of Civil Engineers) (2002): Tsunami Assessment Method for Nuclear Power Plants in Japan.

Uchida, N. and T. Matsuzawa (2011): Coupling coefficient, hierarchical structure, and earthquake cycle for the source area of the 2011 off the Pacific coast of Tohoku earthquake inferred from small repeating earthquake data, Earth, Planets and Space, Vol. 63, pp. 675-679.

Wallace, L. M., Å. Fagereng and S. Ellis (2012): Upper plate tectonic stress state may influence interseismic coupling on subduction megathrusts, Geology, Vol. 40, pp. 895-898.

Wang, K. and S. L. Bilek (2014): Invited review paper: Fault creep caused by subduction of rough seafloor relief, Tectonophysics, Vol. 610, pp. 1-24.

Watanabe, H. (1998): List of Damaging Japanese tsunami (2nd edition), Tokyo University Publishing, 238p. (in Japanese).

Wu, W-N., H. Kao, S-K. Hsu, C-L. Lo and H-W. Chen (2010): Spatial variation of the crustal stress field along the Ryukyu-Taiwan-Luzon convergent boundary, Journal of Geophysical Research, Vol. 115, B11401.

Yamamoto, Y., K. Obana, T. Takahashi, A. Nakanishi, S. Kodaira and Y. Kaneda (2013): Imaging of the subducted Kyushu-Palau Ridge in the Hyuga-nada region, western Nankai Trough subduction zone, Tectonophysics, Vol. 589, pp. 90-102.

Yasuda, T., T. Maruyama, K. Goda, N. Mori and H. Mase (2015): Uncertainty analysis of Nankai Trough earthquake tsunamis using stochastic source model, Journal of Japan Society of Civil Engineers, Ser. B2 (Coastal Engineering),Vol. 71, No. 2, pp. I_295-I_300.

Ye, L., T. Lay and H. Kanamori (2012): The Sanriku-Oki low-seismicity region on the northern margin

of the great 2011 Tohoku-Oki earthquake rupture, Journal of Geophysical Research, Vol. 117, B02305.

Yokose, H., H. Sato, Y. Fujimoto, M. Hannah, T. Mirabueno, T. Kobayashi, K. Akimoto, H. Yoshimura, Y. Morii, N. Yamawaki, T. Ishii and E. Honza (2010): Mid-Pleistocene Submarine Acidic Volcanism of the Tokara Islands, Japan, Journal of Geography (Chigaku Zasshi), Vol. 119, pp. 46-68 (in Japanese with English abstract).

Yue, H. and T. Lay (2011): Inversion of high-rate (1sps) GPS data for rupture process of the 11 March 2011 Tohoku earthquake (M_w9.1), Geophysical Research Letters, Vol. 38, L00G09.

Zhao, D., Z. Huang, N. Umino, A. Hasegawa and H. Kanamori (2011): Structural heterogeneity in the megathrust zone and mechanism of the 2011 Tohoku-oki earthquake (M_w9.0), Geophysical Research Letters, Vol. 38, L17308.

Chapter 3. Examination of Effects of Tsunami Source Uncertainty on Tsunami Height

3.1. Typical factors in parametric studies of uncertainty concerning tsunami resulting from fault motion

Although, in principle, parametric studies use a standard fault model to examine the factors (indicated with a circle) shown in Table 3.1-1, factors determined to have low uncertainty may be excluded.

Table 3.1-1 shows the approach employed for limited sea areas. When assessing probable maximum tsunamis in other sea areas, factors may be selected for implementing parametric studies based on similar examination methods.

Table 3.1-1 Parameters to be examined in parametric studies (X: Factors to implement parametric studies in principle)

	Static parameters							Kinematic parameters		
Region or type of earthquake	Plane Position	Position of large slip region	Strike angle	Dip angle	Dip direction	Slip angle (Rake)	Depth of fault top	Rupture starting point	Rupture velocity	Rise time
In case of heterogeneous model: Interlocking of interplate thrust fault earthquake and tsunami earthquake, or interplate thrust fault earthquake	X*1	X	-	-	-	X*2	-	X	X	X
In case of homogeneous model: Interplate thrust fault earthquake	X*1	-	X	X	-	X	X	-	-	-
Along the Japan Trench (Intraplate normal fault)	X	-	X	X	-	- (Fixed at 270°)	X	-	-	-
In case of homogeneous model: Along the Japan Trench (Tsunami earthquake)	X	-	X	X	-	X*2	X	-	-	-
The Eastern margin of the Japan Sea (Crustal earthquake)	X	X	X	X	X*4	- (Fixed at 90°)	X	-	-	-
Submarine active fault (Upper-crust earthquake)	-	X*5	-	X*5	X*6	X*3	X	-	-	-

*1 Except when applying the standard fault model to the entire seismic region *2 Set according to strike angle considering uncertainty in sliding direction

*3 Set according to dip angle considering the variancevariance of stress field *4 Westward inclination and eastward inclination

*5 Fixed when obvious by survey *6 Set both directions for faults without information

3.2. Range of factors for which uncertainty is relatively high in parametric studies

For the eastern margin of the Japan Sea, the standard fault model configures the dip angle between 30° and 60°, and in cases where the presence of submarine active faults is unknown, the dip is believed to be between 45° and 90° (Southwestern Japan) or between 30° and 60° (Chuetsu region). The orientation of the P axis (principle axis of pressure) in a regional stress field is believed to be held within a range between 90° and 120° for southwestern Japan and between 110° and 140° for the Chuetsu Region (both are clockwise from the north). In these cases, the parameters of the standard fault model have a range.

3.3. Case studies examining the impact that uncertainty about tsunami source has on tsunami height

Here, the impact that uncertainty involving the fault parameters of a tsunami source model has on tsunami height along the coastline is assessed by performing numerical simulations of tsunami. Of the static parameters examined such as strike and dip angle, the impact due to parameters related to uncertainty associated with dynamic fracture of faults such as the fracture initiation point were examined for the Nankai Trough and the eastern margin of the Japan Sea.

3.3.1. Impact of moment magnitude

Because the magnitude of the tsunami height is mainly controlled by the magnitude of slip amount of the fault plane, the effect of moment magnitude (M_W) varies depending upon the scaling law applied. The relationship between M_W and Slippage D for three scaling laws is given below.

(1) Case where an upper limit is not set for the fault plane: $\log D \propto 0.5\, M_W$

(2) Case where an upper limit is set only for the width of the fault plane: $\log D \propto 0.75\, M_W$

(3) Case where an upper limit is set for the length and width of the fault plane: $\log D \propto 1.5\, M_W$

When this relationship is utilized, if M_W is increased 0.1, slip amount will increase by 1.12 times in the case of (1), 1.19 times in the case of (2), and 1.41 times in the case of (3).

Cases where numerical simulations have actually been performed are shown in Figures 3.3.1-1 through 3.3.1-3. Each figure shows the lines of magnification (inclination) anticipated based upon the increase in slip amount. As is clear from the diagrams, the rate of increase in the tsunami height based on the numerical simulations correspond for the most part to the rate of increase of slip amount.

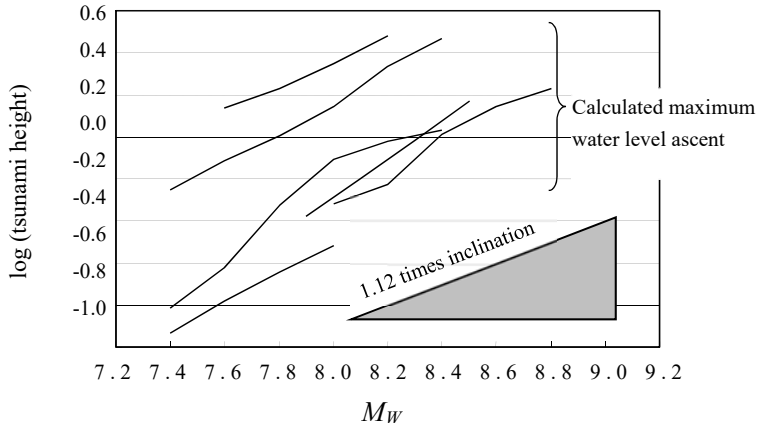

Figure 3.3.1-1 Example of examination of the influence of M_W on tsunami water level (Scaling law (1), Along Japan Trench)

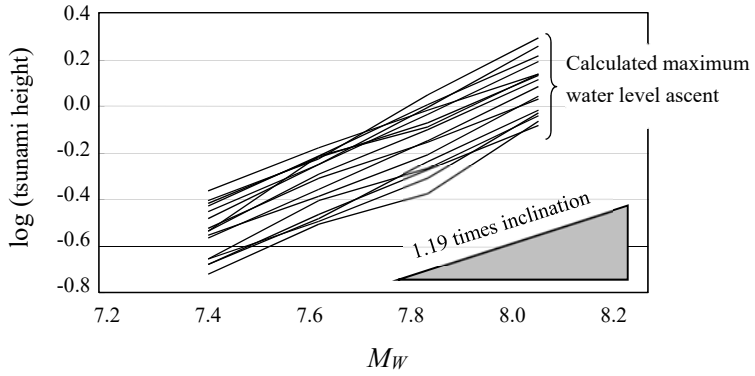

Figure 3.3.1-2 Example of examination of the influence of M_W on tsunami water level (Scaling law (2), Sea area around Southwest Japan)

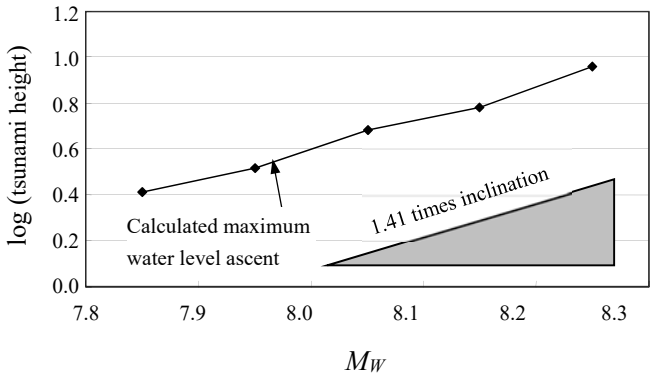

Figure 3.3.1-3 Example of examination of the influence of M_W on tsunami water level (Scaling law (3), Nankai Trough)

3.3.2. Impact of plane position of tsunami source

(1) Example of sea area along the Japan Trench

Figure 3.3.2-1 shows the distribution of the maximum water level ascent along the coastline and the plane position of the examined tsunami source. The horizontal axis is normalized using the maximum value for all cases and is a relative ratio. For the fault models, M_W=7.6, Fault length L=77 km, Fault width W= 46.3 km, and Slippage D= 1.81 m are the same, three cases were configured for the offshore direction so that they would be aligned with a plate boundary surface having a dip angle of 10° (fault depths for the three cases: fault upper edge depth d=15 km, 27 km and 39 km) and three cases for the north-south direction so that there were a total of 3x3 cases. Dip angle δ= 10° and the slip angle λ=85° were uniform.

The basic grid size along the coastline is 320 m. However, somewhat more detailed grids have been used at points where the grid size is 160 m at solid triangles and 80 m at solid star. In the distribution of the maximum water level ascent along the coastline, features are seen such as the tendency for the maximum water level ascent to become greater as the tsunami source is positioned in front of a target point as well as the tendency for the maximum water level ascent to become greater as the tsunami source is positioned in sea areas where the water depth is greater offshore.

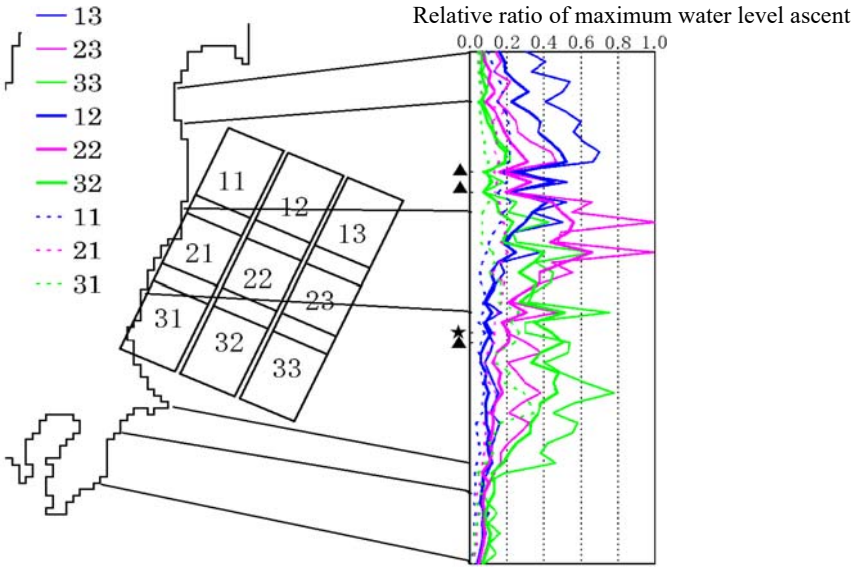

Figure 3.3.2-1 Influence of tsunami source location around the Japan Trench on coastal maximum water level ascent distribution

(2) Example of sea area along the eastern margin of the Japan Sea

Figure 3.3.2-2 shows the distribution of relative ratios of the maximum water level ascent

along the coastline and the plane position for the examined tsunami sources. The fault models were configured so that M_W=7.8, L=120 km, W=17.3 km, Slippage D=8.66 m, as well as δ=60° and λ=90° in a western inclination are uniform, and only the position is changed for the five cases.

The basic grid size along the coastline is 800 m. A 400 m grid size has been used at points where consideration is given to the effect that the Yamato Ridge, Oki Islands and other features have on the tsunami propagation characteristics. In the distribution of the maximum water level ascent along the coastline, features are seen such as the tendency for the maximum water level ascent to increase as the tsunami source is positioned in front of a target point as well as a greater impact due to the propagation route than the position of the tsunami source in cases where the target point is far from the tsunami source.

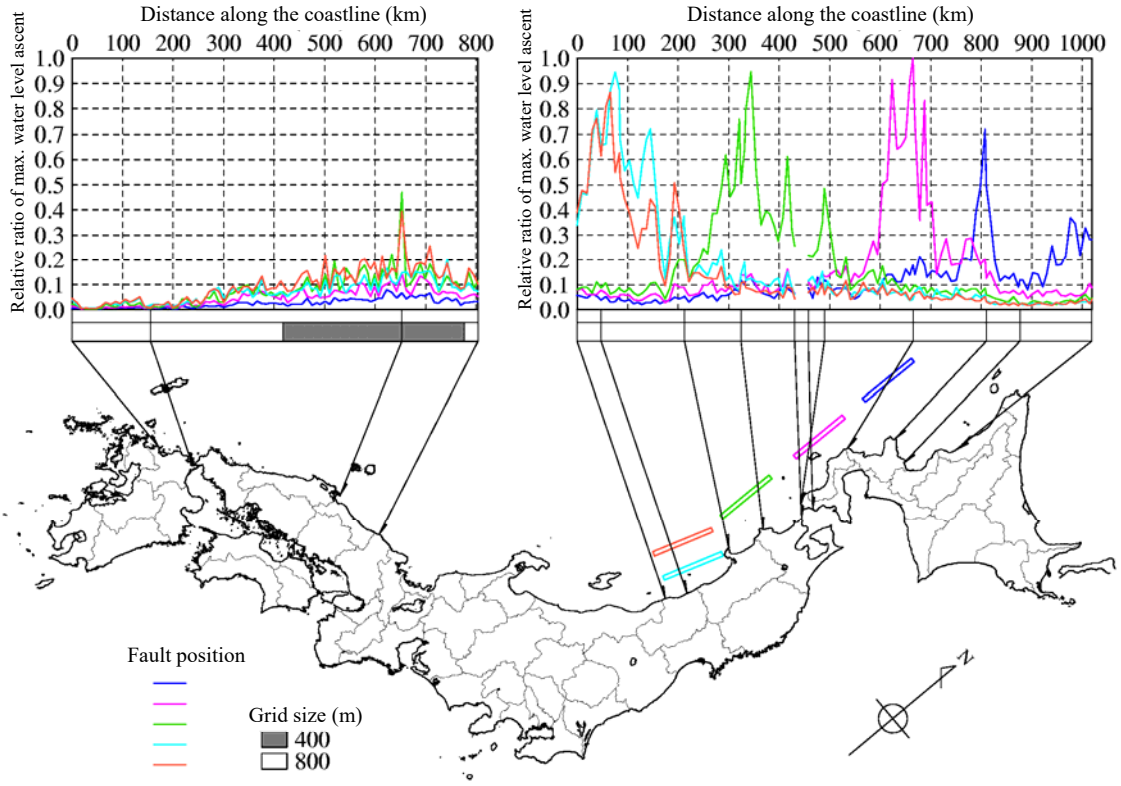

Figure 3.3.2-2 Influence of tsunami source location in the eastern margin of the Japan Sea on coastal maximum water level ascent distribution

3.3.3. Impact of fault upper edge depth

Examples of cases examined where only the depth of the fault upper edge was changed without altering other conditions are shown in Figure 3.3.3-1 (earthquakes in sea areas along the eastern margin of the Japan Sea) and Figure 3.3.3-2 (earthquakes in sea areas along the Japan Trench).

For the examination of earthquakes along the eastern margin of the Japan Sea as shown in Figure 3.3.3-1, fault models were configured for four cases where M_W=7.8, L=120 km, W=17.3 km, Slippage D=8.66 m, λ=90° and Plane position were uniform, and the dip direction and angle were changed. The vertical axes in the figure indicate the ratio of the maximum values in all cases, and the effect that depth of the fault upper edge has on maximum water level ascent varies depending upon the target point, and no clear trends have been able to be discerned.

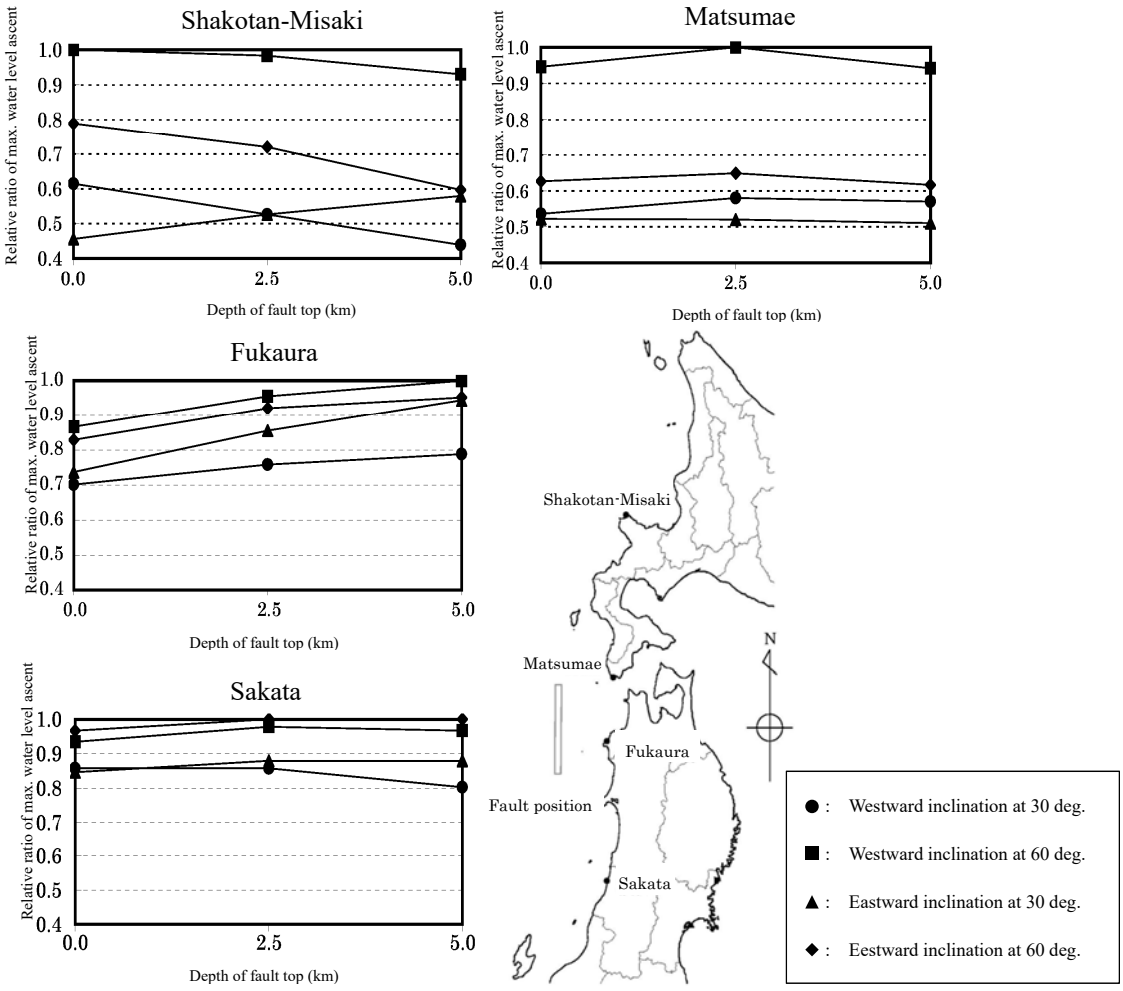

Figure 3.3.3-1 Example of examination of the influence of upper edge depth of fault on maximum water level ascent in the eastern margin of the Japan Sea

For the examination of earthquakes in the sea area along the Japan Trench as shown in Figure 3.3.3-2, Fault (1) (normal fault earthquake) and Fault (2) (tsunami earthquake) were taken into consideration. The fault models for the normal fault earthquake set M_W=8.5, L=219 km, W=59.2 km, Slippage D=7.81 m, δ=45°, λ=270°, and Plane position as uniform, and the fault models for tsunami

earthquake set M_W=8.2, L=200 km, W=50.0 km, Slippage D=7.18 m, δ=20°, λ=95°, and Plane position as uniform. The effect of the depth of the fault upper edge was not straightforward, and there were both points where the maximum water level ascent increased as the fault upper edge depth deepened as well as points where the reverse was observed.

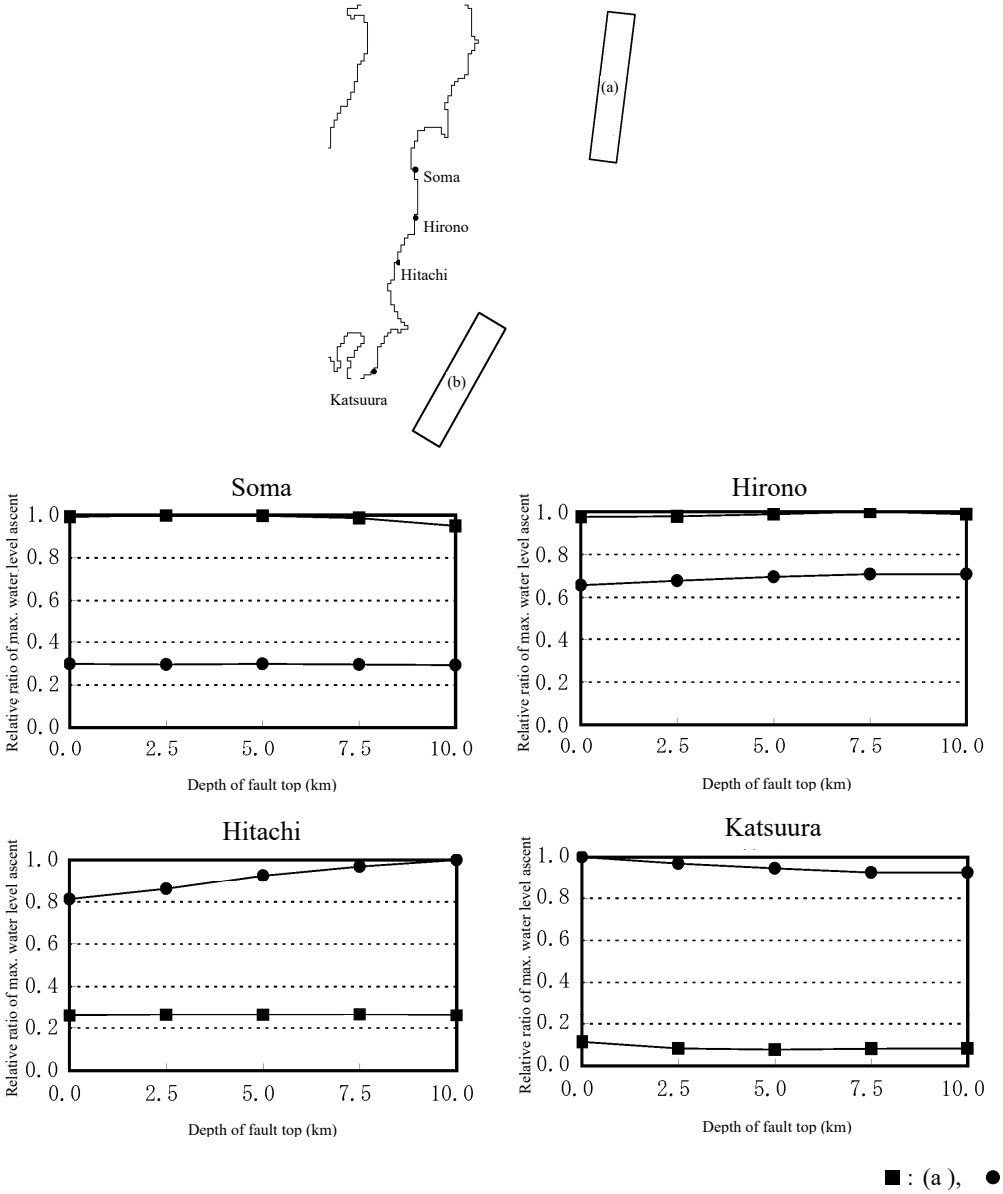

Figure 3.3.3-2 An example of examination of the effect of the upper edge depth of fault on the maximum water level ascent in the sea area along the Japan Trench

3.3.4. Effect of strike

Cases examined where only strike was changed without changing other conditions are shown in

Figure 3.3.4-1 (earthquakes in sea areas along the eastern margin of the Japan Sea) and Figure 3.3.4-2 (earthquakes in sea areas along the Japan Trench).

Figure 3.3.4-1 shows the plane position, distribution of maximum water level ascent along the coastline, and the effect of strike at each point for the examined tsunami sources. The fault models were configured so that, for five cases, M_W=7.8, L=120 km, W=17.3 km, Slippage D=8.66 m, as well as a western inclining δ=60° and λ=90° and d=1 km are uniform, and only strike is varied. By varying strike, points are also seen where the magnitude of the reference strike varies between 0.6 and 1.8 times. Also, there is a tendency for the maximum water rise to be greater at strike where the fault is upright with respect to the target point.

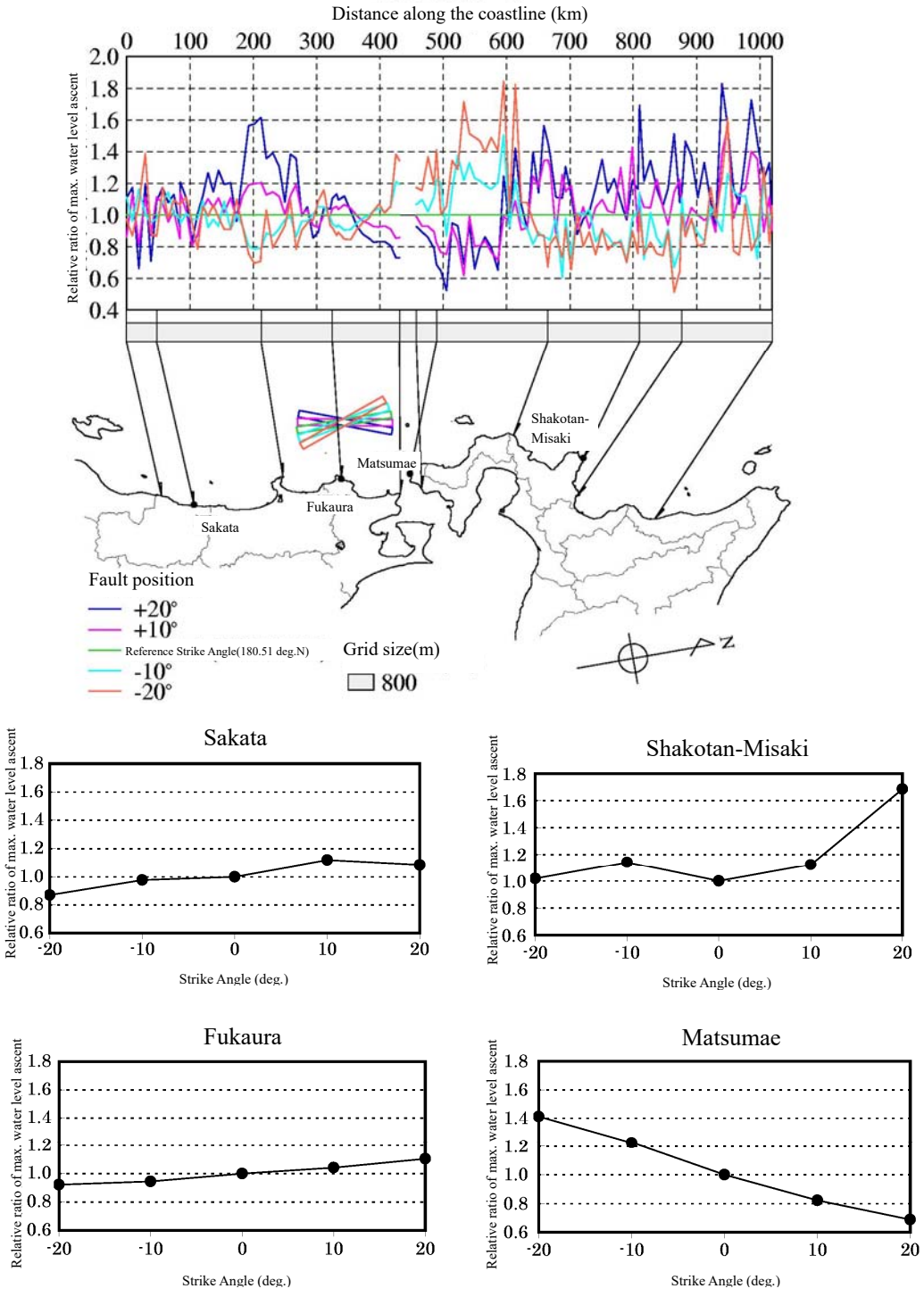

Figure 3.3.4-1 Example of examination of the effect of fault strike on the maximum water level ascent in the eastern margin of the Japan Sea

Figure 3.3.4-2 shows the plane position, distribution of maximum water level ascents along the coastline and the effect of strike at each point for the examined tsunami sources. The fault models

(tsunami earthquakes along sea trenches) were configured so that M_W=8.2, L=200 km, W=50.0 km, Slippage D=7.18 m, as well as δ=20° and λ=95° and d=1 km are the same for five cases, and only strike is varied. By varying strike, points are also seen where the magnitude of reference strike varies between 0.6 and 1.5 times. Also, just as in Figure 3.3.4-1, there is a tendency for the maximum water level ascent to be greater at strike where the fault is upright with respect to the target point.

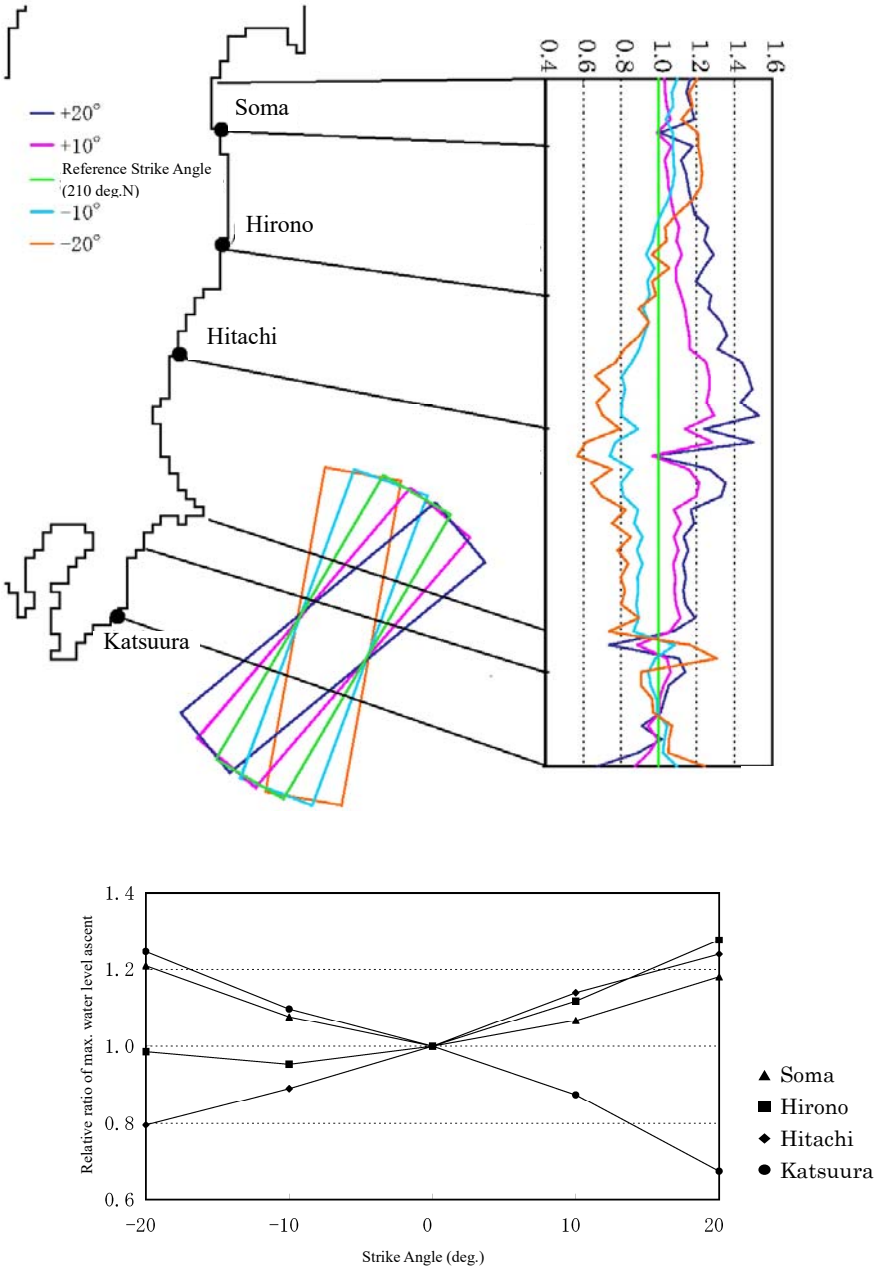

Figure 3.3.4-2 Example of influence of fault strike on the coastal maximum water level distribution along the Japan Trench

3.3.5. Effect of dip direction and angle

(1) Effect of dip direction and angle

Figure 3.3.5-1 shows cases where the effect has been examined of fault dip direction for five tsunami sources along the eastern margin of the Japan Sea. The same model is used for parameters other than dip direction, and computing the ratio of the maximum water level ascent as a western dip/eastern dip, the occurrence probability distribution is shown for each target point position (Shakotan-Misaki, Matsumae, Fukaura and Sakata). The fault models were configured using a combination of conditions where M_W was set between 7.4 and 7.8, thickness of the seismogenic layer at 15 km and 20 km, δ at 30° and 60°, λ=90°, and d=0 km. Although tendencies differ depending upon the target point in a relative comparison of the maximum water level ascent in cases where the fault has a westerly dip and cases where the fault has an easterly dip, basically, the ratio of the maximum water level ascent at all points was mainly distributed around 1.0, and no extreme variances have been established.

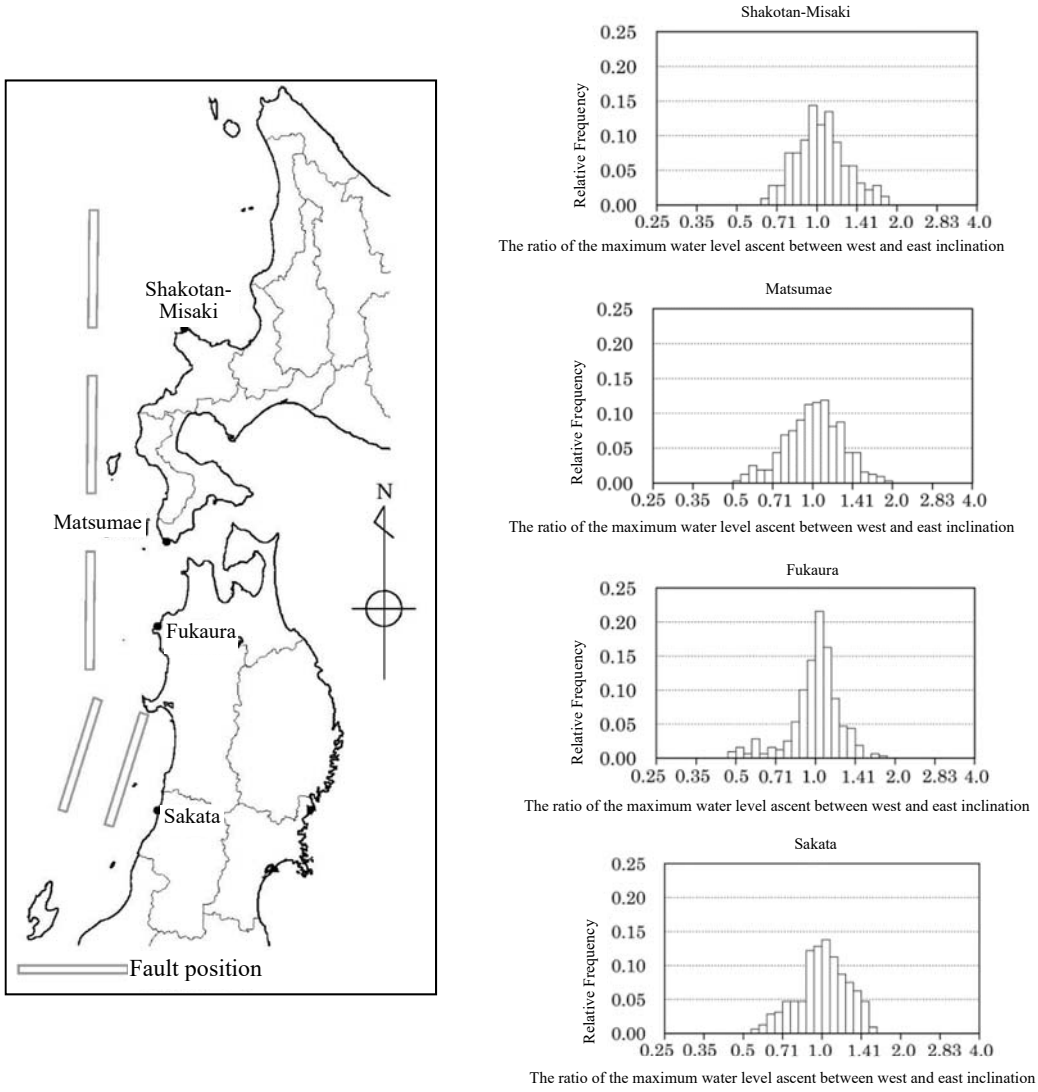

Figure 3.3.5-1 Examination of the influence of the dip direction of the fault in the eastern margin of the Japan Sea on the maximum water level ascent

(2) Effect of fault dip angle

Figure 3.3.5-2 shows examples of examinations conducted of the effect of dip angle for two tsunami sources along the Japan Trench. The fault models for Fault (1) use the same parameters of M_W=7.6, L=77 km, W=46.3 km, D=1.78 m, λ=85°, d=27 km, and Plane position, and the fault models for Fault (2) (tsunami earthquake) use the same parameters of M_W=8.2, L=200 km, W=50.0 km, Slippage D=1.78 m, λ=95°, d=1 km, and Plane position. As may be seen for Katsuura, there are cases where the effect on the dip angle due to target position is manifested significantly in maximum water level ascent as well as cases where almost no effect is seen. In addition, even at the same target point, there are cases where the tsunami source position affects the intensity of the effect of the dip angle as well as cases where the tendency of change is reversed.

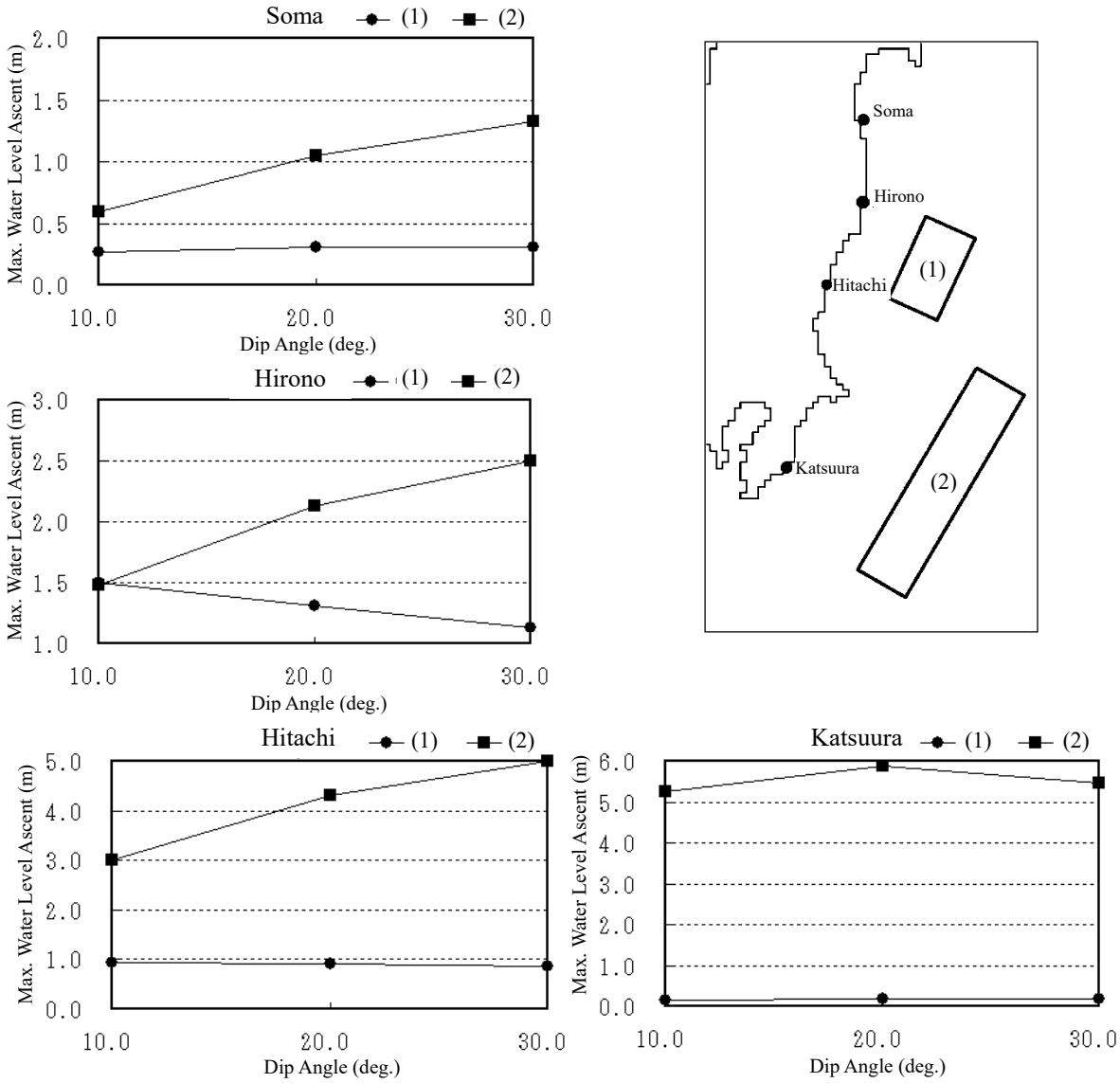

Figure 3.3.5-2 Examination of the influence of the dip angle of the fault on the maximum water level ascent in the sea area along the Japan Trench

3.3.6. Effect of slip angle

Figure 3.3.6-1 shows cases of examinations conducted of the effect of slip angle on tsunami sources along the eastern margin of the Japan Sea, and Figure 3.3.6-2 shows cases of examinations conducted where the tsunami sources are active faults in southwestern Japan.

Figure 3.3.6-1 shows the relationship between the target point and plane position of examined tsunami sources as well as the effect of slip angle for each point. The fault models were configured so

that M_W=7.8, L=120 km, W=17.3 km, Slippage D=8.66 m, as well as a westerly dipping δ=60°, and d=0 km are the same for five cases, and the slip angle was varied. There were four cases, the highest number, in which there were points where the maximum water level ascent was the greatest when the slip angle was 90°.

Similarly, Figure 3.3.6-2 shows the relationship between target point and plane position of examined tsunami sources as well as the effect of slip angle for each point. The fault models were configured so that L=50 km, W=15 km, Slippage D=4.16 m, δ=90°, and d=0 km were the same for six cases, and the slip angle was varied from 105° to 180°, which was the range estimated from the regional stress field. At all of the points, the maximum water level ascent was the greatest when the slip angle was at 105°, which is the angle closest to a pure dip slip.

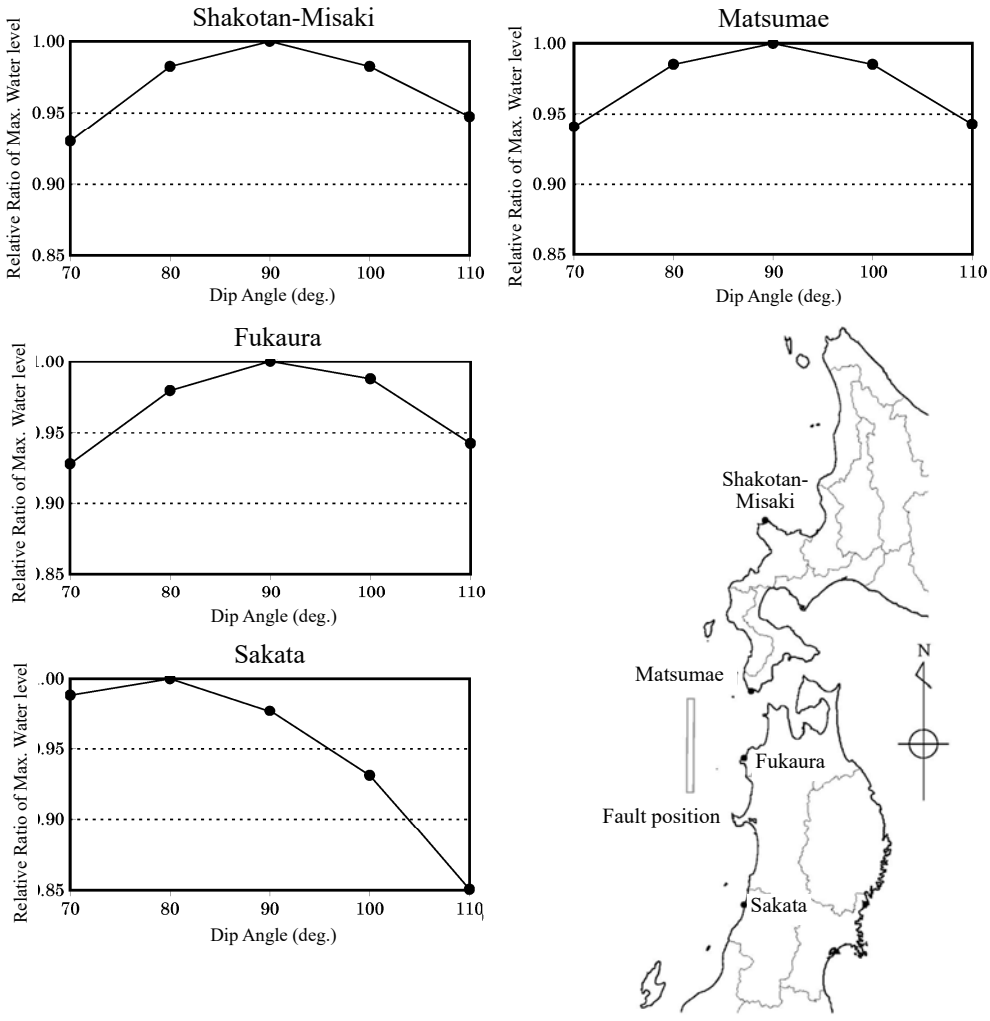

Figure 3.3.6-1 Examples of examination of the influence of slip angle on maximum water level ascent in the eastern margin of the Japan Sea

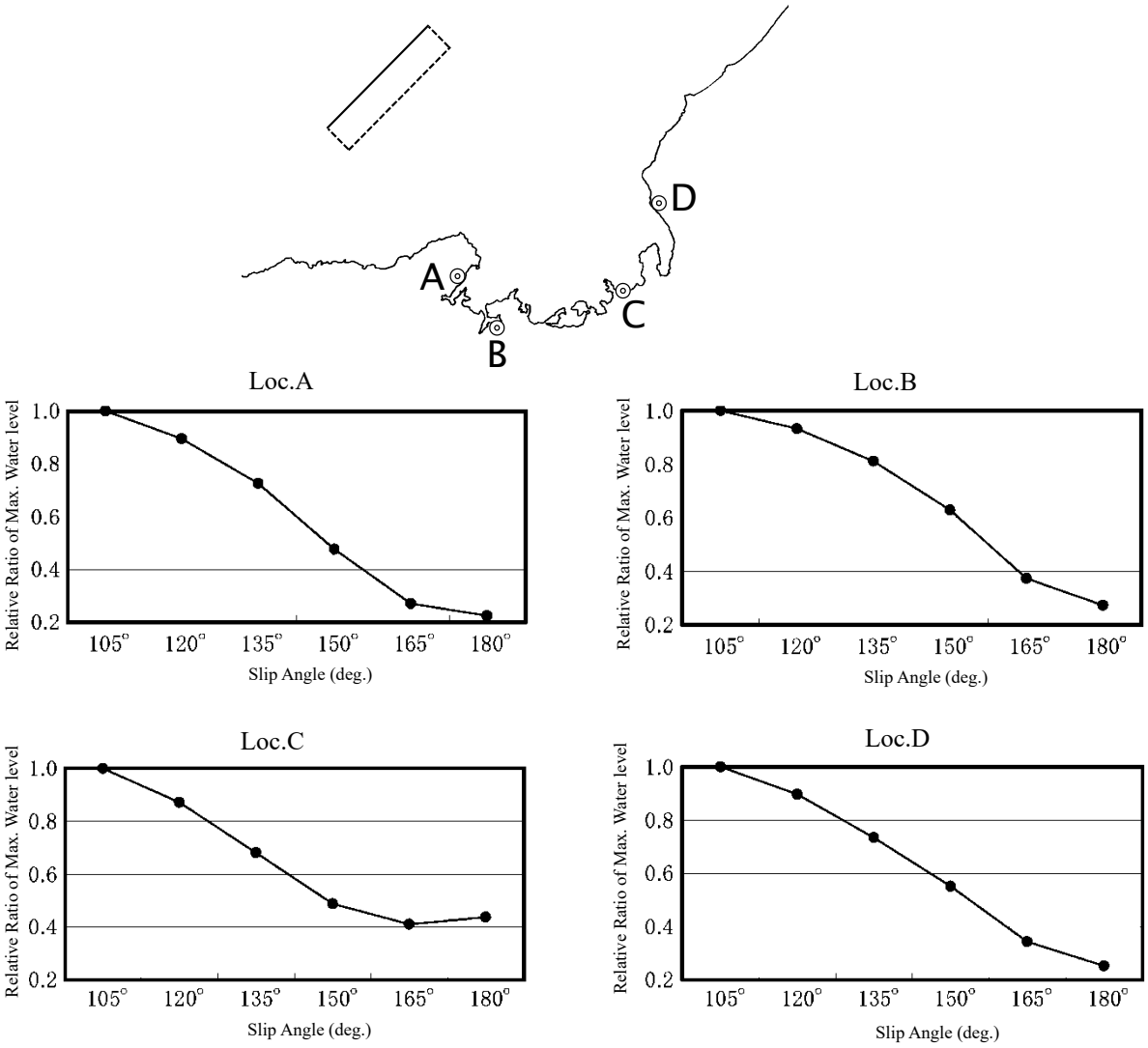

Figure 3.3.6-2 Examples of examination of the influence of slip angle on maximum water level ascent where the tsunami source is an active fault in southwestern Japan

3.3.7. Effect of thickness of the seismogenic layer

In cases where the tsunami source is a seismic region along the eastern margin of the Japan Sea or an active fault in southwestern Japan, the thickness of the seismogenic layer is assumed to be between 15 and 20 km. If the seismic moment (moment magnitude) is considered to be equal, then a change in slip amount is inversely proportional to a change in the width of the fault plane such that 15km/20km=1.33 times. Examples of cases calculated where the tsunami sources are active faults in southwestern Japan are shown in Figure 3.3.7-1.

The fault models, which were examined and shown in Figure 3.3.7-1, were configured using a combination of conditions where M_W was set between 7.1 and 7.5, δ at 45°, 67.5° and 90°, λ between 105° and 180° (AF1) and between 110° and 180° (AF2), and d=0 km. A noticeable trend was observed where the maximum water level ascent in a case, in which the seismogenic layer thickness was set at 15 km, was between 1 and 1.3 times that of a case where thickness was set at 20 km.

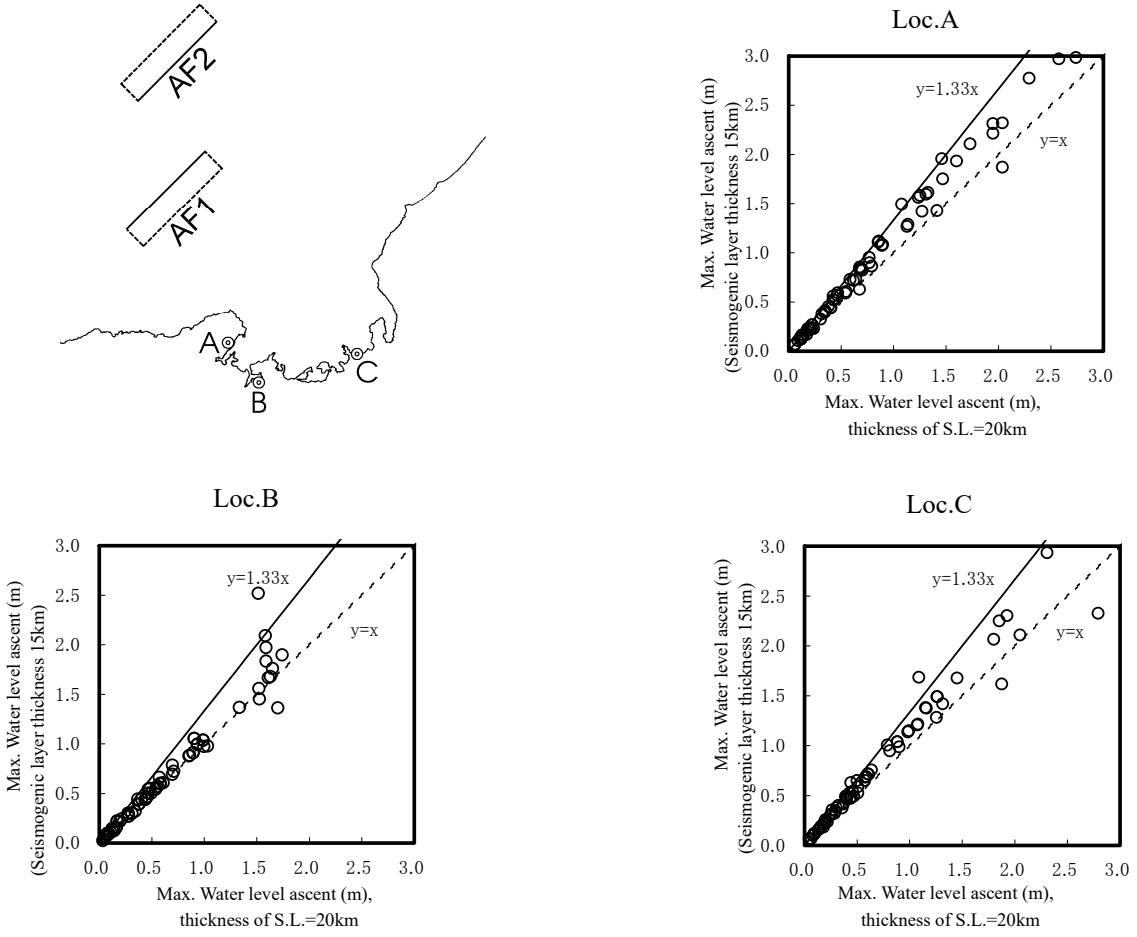

*S.L. = Seismogenic layer

Figure 3.3.7-1 Example of examination of the influence of the thickness of the seismogenic layer on maximum water level ascent in case of active fault in Southwest Japan as tsunami source

3.3.8. Effect of combining multiple segments

The Nankai Trough is comprised of multiple segments. Figure 3.3.8-1 shows changes in the maximum water level ascent at target points along the coastline using combinations of hypothesized

segment partitions (N1 alone, N2 alone, N1+N2, N3+N4, N2+N3+N4, and N1+N2+N3+N4). In cases where multiple segments are taken into consideration, the timing also differs depending on the target point when the waveforms of a tsunami striking from each segment will overlap with other tsunami. Accordingly, it is difficult to find a clear correlation between earthquake energy and the maximum water level ascent along the coastline such that the relationships are specific to the segment partition and target point.

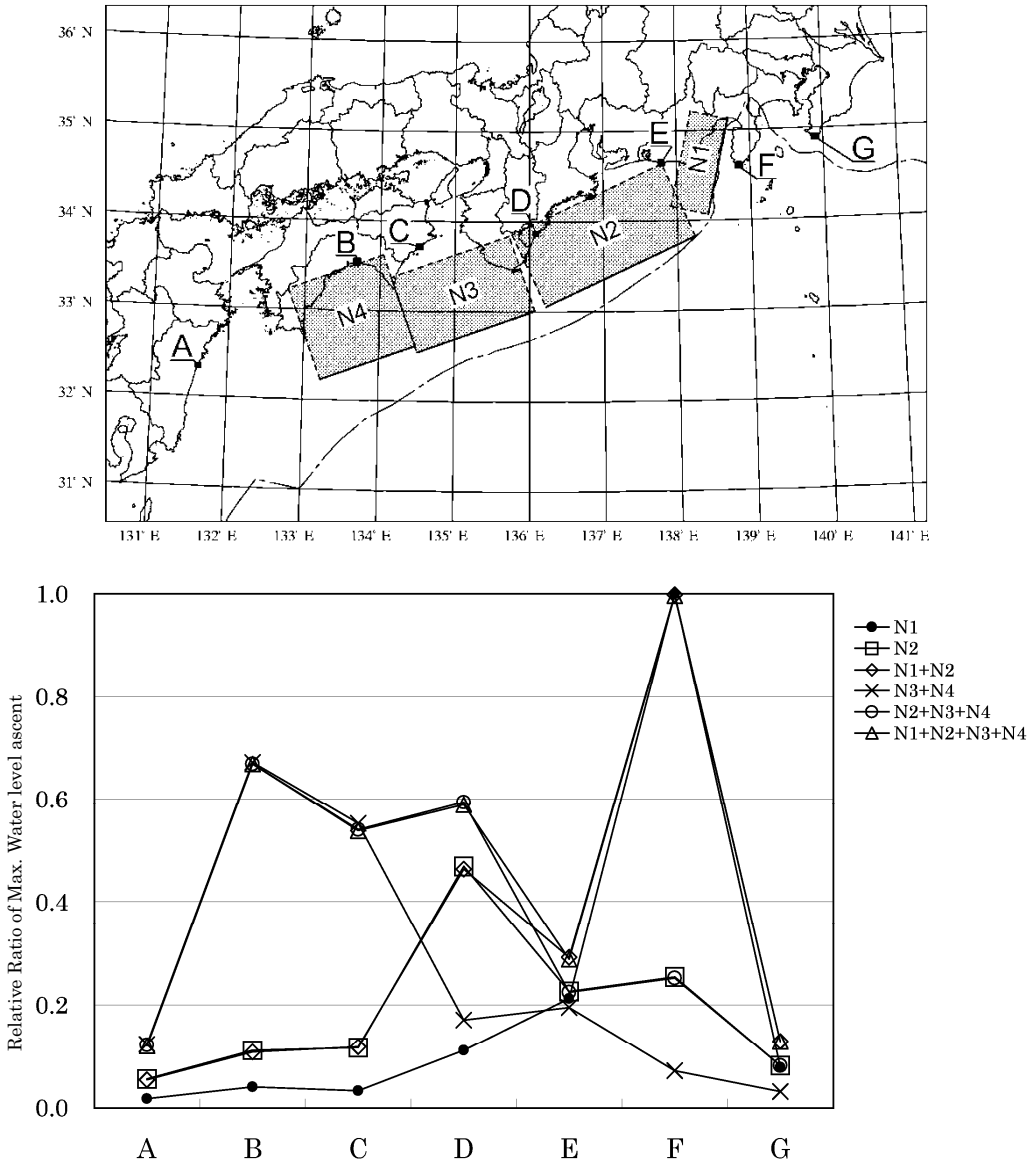

Figure 3.3.8-1 Example of examination of the influence of the combination of segments along the Nankai Trough on the maximum water level ascent

3.3.9. Effect of fault plane shape and stress drop

Figure 3.3.9-1 shows examples where the ratio of fault width to fault length was varied from 0.3 to 0.7 to examine the effect of the shape of fault planes along the Japan Trench. The fault models were configured so that M_W=8.1, D=3.15 m, δ=10° and λ=85° are the same for five cases, and the ratio between width and length was varied. The trends, which showed a change in the maximum water level ascent differ depending upon the target point, are believed to be due to changes in response characteristics and other factors accompanying changes in the basic inherent period as well as propagation characteristics attendant upon the relative positional relationship with the tsunami source.

Figure 3.3.9-2 shows examples with respect to tsunami sources along the eastern margin of the Japan Sea where seismic moment was fixed and slip amount varied in keeping with the change in fault length to examine the effect of static stress drop. The fault models were configured so that M_W=7.8, W=17.3km, westerly dipping δ=60°, d=0 km, and λ=90° are the same for five cases, and the fault length was set at 0.8, 1.0 and 1.25 times the reference model (L=120 km). There are many points where the maximum water level ascent is the highest when the slip angle is 90°. Also, there are many cases showing a tendency for the maximum water level ascent to increase along with an increase in stress drop.

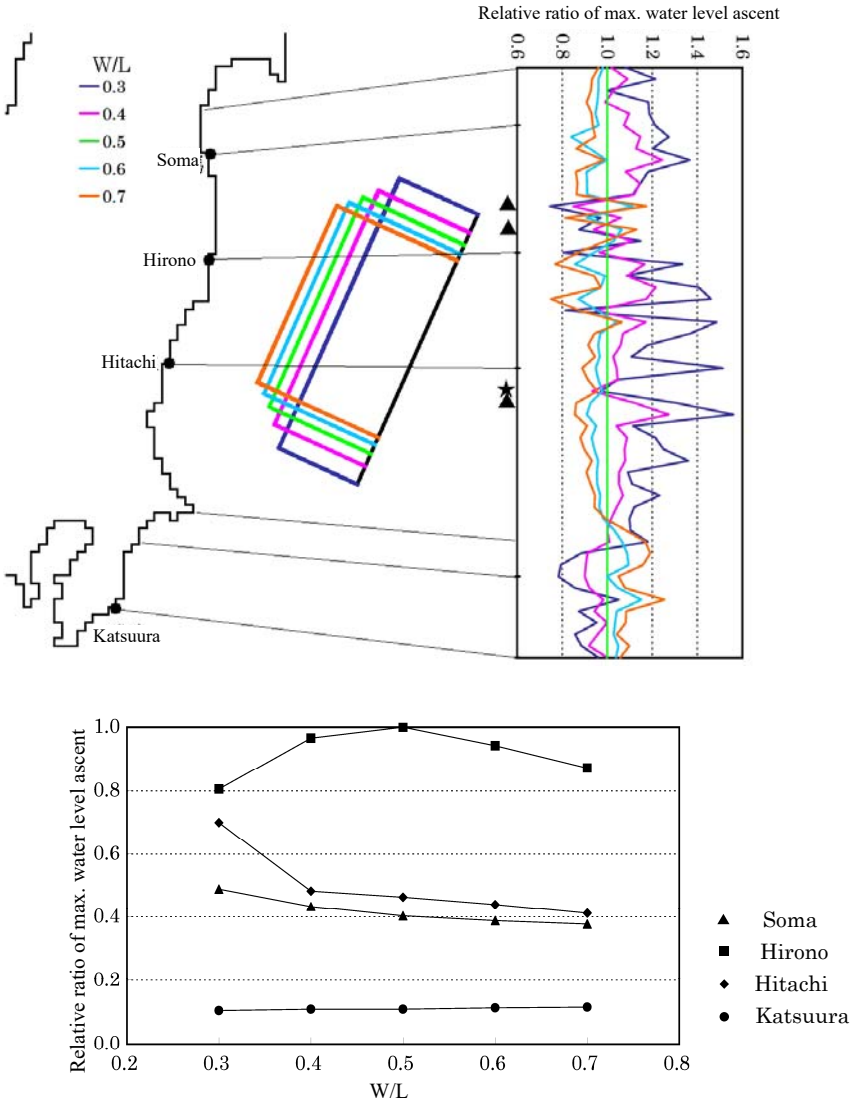

Figure 3.3.9-1 An example of examination of the influence of the fault plane shape on the maximum water level ascent in the sea area along the Japan Trench

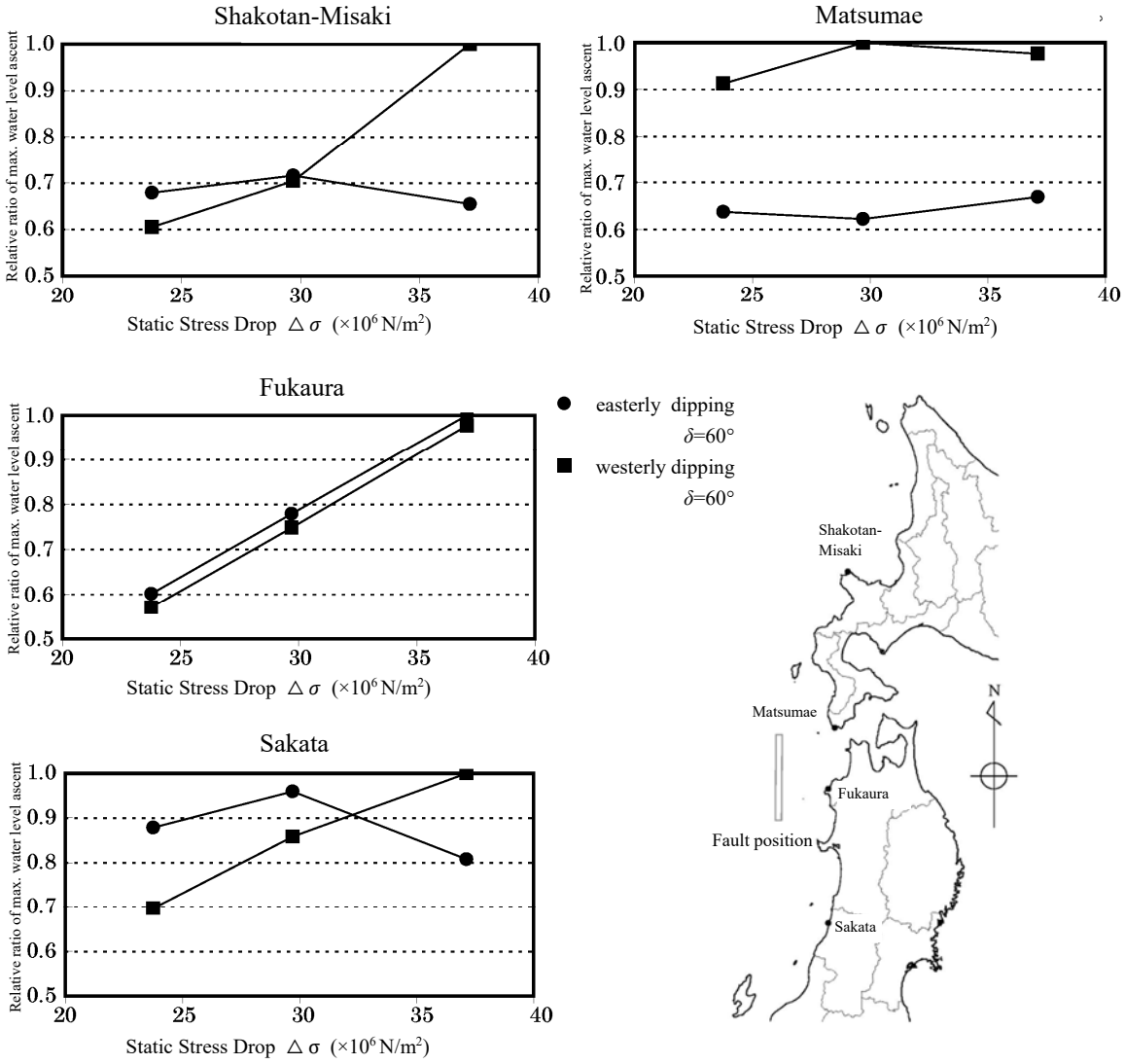

Figure 3.3.9-2 Examples of examination of the influence of stress drop amount in the margin of eastern margin of the Japan Sea on maximum water level ascent

3.3.10. Effect of heterogeneity in fault dislocation

For earthquakes presumed to have a heterogeneous distribution of slip (the 1968 earthquake off the coast of Tokachi, the 1946 Nankai earthquake, and the 1983 earthquake in the central part of the Japan Sea), numerical simulations were conducted in which multiple slip distribution patterns were configured by moving slip distribution rows and columns one at a time to yield a spatial distribution of the ratio of maximum water level ascent in heterogeneous models to homogeneous models, based upon which assessments were conducted of the range of uncertainty and mean magnification between the two. Also, a similar examination was also conducted of cases where heterogeneous models

(asperity area, slip amount, etc.) were configured using the relationship presented by Somerville et al. (1999) and the position of asperity was moved to configure multiple slip distribution patterns.

Figure 3.3.10-1 shows previously estimated heterogeneous models, Table 3.3.10-1 specifications of fault models configured based upon Somerville et al. (1999), and Figure 3.3.10-2 methods for arranging asperity. In Table 3.3.10-1, the number of asperities is assumed to be two, the shape to be square, and the quantities configured based upon Somerville et al. (1999). Figure 3.3.10-2 used a method whereby a fault was divided into 2×3 small blocks. Maximum asperity is arranged in the center of an arbitrary block, and the remaining asperity arranged within the remaining five blocks. The result is the assumption of 6×5=30 fault models.

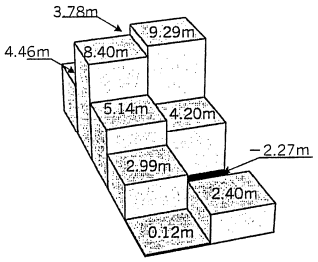

1968 Tokachi-Oki earthquake
(Annaka et al., 1999)

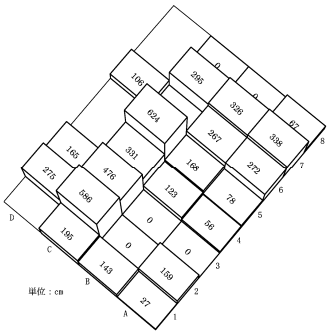

1946 Nankai earthquake
(Drawing based on Tanioka and Satake (1999))

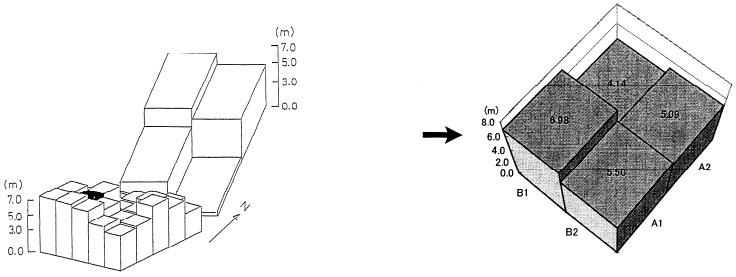

1983 Nihonkai-Chubu earthquake

(Fukuyama and Irikura, 1986)

Right figure: South fault smoothed for simplicity

Figure 3.3.10-1 Basic model of slip distribution based on estimated heterogeneous models

Table 3.3.10-1 Parameters of fault models configured based upon Somerville et al. (1999)

Parameter \ Earthquake	1968 Tokachi-Oki	1983 Nihonkai-Chubu	1946 Nankai
standard fault model	Aida (1978)	Satake (1985)	Tanioka and Satake (1999)
Total area of fault(km^2)	15,000	4,800	48,600
Seismic moment(N·m)	1.74×10^{21}	3.16×10^{20}	1.02×10^{22}
Average dislocation(cm)	405	229	729
Total area of asperity (km^2)	3,363	1,076	10,915
Area of largest asperity(km^2)	2,448	784	7,946
Dislocation of asperity(cm)	813	460	1,465

Seismic moment : With the area A known, $A=1.04\times10^{-10}\times M_0^{2/3}$
Average dislocation : $D=3.36\times10^{-5}\times M_0^{1/3}$
Total area of asperity : $Aa=2.32\times10^{-11}\times M_0^{2/3}$ (22% of A)
Area of largest asperity : $A1=1.69\times10^{-11}\times M_0^{2/3}$
Dislocation of asperity : $Da=D\times2.01$

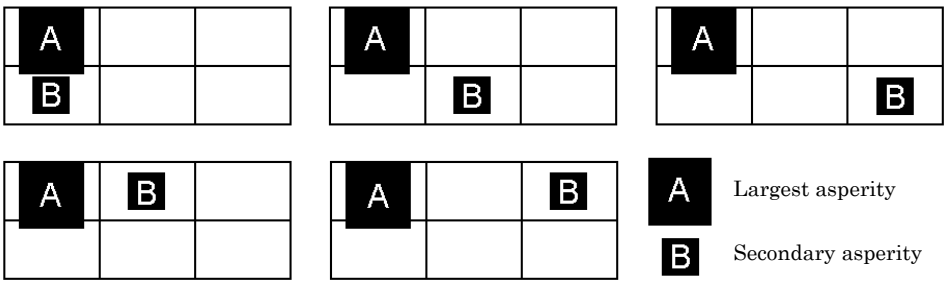

Figure 3.3.10-2 Methods for arranging asperity

Table 3.3.10-2 shows the results of an assessment of mean magnification and variance in a heterogeneous model compared to a homogeneous model. The definitions of geometric mean and log standard deviation are given below.

Geometric mean: $\log K = \frac{1}{N}\sum_{i=1}^{N}\log K_i$

Geometric standard deviation: $\log \varsigma = \left[\frac{1}{N-1}\left\{\sum_{i=1}^{N}(\log K_i)^2 - (\log K)^2\right\}\right]^{\frac{1}{2}}$

where, $K_i = \frac{\text{Result of calculation using heterogeneous model for point } i}{\text{Result of calculation using homogeneous model (mean model) for point } i}$

Assessments were conducted for each individual heterogeneous model, and the table shows the range, geometric mean, median value, and 84% non-exceedance value for all cases. The points of

comparison were the points where run-up height records of tsunami have been recorded for each earthquake.

If the fault area and seismic moment are equal, then, as shown in the table, the homogeneous models provide a lower tsunami height on average than that of the heterogeneous models, so, in order to obtain tsunami heights of the same magnitude, slip amount needs to be revised (increased).

Table 3.3.10-2 Results of an assessment of mean magnification and variance in a heterogeneous model compared to a homogeneous model

1968 Tokachi-Oki

		Model by Somerville et al. (1999)	Model by Annaka et al. (1999)
Ncalculation cases		30	10
Number of points used for comparison		273	273
Geometric mean K	Range	1.280~1.597	1.060~1.358
	Geometric mean	1.446	1.268
	Median	1.466	1.325
	84% cumulative	1.566	1.348
Geometric standard deviation ζ	Range	1.191~1.385	1.221~1.355
	Geometric mean	1.289	1.267
	Median	1.279	1.251
	84% cumulative	1.340	1.310

1946 Nankai

		Model by Somerville et al. (1999)	Model by Tanioka and Satake (1999)
Ncalculation cases		30	24
Number of points used for comparison		149	149
Geometric mean K	Range	1.100~1.542	1.589~2.510
	Geometric mean	1.330	1.987
	Median	1.351	2.023
	84% cumulative	1.445	2.303
Geometric standard deviation ζ	Range	1.267~1.453	1.338~1.670
	Geometric mean	1.364	1.542
	Median	1.376	1.570
	84% cumulative	1.409	1.591

1983 Nihonkai-Chubu

		Model by Somerville et al. (1999)	Model by Fukuyama and Irikura (1986)
calculation cases		30	16
Number of points used for comparison		320	320
Geometric mean K	Range	1.053~1.310	0.998~1.162
	Geometric mean	1.173	1.095
	Median	1.168	1.099
	84% cumulative	1.239	1.151
Geometric standard deviation ζ	Range	1.186~1.379	1.130~1.240
	Geometric mean	1.271	1.175
	Median	1.266	1.169
	84% cumulative	1.347	1.223

3.3.11. Effect of tsunami source position and strike for the Chile tsunami (far-field tsunami)

Using the example of the Chile tsunami, an assessment was conducted that focused on analyzing the sensitivity of variance resulting from uncertainty with respect to the tsunami source of a far-field tsunami. Figure 3.3.11-1 shows a map of the position of tsunami source models and a map of the distribution of initial displacement. The plate boundaries and segment boundaries were taken into account in configuring the tsunami source so that the position in Tsunami source model (1) for the 1960 Chile tsunami was shifted 200, 400 and 600 km to the north. Also, the tsunami source was configured such that strike was also ±10°. The default parameters are based upon Kanamori and Cipar (1974), but the Fault upper edge depth d was set at 1 km.

Figure 3.3.11-2 shows a comparison of the coastal distribution of tsunami height, and Table 3.3.11-1 the results of a comparison with run-up height records of tsunami. As for the reproducibility of the run-up height records of tsunami, the value of variance κ does not change much for any of the tsunami sources. Also, the table shows the sensitivity of parametric studies to Tsunami source fault model (1).

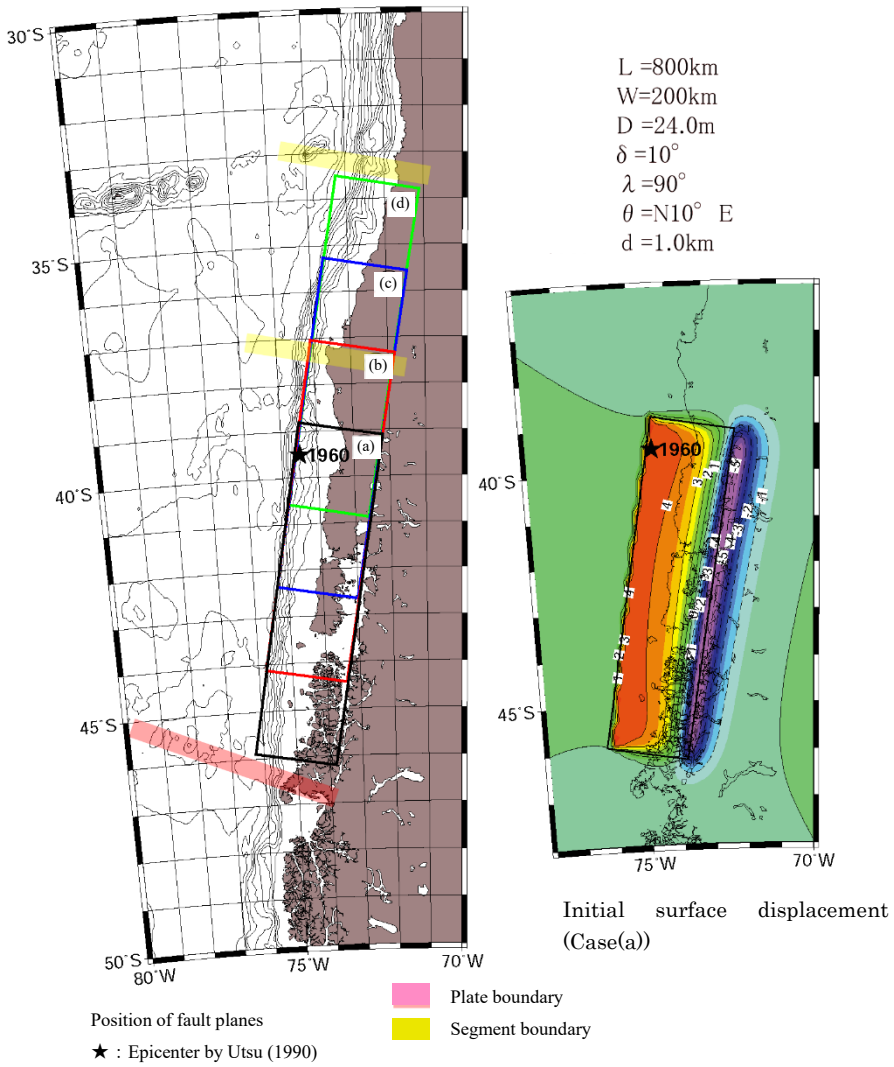

Figure 3.3.11-1 Tsunami source model position and initial surface displacement distribution of Chilean tsunami (Added to the Chile tsunami joint study group (1961))

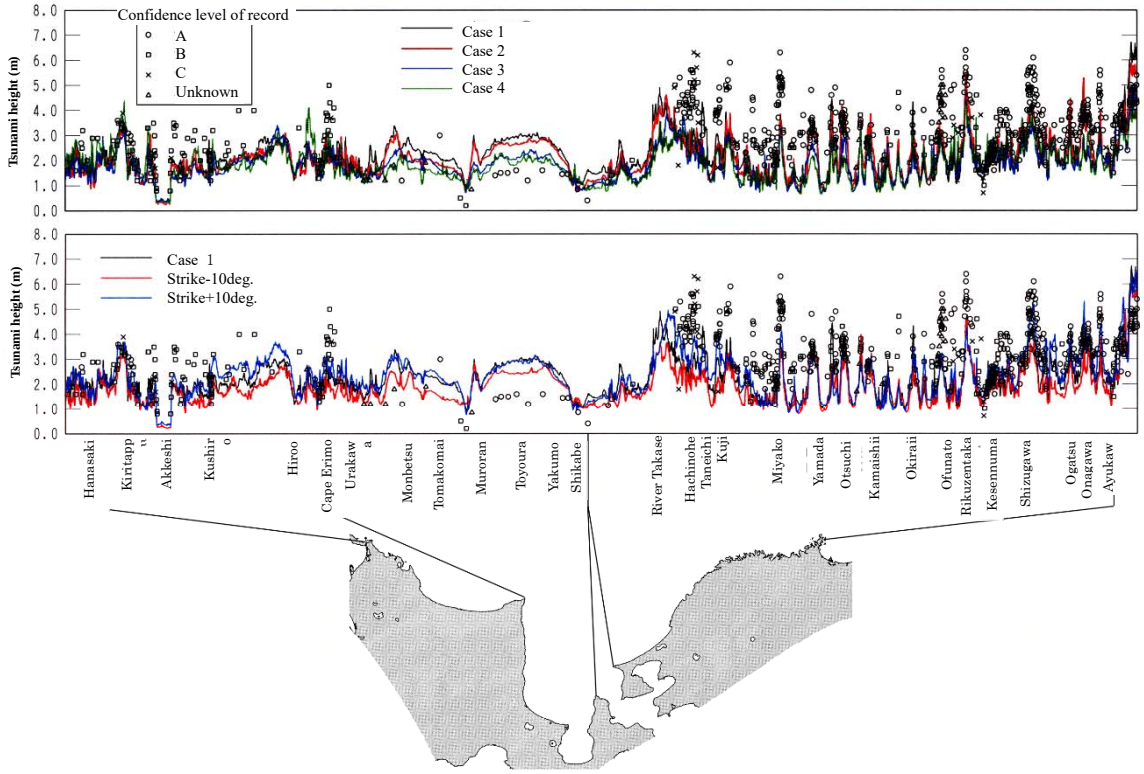

Figure 3.3.11-2 Comparison of coastal distribution of tsunami height by assumed Chilean tsunami (Added to the Chile tsunami joint study group (1961))

Table 3.3.11-1 Comparison result by geometric mean (K) and geometric standard deviation (κ)

Comparison		Case 1	Case 2 200 km North	Case 3 400 km North	Case 4 600 km North	Strike -10deg.	Strike +10deg.
Observation/Calculation	K	1.19	1.15	1.32	1.29	1.34	1.10
	κ	1.43	1.41	1.39	1.42	1.43	1.41
Calculation/Case 1	K	-	1.03	0.90	0.92	0.89	1.08
	ζ	-	1.18	1.20	1.28	1.15	1.18
	$K\times\zeta$	-	1.21	1.08	1.17	1.02	1.28

○Number of points n= 586
○Grid size around comparison points 278m or 93m
○ K: Geometric mean
κ: Aida(1977)'s Geometric standard deviation
ζ: Geometric standard deviation (no bias)

3.3.12. Examination of the effect that kinematic parameters have on tsunami height

In this section we examine the effect of the hypocenter, rupture propagation velocity and rise time on tsunami heights in the eastern margin of the Japan Sea.

(1) Examination conditions

Table 3.3.12-1 shows calculation settings for this examination, and Figure 3.3.12-1 shows the computational region.

1) Hypocenter

- Fault model: A model was developed which has an aggregation of small faults with 10 km long and 5 km wide.
- The relationship between fault area S and Seismic moment M_0 is applied. However, heterogeneity of slip is not taken into consideration.
- A total of six hypocenters are configured at the southern edge, center and northern edge of the fault upper edge and lower edge, respectively.

2) Rupture propagation velocity

The rupture propagation velocity of 3.0 km/s is used as reference case, and those of 2.5 km/s and 3.5 km/s are done for parametric studies.

3) Rise time

The rise time of 0 seconds is used as reference case, and those of 10, 30, and 60 seconds are used for parametric studies.

4) Calculation cases

Table 3.3.12-2 shows a list of the cases examined.

5) Tsunami source

Vicinity of the source region of the 1993 Hokkaido Nansei-Oki earthquake

Table 3.3.12-1 Calculation conditions

Items	Contents
Computational region	All over the Sea of Japan
Calculation grid size	Offshore 1,600m, 800m, 400m, 200m
Basic equations	Nonlinear long wave equations
Initial displacement fields of seafloor	The method of Mansinha and Smylie(1971)
Boundary conditions	Offshore: Open boundary condition (Tsugaru, Tsushima, La Perouse strait) Landward: Full reflection condition (for seafloor exposure, the moving boundary method of Kotani et al.(1998) applied)
Overflow conditions	None
Horizontal eddy viscosity coefficient	$10m^2/s$
Coefficient of friction	Manning's coefficient of roughness: $0.03m^{-1/3}s$
Tide conditions	T.P.±0.0m
Computation time interval	0.5s
Simulating time	6 hours after the occurrence of earthquake

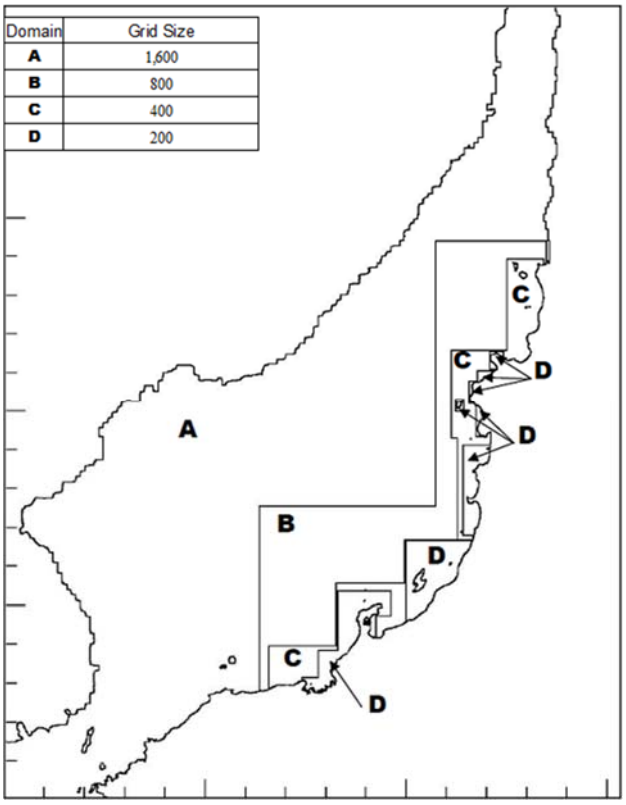

Figure 3.3.12-1 Computational region

Table 3.3.12-2 List of cases

Item	Hypocenter	Rupture propagation velocity	Rise time
Fracture initiation point	1-6 (6 points)	3.0km/s	0s
Fracture propagation velocity	1	2.5, 3.0, 3.5km/s	0s
Fracture propagation velocity+ rise time	1	3.0km/s	0, 10, 30, 60s
Rise time	-	∞	0, 10, 30, 60s

(2) Examination of tsunamis in the vicinity of the source region of the 1993 Hokkaido Nansei-oki earthquake (tsunami source designation: E1C2)

An examination is conducted in which a rectangular fault with a fault width of 28.28 km and a length of 167.1 km is arranged in the vicinity where the 1993 Hokkaido Nansei-oki earthquake occurred (E1C1). As shown in Figure 3.3.12-2, small faults are arranged dividing the area into five equal parts across the width and 16 equal parts across the length. This examination does not take into account large slip areas, and a configuration of uniform slip (4.53 m) is used.

Figure 3.3.12-3 shows the horizontal distributions of the water level for various cases when seafloor displacement ends, and Figures 3.3.12-4 through 3.2.12-6 show the same ones after 85 seconds, 5 minutes, and 10 minutes, respectively. Although differences are observed in tsunami when seafloor displacement ends and when 85 seconds have elapsed after seafloor displacement ended, no significant differences are existed in tsunami after 5 minutes had passed as well as after 10 minutes had passed.

1) Examination of hypocenter

Hypocenters are configured at six points (a) through (f) (Figure 3.3.12-2) and a tsunami analysis conducts to compare tsunami heights along the coastline. Diagrams comparing tsunami heights along the coastline from Hokkaido to Kyoto are shown in Figures 3.3.12-7 through 3.3.12-10, and Figure 3.3.12-11 shows a diagram comparing the tsunami heights at Okushiri Island.

- Overall, there is a tendency that tsunami heights are lower than that of instantaneous overall rupture.
- In the vicinity of tsunami source, there are points where the difference in the tsunami height

is significant with respect to instantaneous overall rupture.

- In cases where the rupture starts from the center of the tsunami source (hypocenters (b) and (e)), there are points where the tsunami height on the northern side of the tsunami source is higher than that of instantaneous overall rupture.
- In the area around Inaho (area around the northern tip of Okushiri Island) (Figure 3.3.12-21), the tsunami height is predominantly higher than that of instantaneous fracture (Fracture initiation points (a), (c), (d) and (f)).

2) Examination of rise time

An examination is conducted where rise time is set at 10, 30, and 60 seconds. In this examination, the hypocenters are not set, and simultaneous rupture is used. Figure 3.3.12-12 shows the results of a comparison of tsunami heights along the coastline from Hokkaido to Kyoto, and Figure 3.3.12-13 shows the results of a comparison of tsunami heights at Okushiri Island.

- Overall, there is a tendency that tsunami heights are lower than that of instantaneous fracture.
- At points near tsunami sources, the tsunami height is significantly lower when the rise time is 60 seconds.
- Although the tsunami height is significantly lower when rise time is 60 seconds, there is little impact on the other side of Okushiri Island as viewed from the tsunami source (e.g. Hotokesawa).

3) Examination of rupture propagation velocity

An examination is conducted where fracture propagation velocity is set at 2.5, 3.0, and 3.5 km/s. In these cases, the examination is conducted by fixing the fracture initiation point at (a). Figure 3.3.12-14 shows the results of a comparison of tsunami heights along the coastline from Hokkaido to Kyoto, and Figure 3.3.12-15 shows the results of a comparison of tsunami heights at Okushiri Island.

- Lower tsunami heights are existed at points far from the hypocenter in the vicinity of the tsunami source.
- Overall, there is a tendency that tsunami heights are lower than that of instantaneous rupture.
- When rupture propagation is taken into account, tsunami height on the northern tip of Okushiri Island is higher when compared with that of instantaneous rupture, but the difference resulting from different fracture propagation velocities is small.
- Of the cases in this examination, the tsunami height at the Inaho when the rupture

propagation velocity is 2.5 km/s is the highest (T.P.+11.3 m).

4) Examination of tsunami superposition

An examination is conducted in which the rupture propagation velocity is set at 3.0 km/s, the hypocenter fixed at (a), and the rise time varies: 0 second, 10 seconds, 30 seconds, and 60 seconds. Figure 3.3.12-16 shows the results of a comparison of tsunami heights along the coastline from Hokkaido to Kyoto, and Figure 3.3.12-17 shows the results of a comparison of tsunami heights at Okushiri Island.

- In the vicinity of the tsunami sources, the tsunami height is somewhat higher for rise time of 10 seconds.
- Overall, there is a tendency that tsunami heights are lower than that of instantaneous rupture.
- In the area around Inaho (area around the northern tip of Okushiri Island), tsunami heights result in a predominantly higher than that of instantaneous rupture (hypocenters (a), (c), (d) and (f)).
- Tsunami heights are somewhat lower than that of the case where only the rupture propagation velocity is taken into account.

5) Analysis of factors where the difference is greater

In the examination of the effect of hypocenters, results are shown (Figures 3.3.12-18 and 3.3.12-19) where the difference in the maximum tsunami heights is greater around Sakaeiso on the Hokkaido coastline (Figure 3.3.12-20) and around Inaho on Okushiri Island (Figure 3.3.12-21).

Figure 3.3.12-22 shows a diagram comparing time histories of the water level at the respective points. The difference in peak heights at around 15 minutes at Inaho is thought to be caused by the superposition of waves propagating around to the north along the coastline of Okushiri Island and the wave propagating along the south of the island (Figure 3.3.12-23).

In order to verify that the difference in tsunami height at Inaho is caused by the superposition of waves propagating along the coastline of Okushiri Island, an examination is conducted of cases where only one portion of the tsunami source ruptures. Snapshots are shown of the tsunami heights around Inaho (Figures 3.3.12-25 and 3.3.12-26). It is verified that the wave, which arrives at the northwestern part of the island from the vicinity of the center of the tsunami source (hypocenter (b)), propagates to the north, and superimposes with the wave propagating along the eastern coastline from the south of the island from around the southern part of the tsunami source (hypocenter (c)), thereby resulting in amplification of the tsunami height at Inaho.

Based on the aforementioned, it is found that, in cases where there are islands, promontories or other geographical features around a tsunami source, the effects of the hypocentral position and rupture propagation velocity may amplify tsunami height by between 20 and 30%.

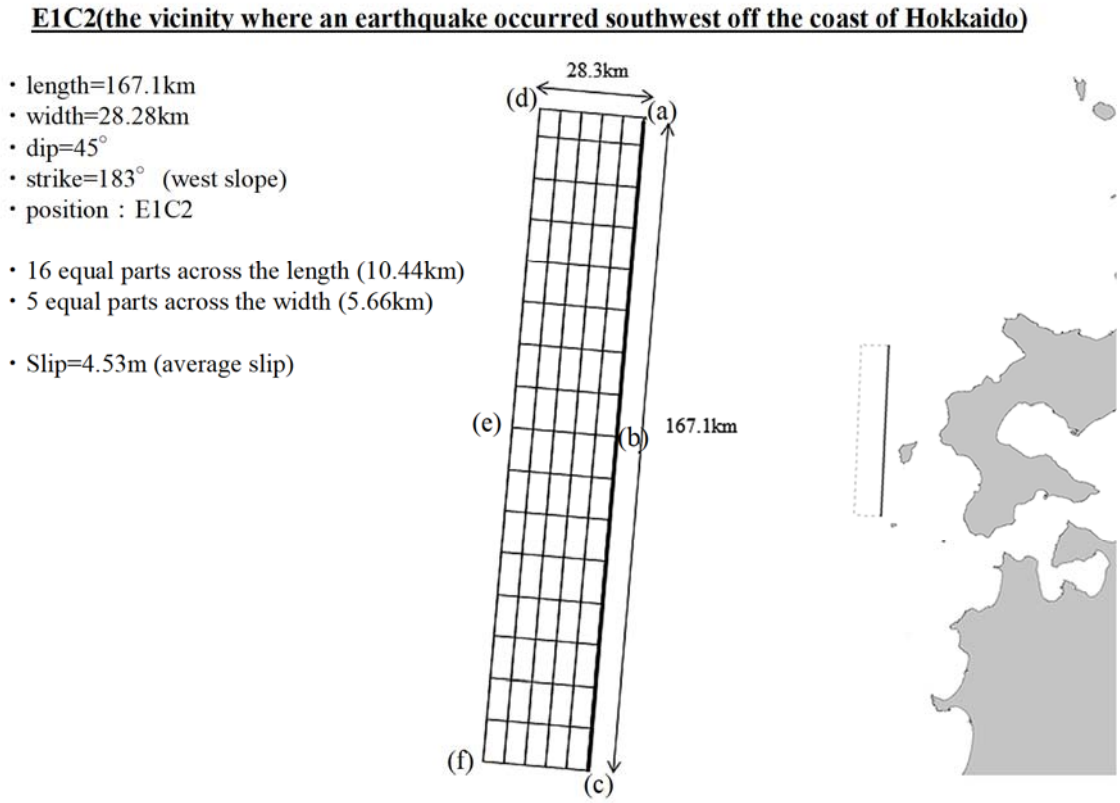

Figure 3.3.12-2 Hypocenters of the fault model (the vicinity where the 1993 Hokkaido Nansei-oki earthquake occurred)

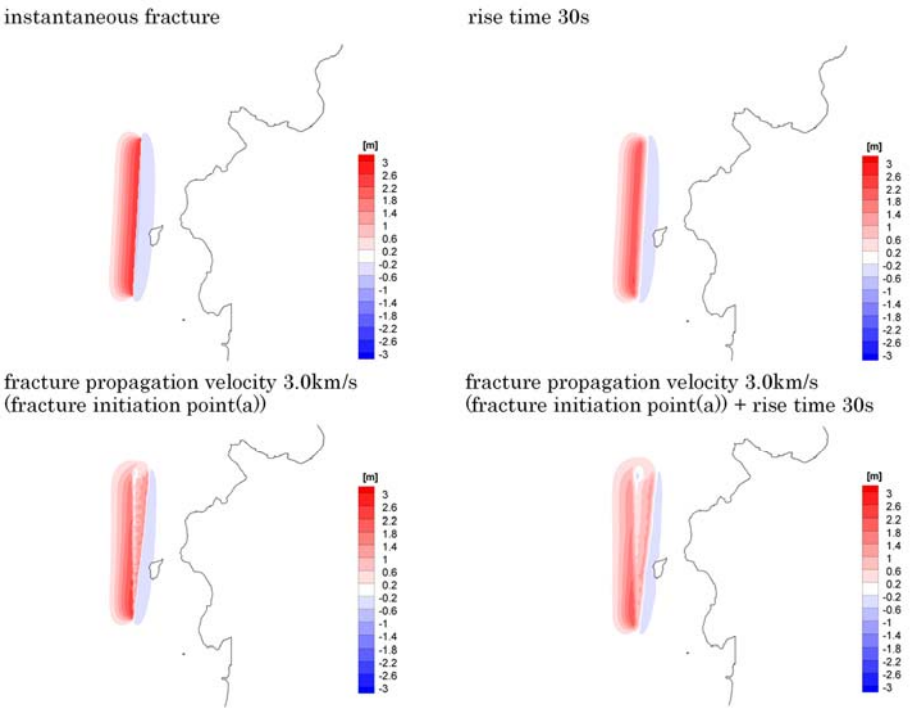

Figure 3.3.12-3 Comparison of the horizontal distribution of tsunami height (when ground deformation ended)

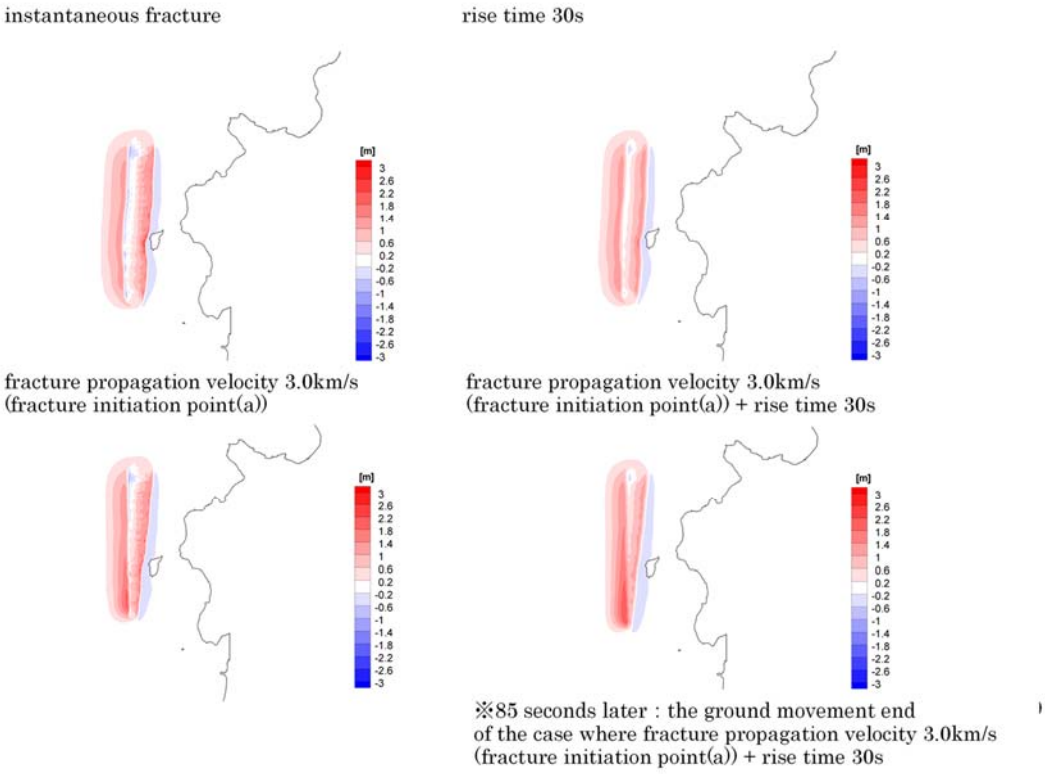

Figure 3.3.12-4 Comparison of the horizontal distribution of tsunami height (85seconds later)

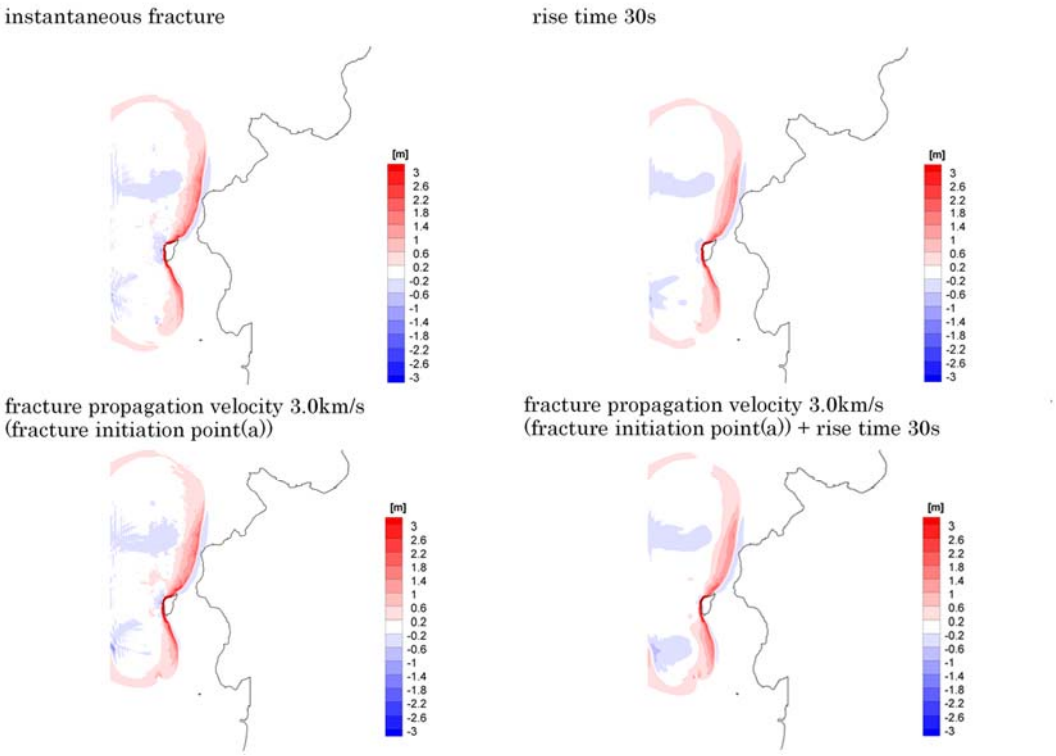

Figure 3.3.12-5 Comparison of the horizontal distribution of tsunami height (5 minutes later)

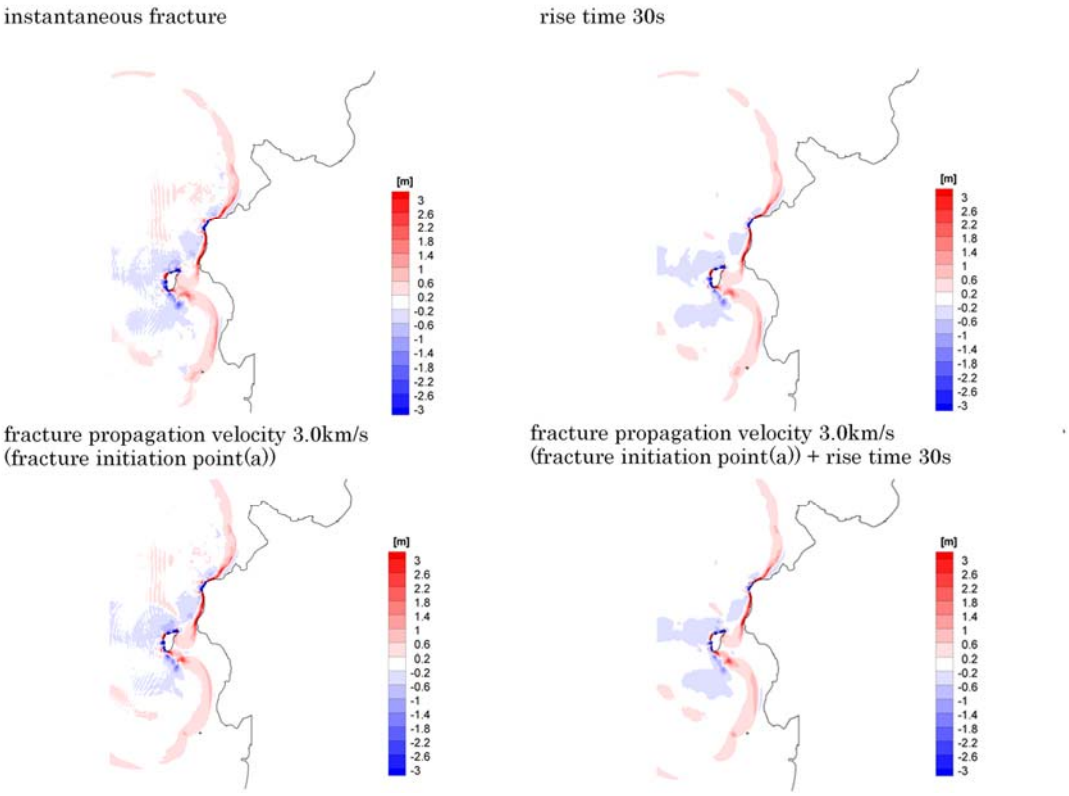

Figure 3.3.12-6 Comparison of the horizontal distribution of tsunami height (10 minutes later)

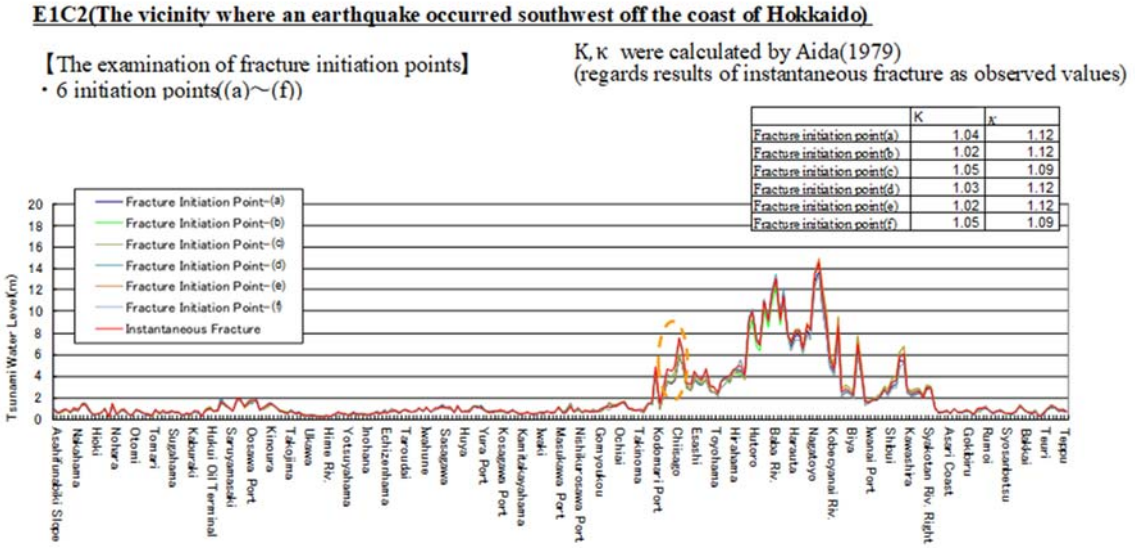

Figure 3.3.12-7 Comparison of tsunami heights along the coastline (Hokkaido to Kyoto): examination of hypocenters (all cases)

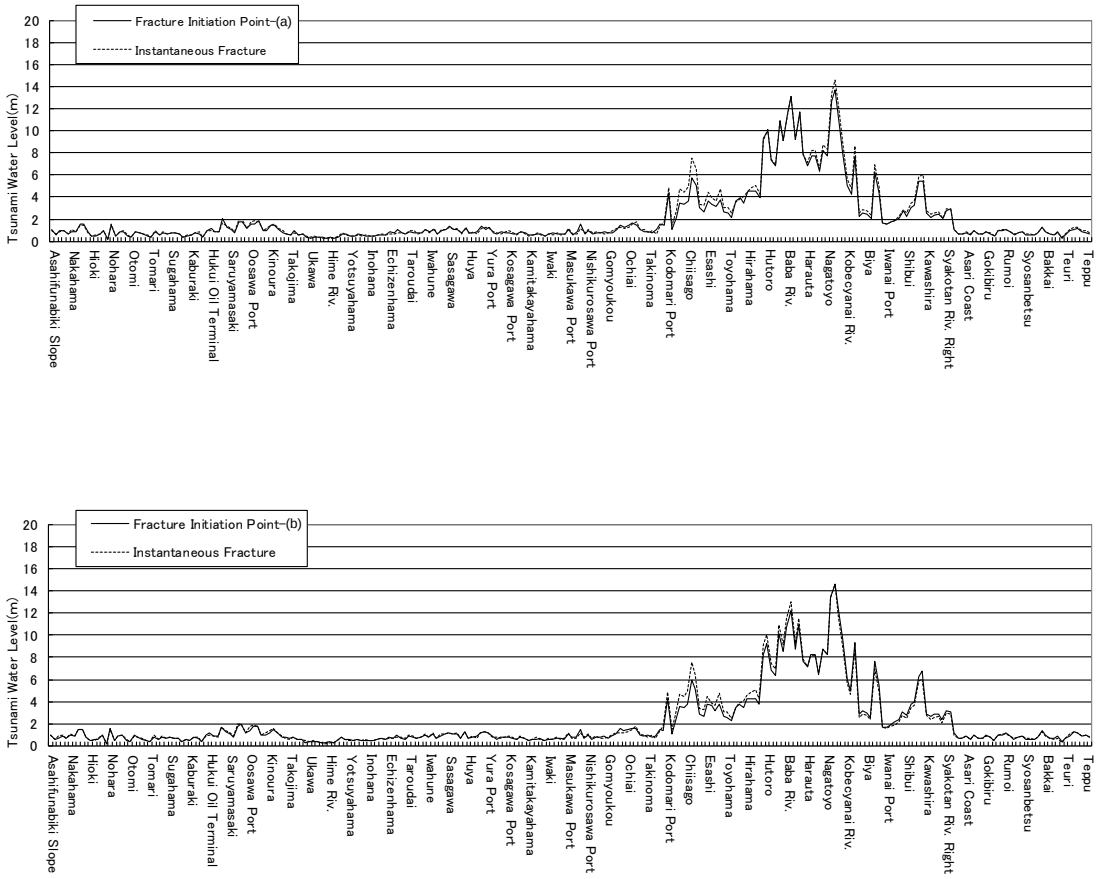

Figure 3.3.12-8 Comparison of tsunami heights along the coastline (Hokkaido to Kyoto): examination of hypocenters (a), (b)

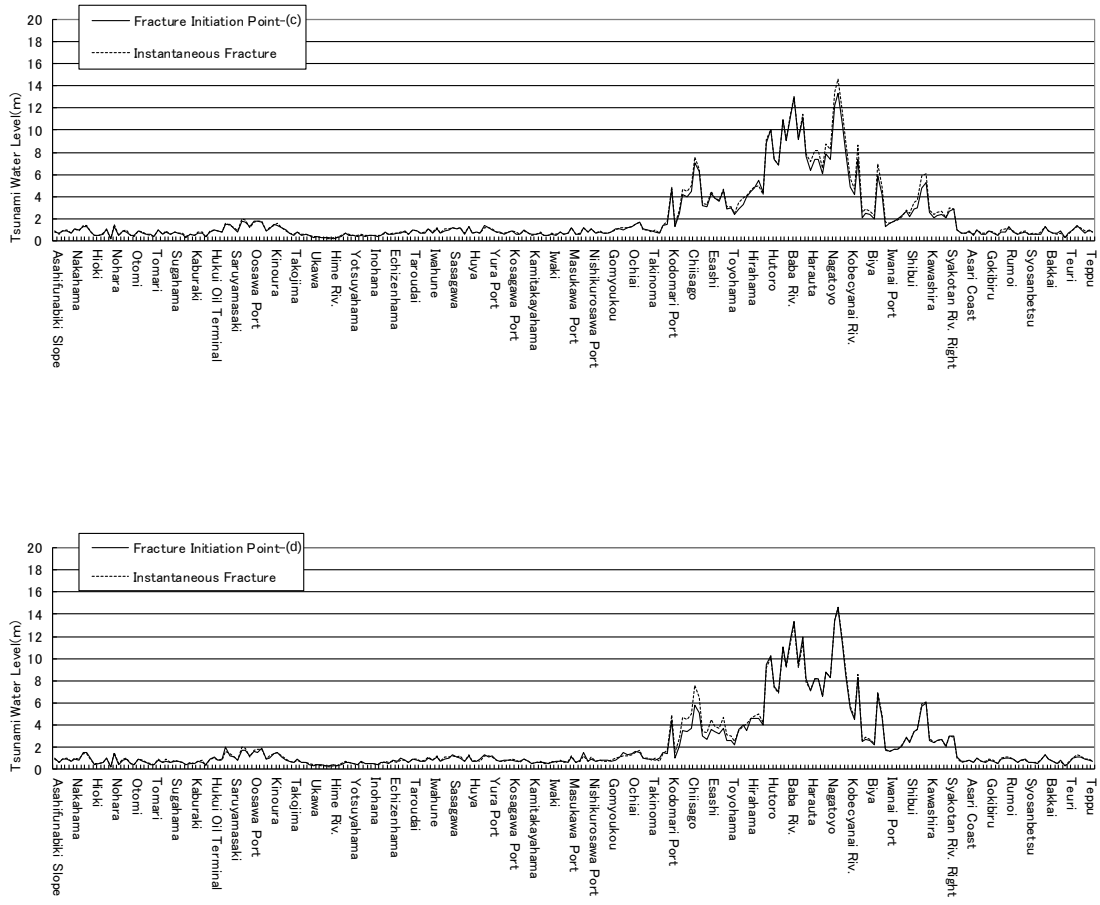

Figure 3.3.12-9 Comparison of tsunami heights along the coastline (Hokkaido to Kyoto): examination of hypocenters(c), (d)

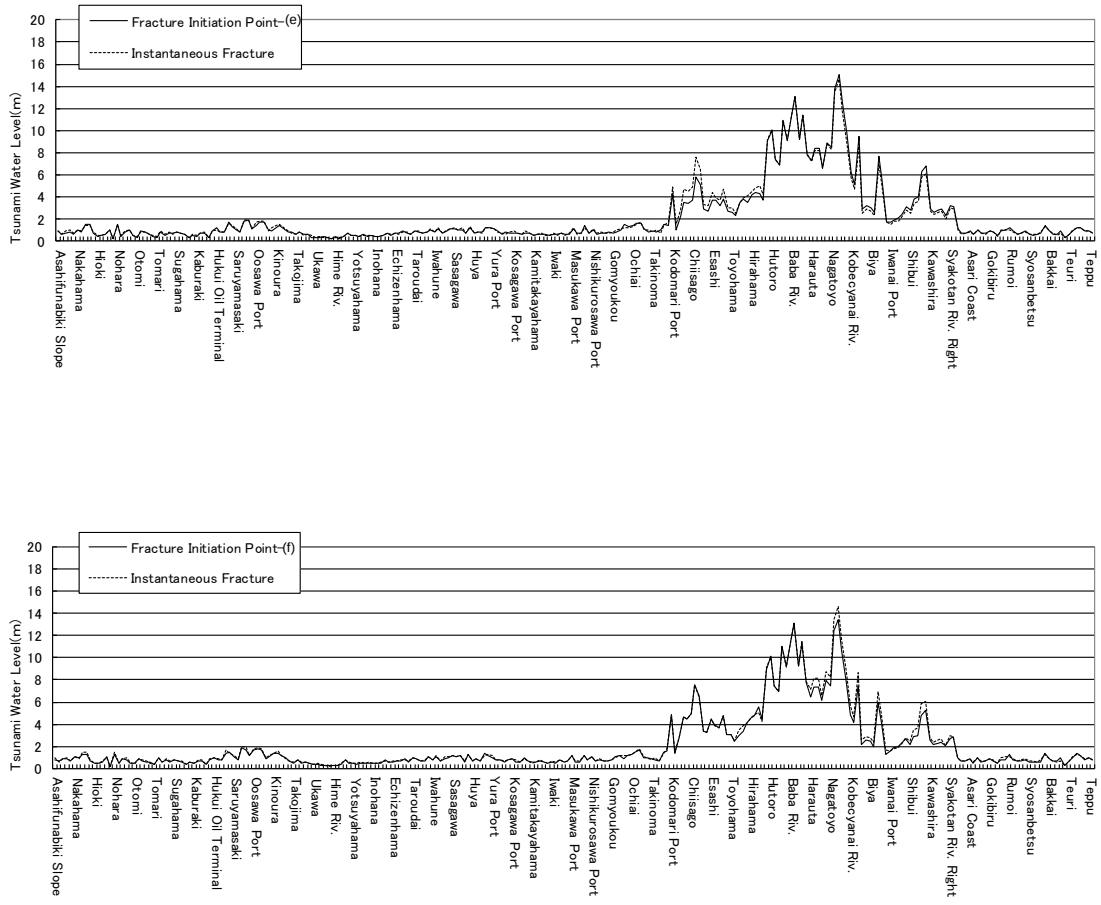

Figure 3.3.12-10 Comparison of tsunami heights along the coastline (Hokkaido to Kyoto): examination of hypocenters (e), (f)

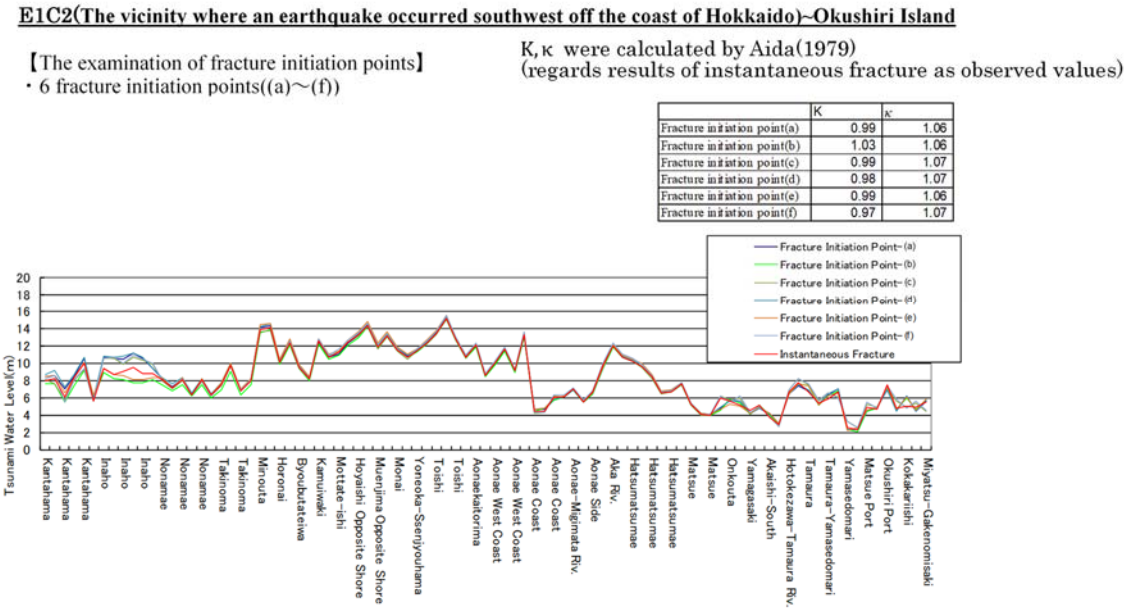

	K	κ
Fracture initiation point(a)	0.99	1.06
Fracture initiation point(b)	1.03	1.06
Fracture initiation point(c)	0.99	1.07
Fracture initiation point(d)	0.98	1.07
Fracture initiation point(e)	0.99	1.06
Fracture initiation point(f)	0.97	1.07

Figure 3.3.12-11 Comparison of tsunami heights along the coastline (Okushiri island): examination of hypocenters (all cases)

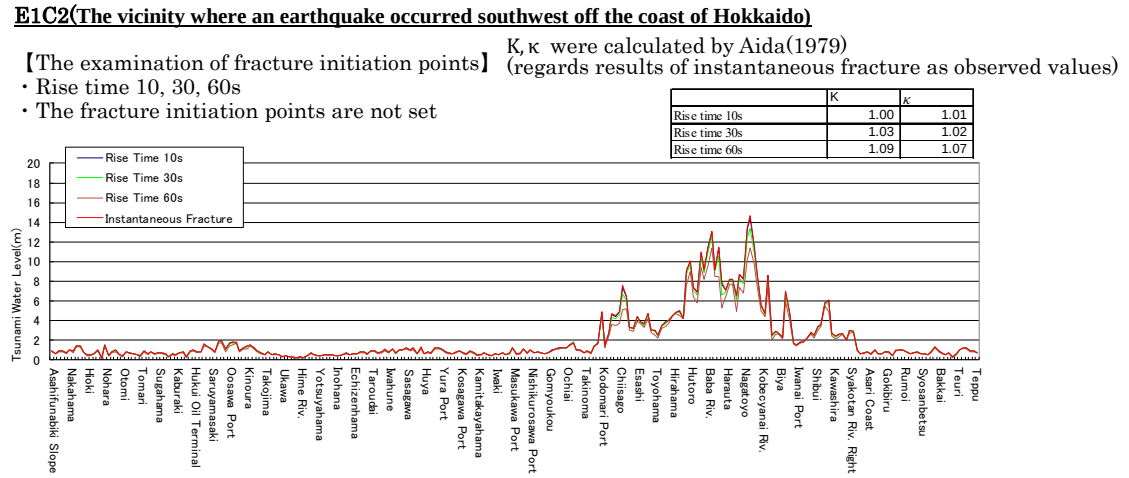

	K	κ
Rise time 10s	1.00	1.01
Rise time 30s	1.03	1.02
Rise time 60s	1.09	1.07

Figure 3.3.12-12 Comparison of tsunami heights along the coastline (Hokkaido to Kyoto): rise time

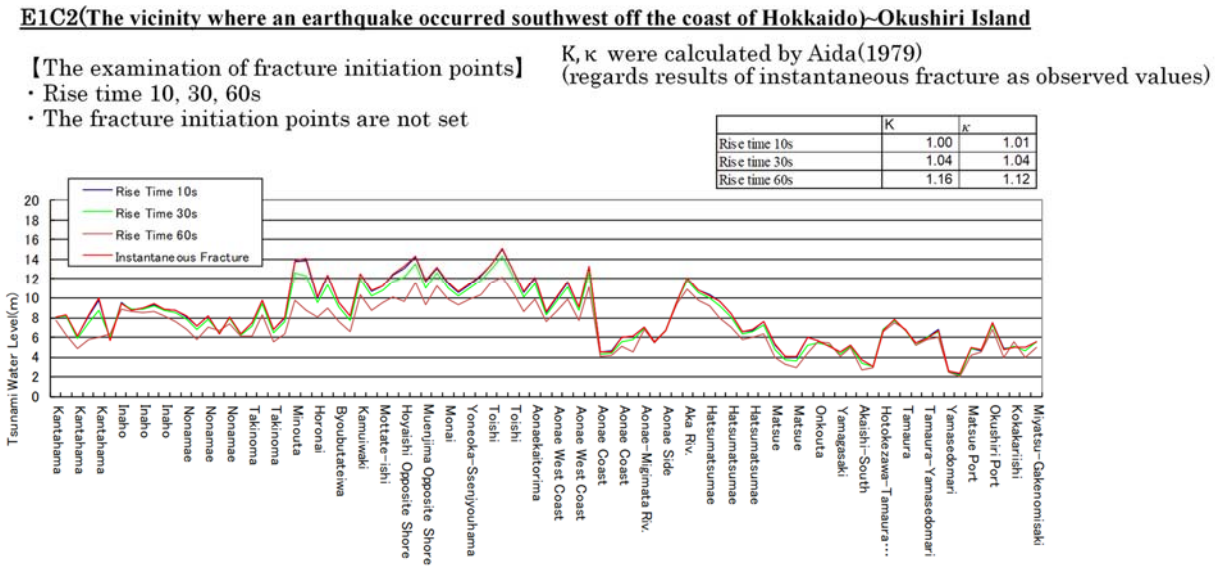

Figure 3.3.12-13 Comparison of tsunami heights along the coastline (Okushiri island): rise time

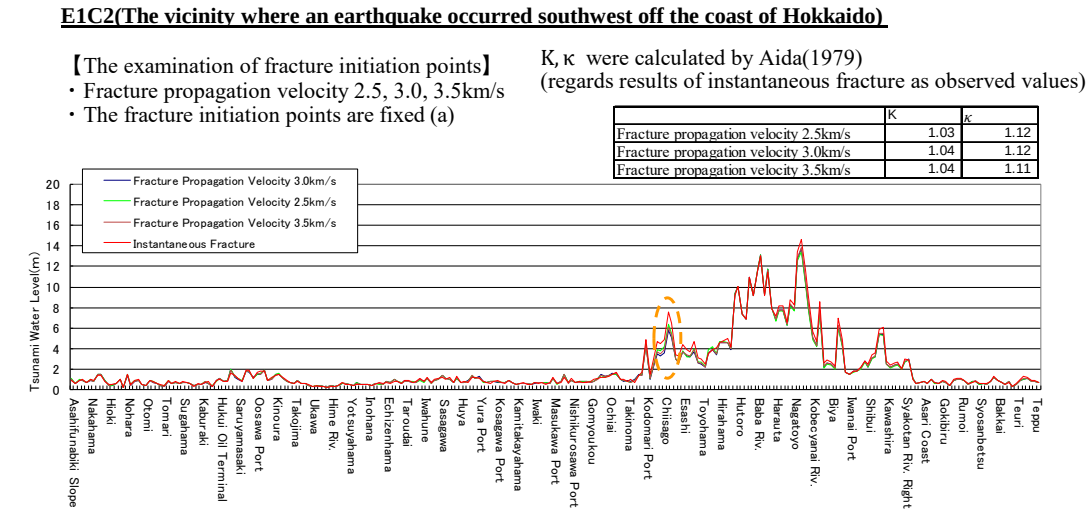

Figure 3.3.12-14 Comparison of tsunami heights along the coastline (Hokkaido to Kyoto): rupture propagation velocity

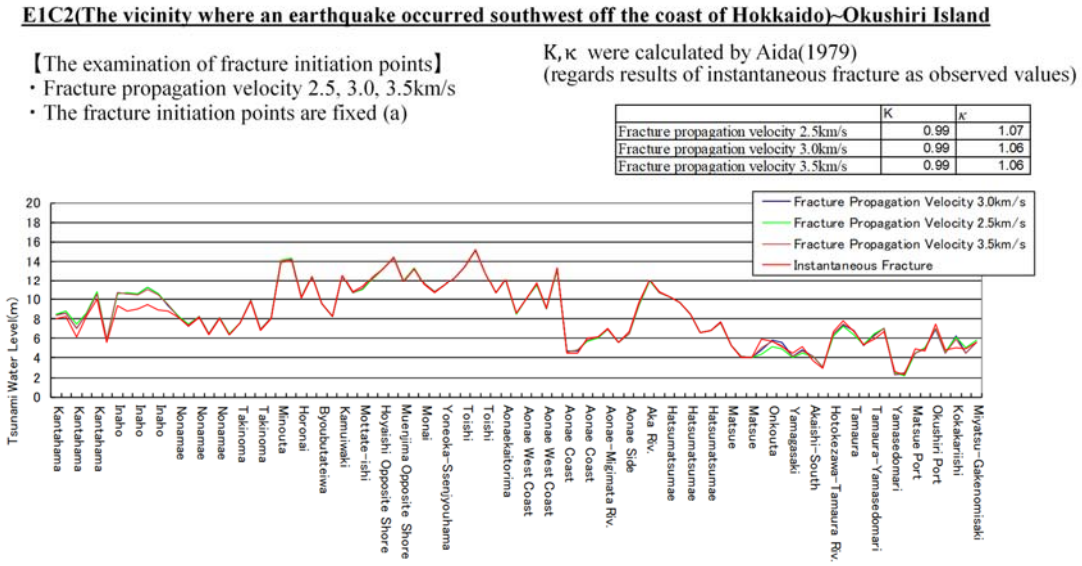

Figure 3.3.12-15 Comparison of tsunami heights along the coastline (Okushiri island): rupture propagation velocity

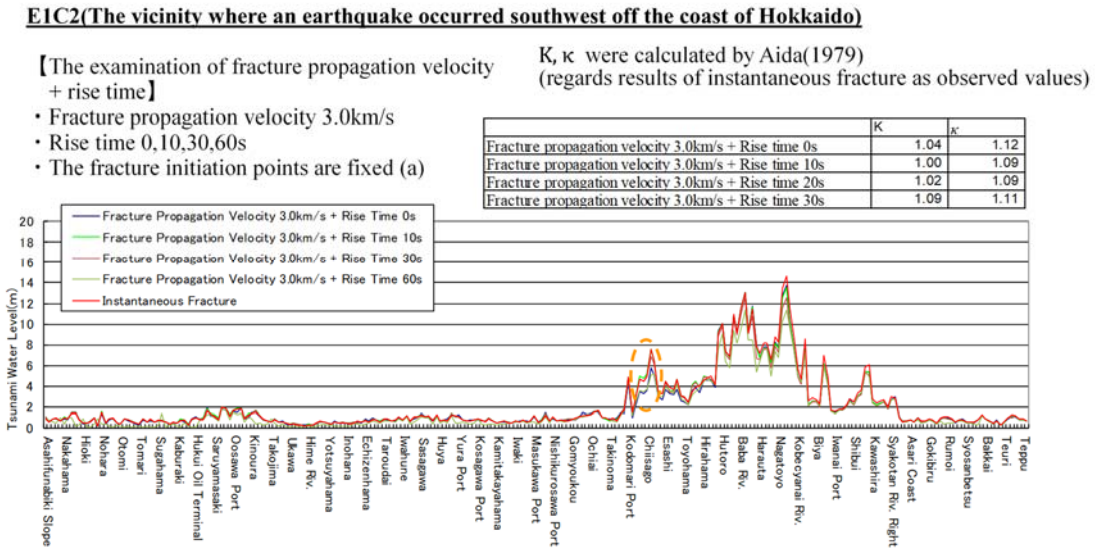

Figure 3.3.12-16 Comparison of tsunami heights along the coastline (Hokkaido to Kyoto): rupture propagation velocity + rise time

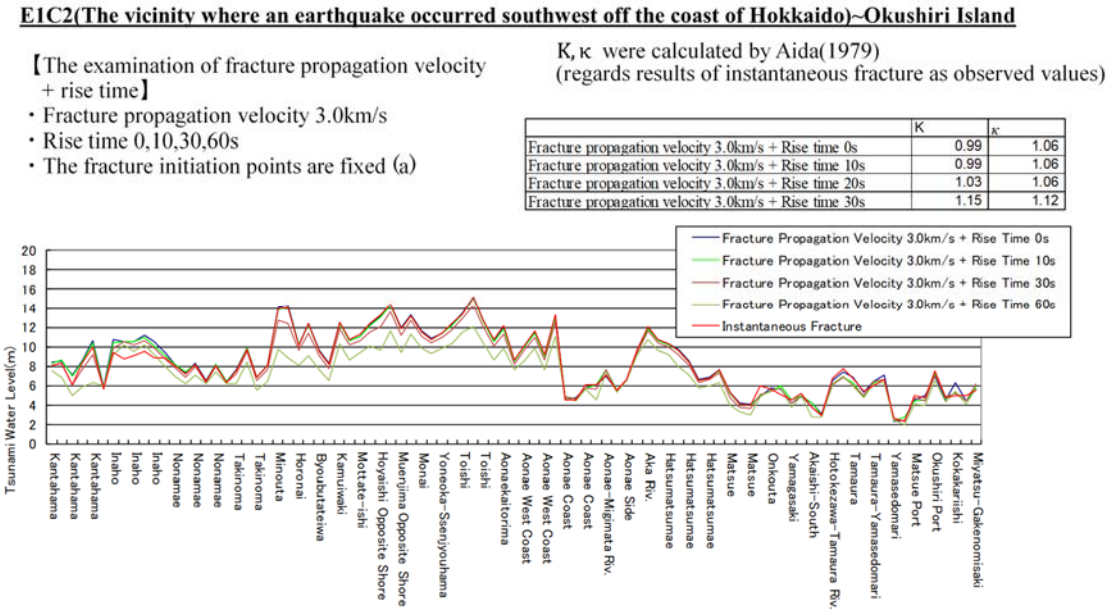

Figure 3.3.12-17 Comparison of tsunami heights along the coastline (Okushiri island): rupture propagation velocity + rise time

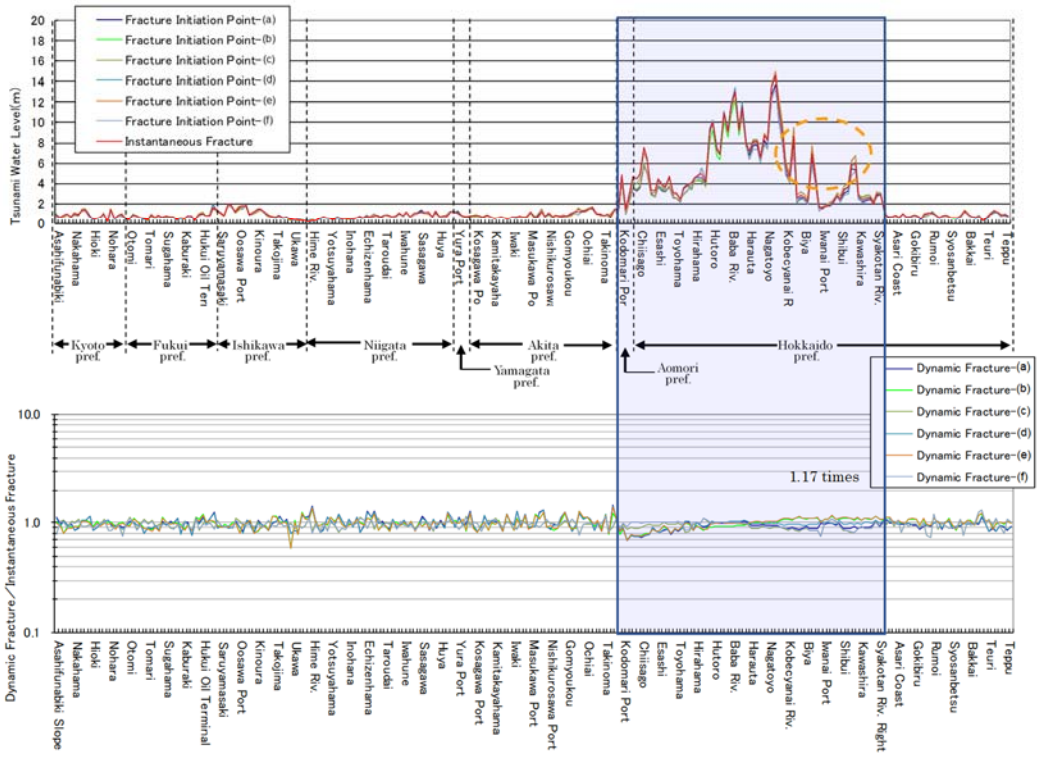

*"Dynamic fracture" refers to consideration of hypocenter or rupture propagation velocity.

Figure 3.3.12-18 The points with larger difference from the case of instantaneous rupture (the coast of Hokkaido)

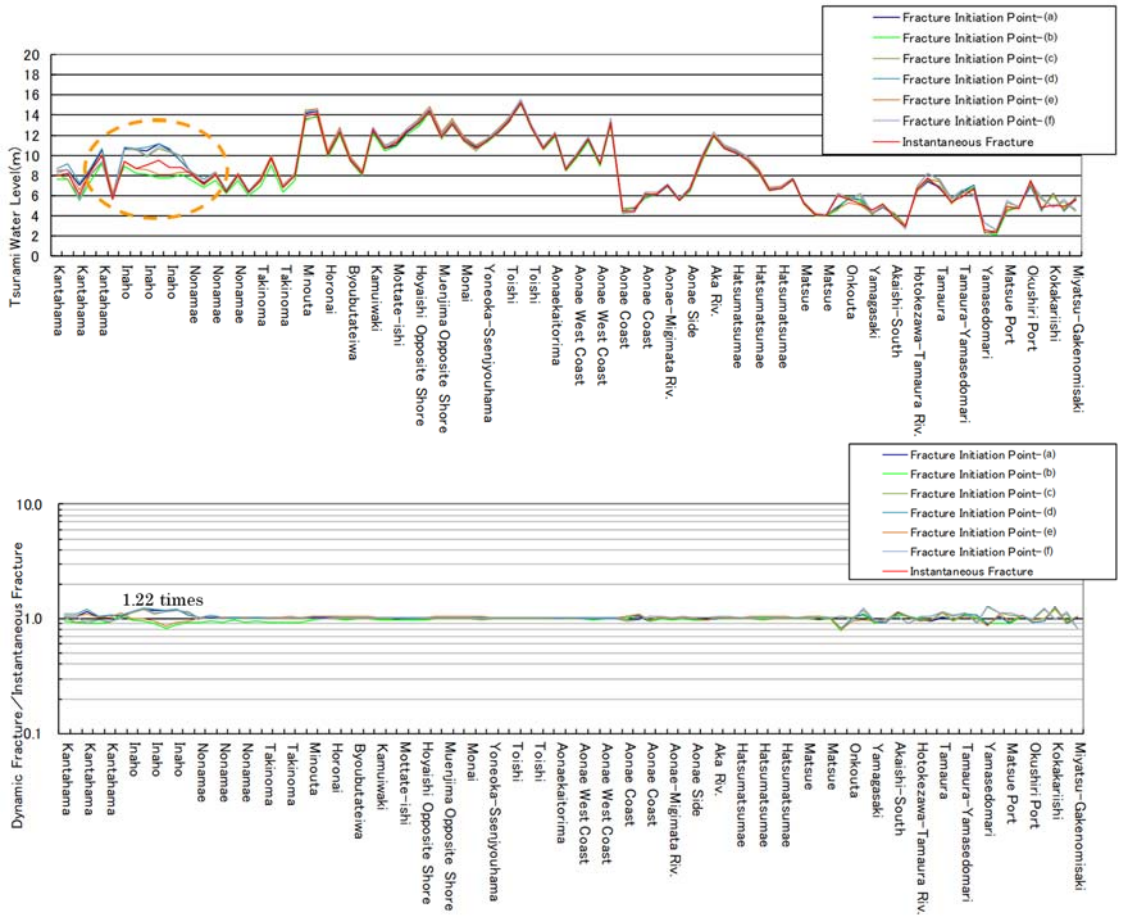

*"Dynamic fracture" refers to consideration of hypocenter or rupture propagation velocity.

Figure 3.3.12-19 The points with larger difference from the case of instantaneous rupture (the coast of Okushiri island)

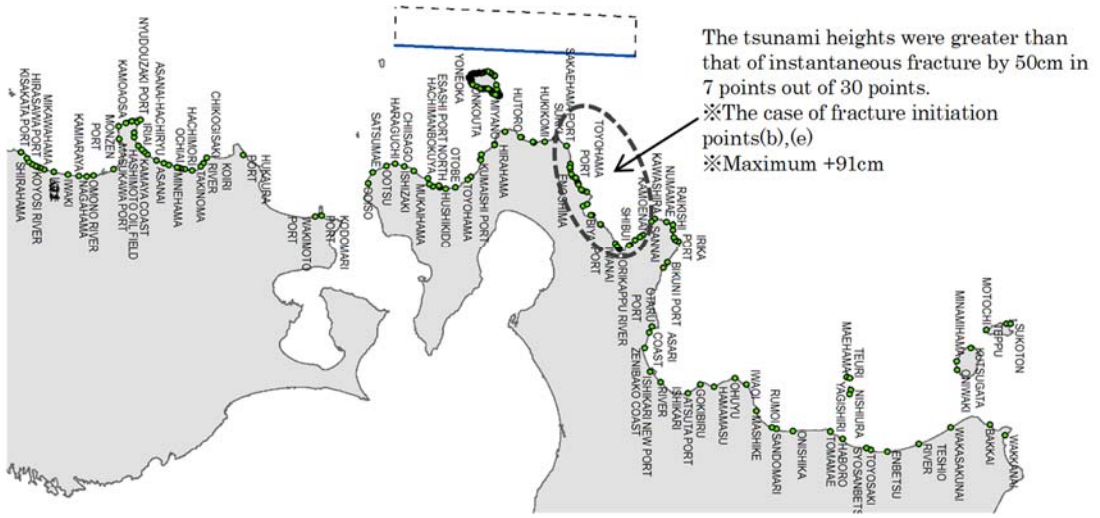

Figure 3.3.12-20 The points with larger difference from the case of instantaneous rupture (the coast of Hokkaido)

Figure 3.3.12-21 The points with larger difference from the case of instantaneous rupture (the coast of Okushiri island)

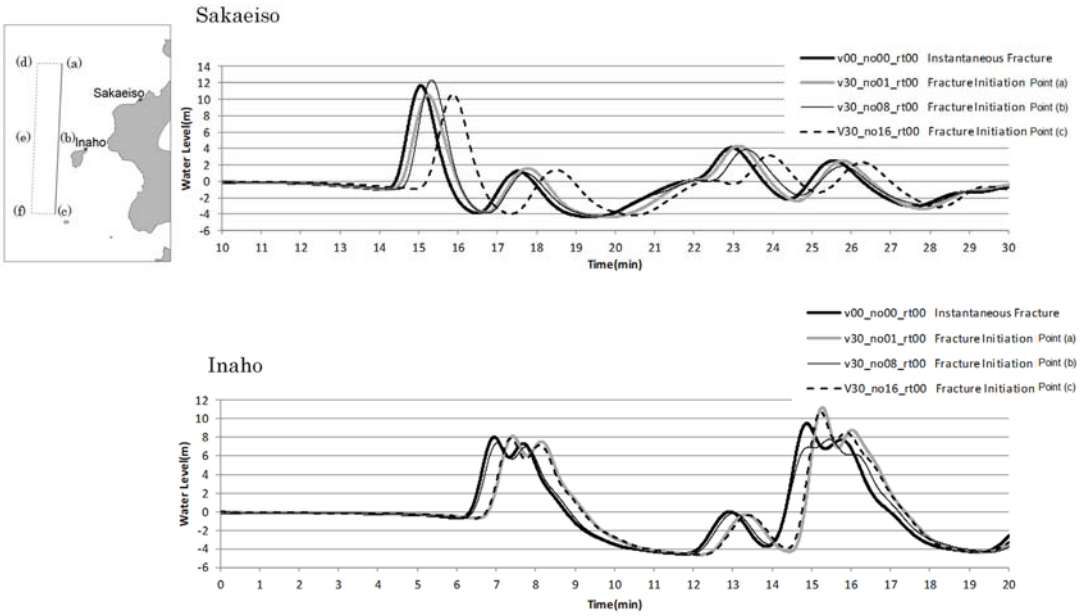

Figure 3.3.12-22 Comparison of the time histories of water level at Sakaeiso and Inaho

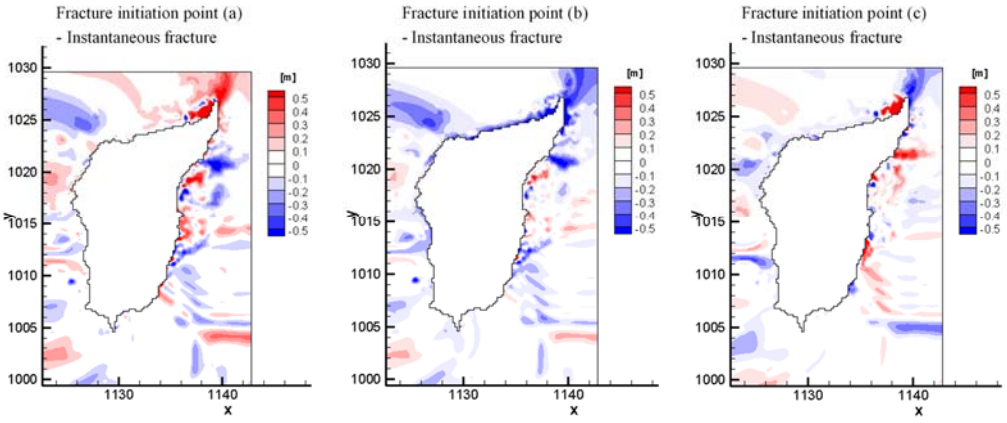

Figure 3.3.12-23 The difference of the maximum water level ascent around Okushiri island (examination of hypocenter – instantaneous fracture)

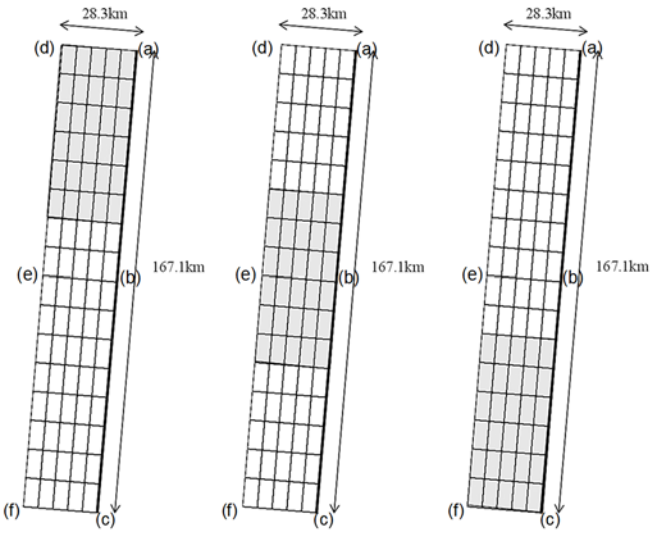

Figure 3.3.12-24 Patterns of partial rupture of the fault plane (the shade area indicates the partial fracture)

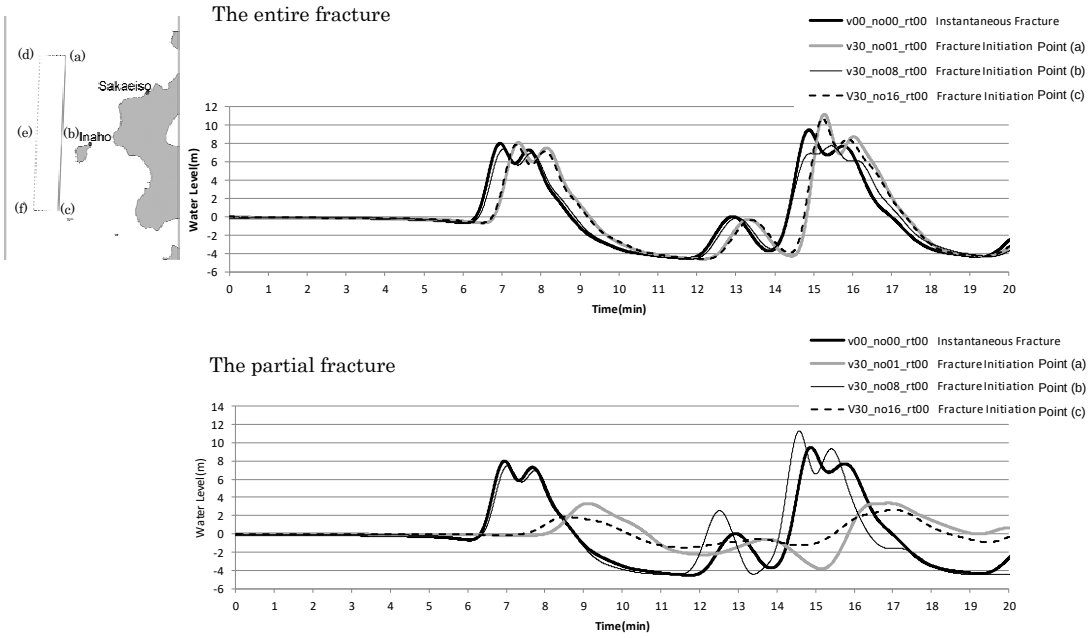

Figure 3.3.12-25 Comparison of the time histories of water level at Sakaeiso and Inaho (the upper: the entire fracture, the lower: the partial rupture)

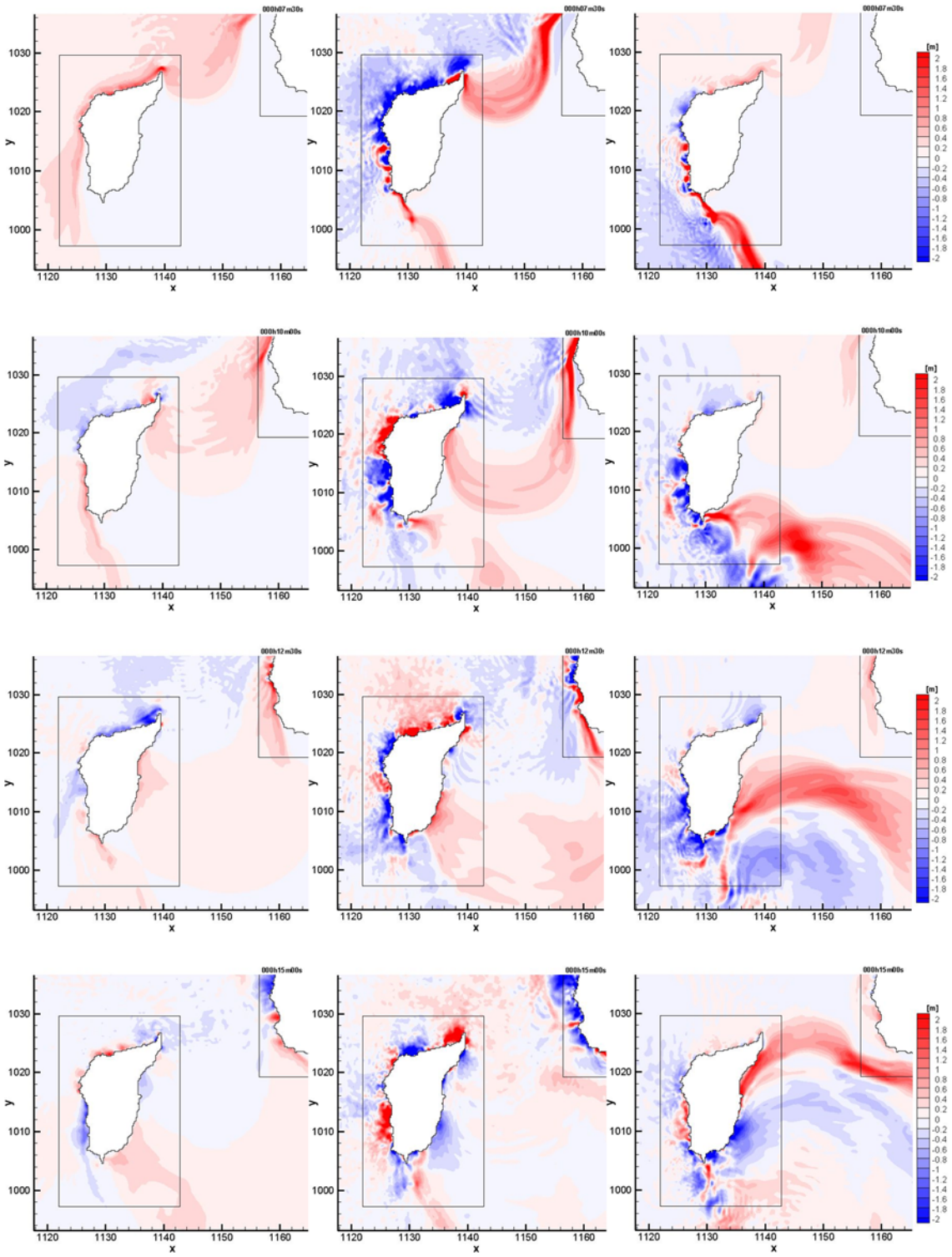

Figure 3.3.12-26 Horizontal distributions of the maximum water level ascent (from above, 7.5 min. later, 10 min. later, 12.5 min. later, 15 min. later)

(4) Summary

The examination was conducted of the effect that the hypocenter, rupture propagation velocity, and rise time have on tsunami height along the eastern margin of the Japan Sea. Based on the examination results, there is an overall tendency for tsunami height to be lower when the hypocenter or other elements are taken into consideration, but because there are some local points where the tsunami height is around 20 to 30% higher, particular care needs to be given to points having specific features such as those described below.

- Points that are near the tsunami source and the case that the effect of first wave is large
- Points that are significantly affected by islands
- Points that are significantly affected by promontories or peninsulas
- Points that are in a bay and are significantly affected by reflected waves

In addition, in cases where the tsunami height is relatively higher in cases of instantaneous fracture, it is desirable to perform calculations that take into account rupture propagation velocity and rise time for the benefit of verification.

[Appendix 3 References]

Aida, I. (1977): Simulations of Large Tsunamis Occurring in the Past off the Coast of the Sanriku District., Bulletin of the Earthquake Research Institute, University of Tokyo, Vol. 52 (1), pp. 71-101 (in Japanese).
https://repository.dl.itc.u-tokyo.ac.jp/?action=repository_action_common_download&item_id=33218&item_no=1&attribute_id=19&file_no=1

Annaka, T., K. Ohta, H. Motegi, I. Yoshida, M. Takao and H. Soraoka (1999): Tsunami Inversion Based on the Shallow Water Theory, Proceedings of Coastal Engineering, JSCE, Vol. 46, pp. 341-345 (in Japanese).
https://www.jstage.jst.go.jp/article/proce1989/46/0/46_0_341/_pdf/-char/ja.

Committee for the Field Investigation of the Chilean Tsunami of 1960 (1961): The Chilean tsunami of May 24, 1960, Earthquake Research Institute, The University of Tokyo, 397p. (in Japanese).
http://iss.ndl.go.jp/books/R100000039-I000797416-00.

Fukuyama, E. and K. Irikura (1986): Rupture process of the 1983 Japan Sea (Akita-Oki) earthquake using a waveform inversion method, Bulletin of the Seismological Society of America, Vol. 76:6, pp. 1623-1640.

Kanamori, H. and J. J. Cipar (1974): Focal process of the great Chilean earthquake May 22, 1960,

Phys. Earth Planet. Interiors, Vol. 9 pp. 128-136.

Kotani, M., F. Imamura. and N. Shuto (1998): New method of tsunami runup and estimation of damage using GIS data, Proceedings of Coastal Engineering, JSCE, Vol. 45, pp. 356-360 (in Japanese). http://library.jsce.or.jp/jsce/open/00008/1998/45-0356.pdf

Mansinha, L. and D. E. Smylie (1971): The displacement fields of inclined faults, Bulletin of the Seismological Society of America, Vol. 61, No. 5, pp. 1433-1440.

Somerville, P., K. Irikura, R. Graves, S. Sawada, D. Wald, N. Abrahamson, Y. Iwasaki, T. Kagawa, N. Smith and A. Kawada (1999): Characterizing Crustal Earthquakes Slip Models for the Prediction of Strong Ground Motion, Seismological Research Letters, Vol. 70, No. 1, pp. 59-80.

Tanioka, Y. and K. Satake (1999): Slip Distribution of the 1946 Nankai Earthquake Evaluated from the Tsunami Records, Chikyu Extra Vol. 24 (in Japanese).